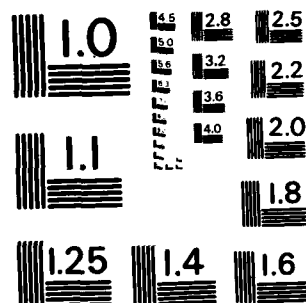MICROCOPY RESOLUTION TEST CHART

NATIONAL BUREAU OF STANDARDS - 1963 - A

AD A130745

ELECTRONIC PROPERTIES OF SEMICONDUCTOR INTERFACES

Final Technical Report

by

F.Flores, C.Tejedor, F.Guinea and J.Sánchez-Dehesa

February 1983

DTIC
SELECTE
JUL 1 1983
S
D
A

SECURITY CLASSIFICATION OF THIS PAGE *(When Data Entered)* R&D 4021-EE

REPORT DOCUMENTATION PAGE	READ INSTRUCTIONS BEFORE COMPLETING FORM

1. REPORT NUMBER	2. GOVT ACCESSION NO. AD-A130 945	3. RECIPIENT'S CATALOG NUMBER

4. TITLE *(and Subtitle)*	5. TYPE OF REPORT & PERIOD COVERED
Electronic Properties of Semiconductor Interfaces	Final Technical Report Dec 81 - Feb 83
	6. PERFORMING ORG. REPORT NUMBER

7. AUTHOR(s)	8. CONTRACT OR GRANT NUMBER(s)
F. Flores, C.Tejedor, F.Guinea and J.Sánchez-Dehesa	DAJA37-82-C-0118

9. PERFORMING ORGANIZATION NAME AND ADDRESS	10. PROGRAM ELEMENT. PROJECT, TASK AREA & WORK UNIT NUMBERS
Departamento de Fisica del Estado Solido Universidad Autonoma Cantoblanco, Madrid 34, Spain	6.11.02A 1T161102BH57-03

11. CONTROLLING OFFICE NAME AND ADDRESS	12. REPORT DATE
USARDSG-UK Box 65, FPO NY 09510	Feb 83
	13. NUMBER OF PAGES 98

14. MONITORING AGENCY NAME & ADDRESS*(If different from Controlling Office)*	15. SECURITY CLASS. *(of this report)*
	Unclassified
	15a. DECLASSIFICATION/DOWNGRADING SCHEDULE

16. DISTRIBUTION STATEMENT *(of this Report)*

Approved for Public Release, distribution unlimited

17. DISTRIBUTION STATEMENT *(of the abstract entered in Block 20, if different from Report)*

18. SUPPLEMENTARY NOTES

19. KEY WORDS *(Continue on reverse side if necessary and identify by block number)*

Heterojunctions. Junctions. Superlattices. Metal-semiconductor interfaces. Etched junctions. Barrier height. Wannier functions. Non-abrupt junctions. Metal-semiconductor interdiffusion.

20. ABSTRACT *(Continue on reverse side if necessary and identify by block number)*

The objective was to analyze the electronic properties of different semiconductor interfaces. The Wannier function formalism has been applied to the GaAs-AlAs (111) and (100) heterojunctions and superlattices. Ionic relaxations, band discontinuities and interface states have been obtained. Abrupt Si-metal interfaces and Si-interlayer-metal junctions have been analyzed by means of a selfconsistent tight-binding approach. The barrier height has

(...../....)

DD FORM 1473 EDITION OF 1 NOV 65 IS OBSOLETE

20. Abstract (cont)
been obtained by calculating the interface density of states and
the neutral level of the junction. Our results show that the
barrier height is mainly determined by the coupling between tne
semiconductor and the last layer just sitting on top of the same
semiconductor.

CONTENTS

ABSTRACT

Some electronic properties of GaAs-AlAs heterojunctions and of metal-semiconductor junctions are presented in this Report.

GaAs-AlAs heterojunctions have been analyzed by means of a selfconsistent localized scheme, based on a Wannier function approach. Finite superlattices for (100) and (111) directions have been considered, and their structural properties have also been discussed. Our results show small ionic relaxations at the (100)-interfaces, and no appreciable relaxation at the (111)-heterojunction. The electronic selfconsistent calculation gives a small transfer of charge from AlAs to GaAs, so that a potential barrier between both semiconductors appears. By calculating this barrier, we have obtained the energy difference between the top of both semiconductor valence bands, and found good agreement with the experimental evidence.

Abrupt metal-semiconductor junctions have been analyzed by a selfconsistent tight-binding calculation. Realistic results for the junction have been obtained in a (111)-Si-Ag interface. General junctions for Si have been discussed within the same context, and we have shown that: (i) the barrier height increases with the strength of the metal-semiconductor coupling; (ii) the barrier height is essentially determined by the coupling between the semiconductor and the *last* metal layer.

Etched metal-semiconductor junctions have been analyzed in a similar way. We present a realistic calculation of a Si-H-Ag junction. More general cases for Si have been explored by changing the parameters of the interface. Our results show: (i) The barrier height presents small changes (of up to 0.2 eV) depending on the ad-atom electronegativities. For ad-atoms of low (high) electronegativity, we find higher (smaller) barrier heights. (ii) The barrier height has been

found to be practically determined by the coupling between the semiconductor and the ad-atom interlayer.

Finally, non-abrupt III-V semiconductor-metal junctions have been analyzed and shown to interdiffuse as a function of the metal-semiconductor heat of reaction and of the heat of reaction for the semiconductor.

CHAPTER I. HETEROJUNCTIONS

I.1. INTRODUCTION

Semiconductor-semiconductor junctions have become an important subject with many potential applications. Our work on this topic has been concentrated in the analysis of GaAs-AlAs superlattices (SL).

In the last few years much progress has been made in the technology of artificial crystals constituted by periodic layers of two semiconductors. These superlattices show, under certain conditions, very interesting properties such as extremely high carrier mobility (Hess and Holonyak Jr. 1981) or negative differential resistance (Esaki and Chang 1974). A SL which has received a great deal of attention is GaAs-Al_xGa_{1-x} as grown by molecular-beam-epitaxy. Several experimental techniques (Dingle et al.1974, 1975, Manuel et al.1976, Sai-Halasz et al.1978, van der Ziel and Gossard 1978, Barker et al.1978, Merlin et al.1980, Colvard et al.1980, Holonyak Jr. et al.1980, 1981, Weisbuch et al.1981a, 1981b, Gormik et al.1981, Piczuk et al.1981a, 1981b) have been used to study the vibrational and electronic properties of this system. The Kroning-Penney model has been extensively used to interpret the phenomenology. Such a model may be adequate when the layer thickness is so large that regions with bulk properties of each semiconductor exist. However, the theoretical analysis is more difficult in those systems where ultra-thin layers form the SL. Fortunately, in such cases the experiments have been performed in samples where $x = 1$ (van der Ziel and Gossard 1978, Barker Jr.et al.1978, Merlin et al.1980, Colvard et al.1980). This makes possible a calculation of the properties of these $(GaAs)_m-(AlAs)_n$ SL's where m and n are the number of layers of each semiconductor in a period of the crystal. Some efforts (Caruthers and Lin Chung 1978, Osbourn and Smith 1979, Schulman and McGill,

1979, 1981, Andreoni and Car 1980, Schulman and Chang 1981)
have been made to study such systems by means of model
hamiltonians. However, to our knowledge, just only one self-
consistent calculation (Pickett et al.1978) has been carried
out for (110) oriented GaAs-AlAs SL's. This implies hetero-
polar interfaces with properties essentially different to the
homopolar ones of the experimental samples which have been
grown in the (001) direction. In this project, we have
analysed several SL's with polar interfaces, both (001) and
(111) by means of a self-consistent calculation of their
electronic and structural properties. Besides the electronic
self-consistency, similar to the one obtained in the
computations published for other interfaces as (GaAs-AlAs)
(110) (Pickett et al.1978), (ImAs-GaSb) (100) (Ihm et al.1979)
and (Ge-GaAs) (Kunc and Martin 1981), we extend the self-
consistency to the ions which are free to move in order to
reach their equilibrium positions. The method is a minimization
of the total energy in terms of a localized basis which makes
easier its comparison with calculations where a tight-binding
model hamiltonian is used. Since the experiments are usually
performed in (001) SL's , we will devote more attention to
this case. In particular, we will analyze several systems with
different layer thickness in order to see when the SL can be
considered as a junction of the two semiconductors or as a
completely new crystal.

I.2. SELF-CONSISTENCY. LOCAL DENSITY FORMALISM

I.2.1. The method

We use a method which has given satisfactory results for
other problems (Tejedor and Vergés 1979, Vergés and Tejedor
1979a, 1979b, Sánchez-Dehesa et al.1981a, 1981b, 1981c). In
order to describe the electronic structure of the crystal, we
use a Wannier functions (WF) representation (Kohn 1973). This
localized basis presents an important advantage in our case
of fully occupied bands. By means of a unitary transformation

between the eigenstates $\psi_m^{\vec{k}}(\vec{r})$ and the WF $a_m(\vec{r}-\vec{R})$ (where the index m sums over the valence bands), both the charge density, $\rho(\vec{r})$, and the kinetic energy, T, can be written in terms of the WF as follows (Vergés and Tejedor 1979a, 1979b):

$$\rho(\vec{r}) = 2 \sum_m^{VB} \sum_{\vec{k}}^{BZ} \psi_m^{\vec{k}*}(\vec{r}) \psi_m^{\vec{k}}(\vec{r}) = 2 \sum_m^{VB} \sum_{\vec{R}} a_m^*(\vec{r}-\vec{R}) a_m(\vec{r}-\vec{R}) \qquad (I.1)$$

$$T = 2 \sum_m^{VB} \sum_{\vec{k}}^{BZ} \langle \psi_i^{\vec{k}}(\vec{r}) | -\frac{\nabla^2}{2} | \psi_i^{\vec{k}}(\vec{r}) \rangle =$$

$$= 2 \sum_m^{VB} \sum_{\vec{R}} \langle a_m(\vec{r}-\vec{R}) | -\frac{\nabla^2}{2} | a_m(\vec{r}-\vec{R}) \rangle \quad , \qquad (I.2)$$

where the sum in $\vec{k}$ runs over the first Brillouin zone, whereas the sum in $\vec{R}$ runs over all the lattice positions. Accordingly, within a local approximation, the total energy of the system can be expressed as a function of the valence WF and an ionic pseudopotential, $v_i(\vec{r})$. Thus, the energy can be written as

$$E_T = E_e + E_{bs} \quad , \qquad (I.3)$$

where E_e takes account of the purely electrostatic interaction of a set of ionic pseudopotentials, all embedded in a compensating uniform negative background (the zero Fourier component of ρ), while all the other contributions are included in the band-structure term E_{bs}. The electrostatic term is split as usual (Vergés and Tejedor 1979b) into two parts: (i) the Ewald energy E_{EW}, containing the interaction of a set of point ions with the electronic background, and (ii) the correction coming from the spatial dependence of the ionic pseudopotential $v_i(\vec{r})$:

$$E_e = E_{EW} + \frac{\bar{\rho}}{N_i} \left\{ \sum_l \int d\vec{r} \left[v_i^{al}(\vec{r}) + \frac{z_a}{r} \right] + \sum_l \int d\vec{r} \left[v_i^{cl}(\vec{r}) + \frac{z_c}{r} \right] \right\} \quad , \qquad (I.4)$$

where the sums in l run over the types of anions and cations in the supercell. In eq.(I.4) $\bar{\rho}$ is the mean electronic charge and z_a and z_c are the ionic charges, i.e. 3 and 5 in our case.

The Ewald energy is computed by standard methods (Harrison 1966, Sánchez-Dehesa 1982) and is given by

$$E_{EW} = (\frac{1}{\sqrt{2}} - 2) - \frac{N_a Z_a^2 + N_c Z_c^2}{N} +$$

$$+ \frac{4\pi}{N_i \Omega} \sum_{g \neq 0} \frac{\left[N_a Z_a S_z(\vec{g}) + N_c Z_c S_c(\vec{g})\right]\left[N_a Z_a S_a^*(\vec{g}) + N_c Z_c S_c(\vec{g})\right]}{g^2} *$$

$$* \exp(-g^2/4\alpha)\left[1 - \frac{1}{2}\exp(-g^2/4\alpha)\right] , \qquad (I.5)$$

where N_a and N_c are the numbers of anions and cations in the supercell with volume Ω, and $N_i = N_a + N_c$. The structure factor is defined as usual:

$$S_j(\vec{g}) = \frac{1}{N_j} \sum_{\vec{v}_j} \exp(-i\vec{g} \cdot \vec{v}_j) , \qquad (I.6)$$

where $\vec{v}_j$ are the positions of the anions and cations (j=1,2), respectively, within the supercell. In eq.(I.5) several terms coming from sums in real space do not appear because we take the parameter α high enough to guarantee their cancellation. The actual value in our computation is $\alpha = 1.2$ a.u., which gives a fast convergence in the sums involved in eq.(I.5).

The band structure energy per ion has the expression

$$E_{bs} = \frac{1}{N_T}\left\{\sum_m^{VB} \sum_{\vec{R}} 2\langle a_m(\vec{r}-\vec{R})\left|-\frac{\nabla^2}{2}\right|a_m(\vec{r}-\vec{R})\rangle +\right.$$

$$+ \int d\vec{r}\rho(\vec{r})\epsilon_{xc}[\rho(\vec{r})] + \int d\vec{r}V_i(\vec{r})[\rho(\vec{r})-\bar\rho] +$$

$$\left.+ \int d\vec{r}\frac{V_H(\vec{r})}{2}[\rho(\vec{r})-\bar\rho]\right\} , \qquad (I.7)$$

where N_T is the total number of ions in the crystal. The four contributions to E_{bs} are the kinetic, T, the exchange and correlation, E_{xc}, the ion-electron, E_I, and the Hartree, E_H, energies respectively. The last two terms do not contain the zero Fourier component of ρ, which is included in E_e. In order to elude the cumbersome spatial integrals in eq.(I.7), the evaluation of E_{bs} will be obtained in reciprocal space as will

be detailed below (Vergés and Tejedor 1979b).

Once the total energy is written in terms of the WF's, a self-consistent solution is obtained by a minimization of that total energy as a function of a set of variational parameters included in a set of trial WF's. The whole scheme to get trial WF's from localized functions was proposed by Kohn (1973) and it is simple enough to allow the calculation of different crystal properties (Tejedor and Vergés 1979, Vergés and Tejedor 1979a,b, Sánchez-Dehesa et al.1981a,b,c). In particular, it has been used to analyze stacking faults in silicon (Sánchez-Dehesa et al.1981b) by a model where a ficticious SL is used. Satisfactory results were obtained, so that we will follow here the same procedure and only a few technical points need more attention. The whole procedure is sketched in the following diagram:

```
                    ┌─────────────────────────┐
                    │ Choice of a set of      │
                    │ variational parameters β│
                    └───────────┬─────────────┘
                                │
                                ▼
┌─────────────────────────┐   ┌──────────────────────┐
│ Calculation of T        │◄──│ Variation of the     │
│ and ρ from the WF's a   │   │ parameters β         │
└───────────┬─────────────┘   └──────────────────────┘
            │                             ▲
            ▼                             │
        ┌──────────────────────┐          │
   ┌───►│ Calculation of       │          │
   │    │ E_bs = E_I+E_H+T+E_xc│          │
   │    └───────────┬──────────┘          │
   │                │                     │
┌──┴──────────┐     ▼                ┌────┴──────────────────┐
│ Structural  │  ┌──────────────┐    │         NO            │
│ parameters  │─►│ Calculation  │──► │ Is E_T a minimum?     │
│ and ionic   │  │ E_T = E_bs+E_e│   │        YES            │
│ pseudopotent│  └──────────────┘    └───────────┬───────────┘
└─────────────┘                                  │
                                                 ▼
                                    ┌───────────────────────┐
                                    │ Self-consistent       │
                                    │ WF   a_m(r⃗,β)        │
                                    └───────────────────────┘
```

$E_{bs} = E_I + E_H + T + E_{xc}$

$E_T = E_{bs} + E_e$

Is E_T a minimum?

Self-consistent WF $a_m(\vec{r},\beta)$
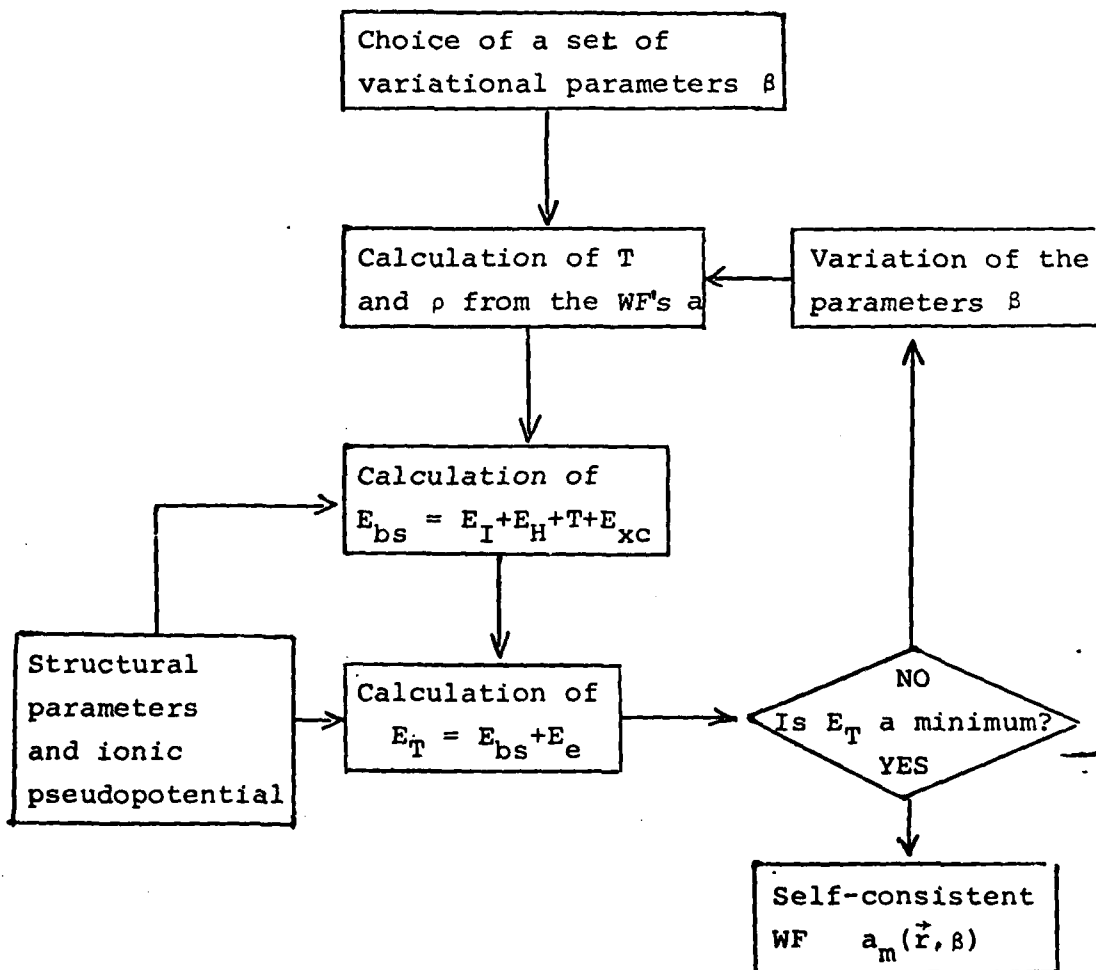
The procedure begins with a set of sp^3 Slater type orbitals (STO) centred at the positions where ionic pseudo-potentials are placed to describe the effect of the nuclei and core electrons. In order to have a good starting point for the SL calculation, we have previously computed the WF and lattice constant for GaAs and AlAs perfect semiconductors in zincblende structure. We apply our method with the ionic pseudopotentials to be used later on for the (110) GaAs-AlAs superlattice (Pickett et al.1978), taking into account that the pseusopotential must be normalized to the volume of the unit cell, so that it must be adequately varied when the introduction of ionic relaxations changes that volume. The parameters of the STO involved in the valence WF's and the lattice constants are the results we are interested in, because this information is required as a starting point in the SL calculation. Moreover, the value of the lattice constant is a test of the correctness of our approach. Table I.1 gives the different contributions to the total energy of the GaAs zincblende crystals as a function of the lattice constant. By using these results we have obtained 5.556 Å and 5.544 Å for the lattice parameters of AlAs and GaAs respectively, when the necessary sums (Tejedor and Vergés 1979, Vergés and Tejedor 1979b) running over the reciprocal lattice vectors contain only the terms corresponding to $|\vec{g}| \leqslant 8\pi/a$. The agreement with the experimental values (Weast 1980), 5.660 Å and 5.653 Å respectively, improves when more $\vec{g}$-vectors are included, but in the SL case that means a numerical task beyond our possibilities, so that we take that maximum value of $|\vec{g}|$ in our calculations. As a different test of our results we present in Table I.2 the Fourier components, $V(\vec{g})$, of the total self-consistent potential (Tejedor and Vergés 1979) with origin midway between ions:

$$V(\vec{g}) = \frac{e^{-i\vec{g}\cdot\vec{\tau}}}{2} \left\{ V_S \cos(\vec{g}\cdot\vec{\tau}) - iV_A \sin(\vec{g}\cdot\vec{\tau}) \right\} \quad ,$$

where $\vec{\tau} \equiv \frac{a}{8}(1,1,1)$, $V_S = 2(V_c+V_a)$ and $V_a = 2(V_c-V_a)$. The agreement with other theoretical estimations supports the adequacy of our calculation (Caruthers and Lin Chung 1978,

TABLE I.1.- Different contributions to the total energy (in a.u.) of GaAs and AlAs zincblende-type crystals as a function of the lattice constant a (in a.u.).

a	10.2678		10.4817		10.6956	
	GaAs	AlAs	GaAs	AlAs	GaAs	AlAs
E_i	-0.9037	-0.9167	-0.9429	-0.9537	-0.9791	-0.9794
E_H	0.2319	0.2345	0.2473	0.2486	0.2607	0.2568
T	1.4036	0.1399	1.3674	1.3617	1.3324	1.3207
E_{xc}	-1.2234	-0.1224	-1.2063	-1.2067	-1.1888	-1.1881
E_{bs}	-0.4916	-0.5072	-0.5346	-0.5501	-0.5749	-0.5900
$\alpha_1 Z$	0.7972	0.8076	0.7494	0.7592	0.7053	0.7145
E_{ew}	-4.3812	-4.3812	-4.2918	-4.2918	-4.2060	-4.2060
E_T	-4.0756	-4.0808	-4.0770	-4.0827	-4.0755	-4.0815

8

TABLE I.2.- Symmetric (S) and antisymmetric (A) components of the self-consistent potential, i.e. $V_S = 2(V_c + V_a)$ and $V_A = 2(V_c - V_a)$, where c and a stand for cation and anion respectively. The superindices give the value $(g \frac{a}{2\pi})^2$. B: Caruthers and Lin Chung 1978. C: Walter and Cohen 1969. D: Stukel and Euwema 1969.

	GaAs			AlAs		
	This work	B	C	This work	B	D
V_S^3	-0.2138	-0.2408	-0.245	-0.2017	-0.2600	-0.2200
V_A^3	0.0528	0.0592	0.062	0.0641	0.0400	0.0725
V_A^4	0.0428	0.0350	0.050	0.0591	0.0420	0.0625
V_S^8	0.0105	0.0102	-0.005	0.0263	0.0456	0.0800
V_S^{11}	0.0418	0.0713	0.075	0.0512	0.0710	0.0700
V_A^{11}	0.0026	0.0231	0.003	-0.0063	0.0210	-0.0075
V_A^{12}	-0.0039	0.0120	0.0	0.0026	0.0200	0.0

Walter and Cohen 1969, Stukel and Euwema 1969). The other
result we need is the valence WF. They are built up from trial
functions for each bond given by

$$f_{\vec{v}_i}(\vec{r}) = \sin\lambda\phi_{\vec{v}_i}(\vec{r}) + \cos\lambda\phi_{\vec{v}_i}(\vec{r} - \frac{a}{4}\vec{v}_i) \quad , \qquad (I.8)$$

where $\phi_{\vec{v}_i}(\vec{r})$ is a sp^3 Slater-type orbital (STO) centered at
one ion and pointing along the bond direction labelled by $\vec{v}_i$.
Besides the variational parameter λ, which gives the relative
weight of each one of the two sp^3 orbitals, other parameters
varying in the minimization are the exponents of the STO.
Table I.3 shows our results for all those variational

TABLE I.3.- Variational parameters obtained by minimizing the
total energy of GaAs and AlAs described in a
zincblende (ZNB) and SL framework respectively.
The STO of Ga and As have the functional form
corresponding to states of the fourth atomic shell,
and the orbitals of Al the form corresponding to
the third atomic shell.

	GaAs		AlAs	
	ZNB	SL	ZNB	SL
λ	1.0397	1.0462	1.0139	1.0153
β^a_{4s}	2.4754	2.4779	2.4705	2.4744
β^a_{4p}	1.6885	1.6910	1.7051	1.7048
$\beta^c_{4s,3s}$	2.2764	2.2701	1.5588	1.4890
$\beta^c_{4p,3p}$	1.4912	1.4937	1.0384	1.0351

parameters for AlAs and GaAs with zincblende structure and
the calculated lattice constant given above.

Since these results will be used later on in our computations of SL, it is convenient to check them for perfect crystals described in the SL framework. To this end, we have considered a (001) type SL, and introduced the same condition $|\vec{g}| \leqslant 8\pi/a$ given above, which amounts to using 129 reciprocal vectors. In Table I.3 the variational parameters obtained for this case are compared with the ones obtained in the zincblende structure. The agreement can be considered satisfactory. As far as the contributions to the total energy are concerned, we get results which differ less than 10^{-4} a.u. from the ones given in Table I.1 for the calculation in zincblende structure. All these results seem to support that we can use confidently the parameters obtained in a zincblende structure for different types of SL's.

Once the perfect crystal has been analyzed, the results so obtained are used to start the SL calculation. The ions are placed at their ideal positions in a perfect SL with a lattice constant which is the average of the two constants obtained above for each zincblende crystal. With this choice no missmatch of the two lattices is allowed, which is a good approach because of the very similar parameters of these semiconductors. For this lattice constant, the total energy is self-consistently computed. The calculation is repeated for several lattice constants around that initial value, so that a more precise minimization is achieved. In a final step the process is completed by allowing ionic relaxation at the interfaces, a feature never previously calculated for these SL's. Each one of the necessary steps is fulfilled in the following way. The valence WF's of the superlattice are variationaly computed with the same procedure from a set of linear combinations of sp^3 STO. Now the symmetry along the superlattice direction has been broken so that both the exponents of the orbitals and the mixture coefficients can be different for each bond. This implies many variational parameters and consequently a rather cumbersome numerical task. Therefore we adopt the approach which gave us excellent results in the case of the stacking fault of silicon (Sánchez-Dehesa et al.1981b). Just the parameters of the atoms at the

interfaces are treated variationaly, fixing those corresponding to the inner layers to their bulk values previously calculated at the zincblende structure. In order to test the results of this enormously simplified approach we have made some particular calculations by also minimizing with respect to the parameters of inner layers. The total energy decreases so little with this degree of freedom in which no significant variation appears, that this simplified approach can be considered as rather effective. In this scheme, the computation starts by taking, for the interface bonds, the bulk parameters as the initial values for the minimization procedure.

As far as other technical points are concerned, they are treated as detailed in Sánchez-Dehesa et al.(1981b), in particular the special points scheme used to perform integrals in reciprocal space.

In spite of the fact that the following sections are devoted to the analysis of different SL's, we can advance here the general trend of the results. The main variation obtained with the minimization corresponds to the mixture parameter λ at the interface as well as to the coefficients, obtained in the orthogonalization procedure, of each WF given in terms of the bond orbitals (I.8). However, the exponents of the STO do not vary significantly. Such a result could be expected because something similar happens in a much more drastic situation as that of the change from free atoms to ions forming a crystal (Tejedor and Vergés 1979, Vergés and Tejedor 1979a).

I.2.2. Results

I.2.2.1. (001) Superlattices

In this section we discuss the results obtained when the method avobe described is applied to SL oriented along the (001) direction, which are those of experimental interest. We concentrate upon $(GaAs)_m-(AlAs)_m$ systems with $m = 1,2,3$, in order to analyze the effect of layer thickness on the

properties of the SL. Experimental information (Barker Jr. et al.1978) for such very thin SL's indicates that these crystals must be considered as three-dimensional (3D) with properties rather different to those of thicker SL's, where two-dimensional (2D) confination appears. Our results allow to analyze how the transition in the 3D-2D behaviour occurs and, in particular, the way in which transfer of charge and ionic relaxations takes place at the interface of thicker SL and heterojunctions.

Figures I.1, I.2 and I.3 show the supercell used in the calculation for the cases m = 1, 2 and 3, respectively. Straight lines joining the ions represent the bonds (eq.(I.8)) from which a set of trial WF's is built up as described above. As in many other systems (Tejedor and Vergés 1979, Vergés and Tejedor 1979a,b, Sánchez-Dehesa et al.1981a,b,c), our results show that each valence WF can be associated with one of those bonds because its weight in the neighbouring bonds decreases very quickly. Therefore, we refer hereafter sometimes to a particular valence WF as a particular bond. As mentioned above, we start by self-consistently solving the problem of a perfect (without ionic relaxations at the interface) SL in order to determine the size of the supercell. This can be represented by the bond length l_m in each case $(GaAs)_m-(AlAs)_m$. We get $l_1 = 2.404$ Å, $l_2 = 2.370$ Å and $l_3 = 2.380$ Å, which are very close to $l_{GaAs} = 2.401$ Å and $l_{AlAs} = 2.406$ Å obtained in zincblende structure. This can be taken as a satisfactory test of the consistency of our SL calculations. Once the bond length has been determined for the inner ions, the distance between ionic layers at the interface is allowed to vary looking for equilibrium positions. Such step is made only for m = 3 because it does not mean a new variational freedom in the other two cases where all the ions can be considered as being at an interface. For m = 3 we get that both the distances Al-As and Ga-As at the interface increase in a 2.5 % of their bulk value. This implies that the period of $(GaAs)_3(AlAs)_3$ SL's is 1.008 times that of the ideal one. Let us now discuss the values of the variational parameters at this minimum of the total energy.
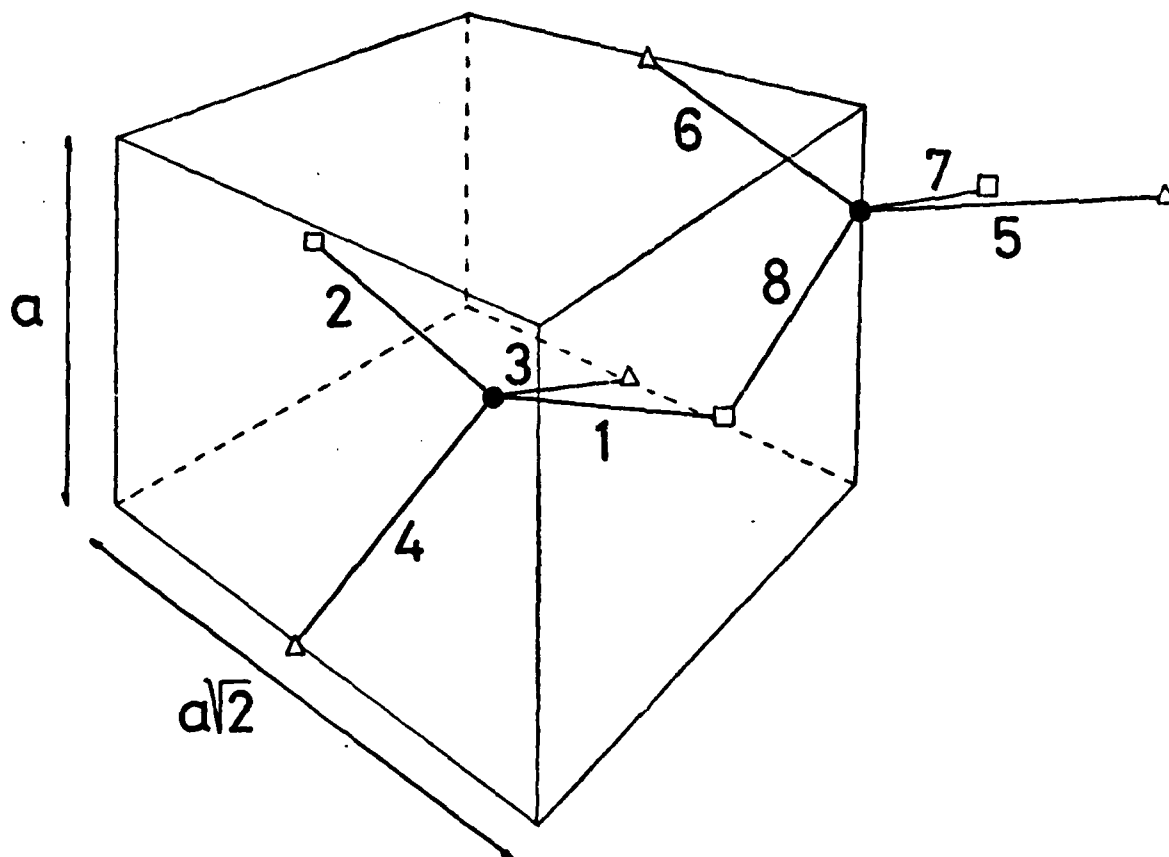
FIGURE I.1.- Supercell used in the calculation of a
$(GaAs)_1$-$(AlAs)_1$ SL oriented along the (001)
direction. Heavy lines represent the bonds
from which WF's are built up. Parameter a
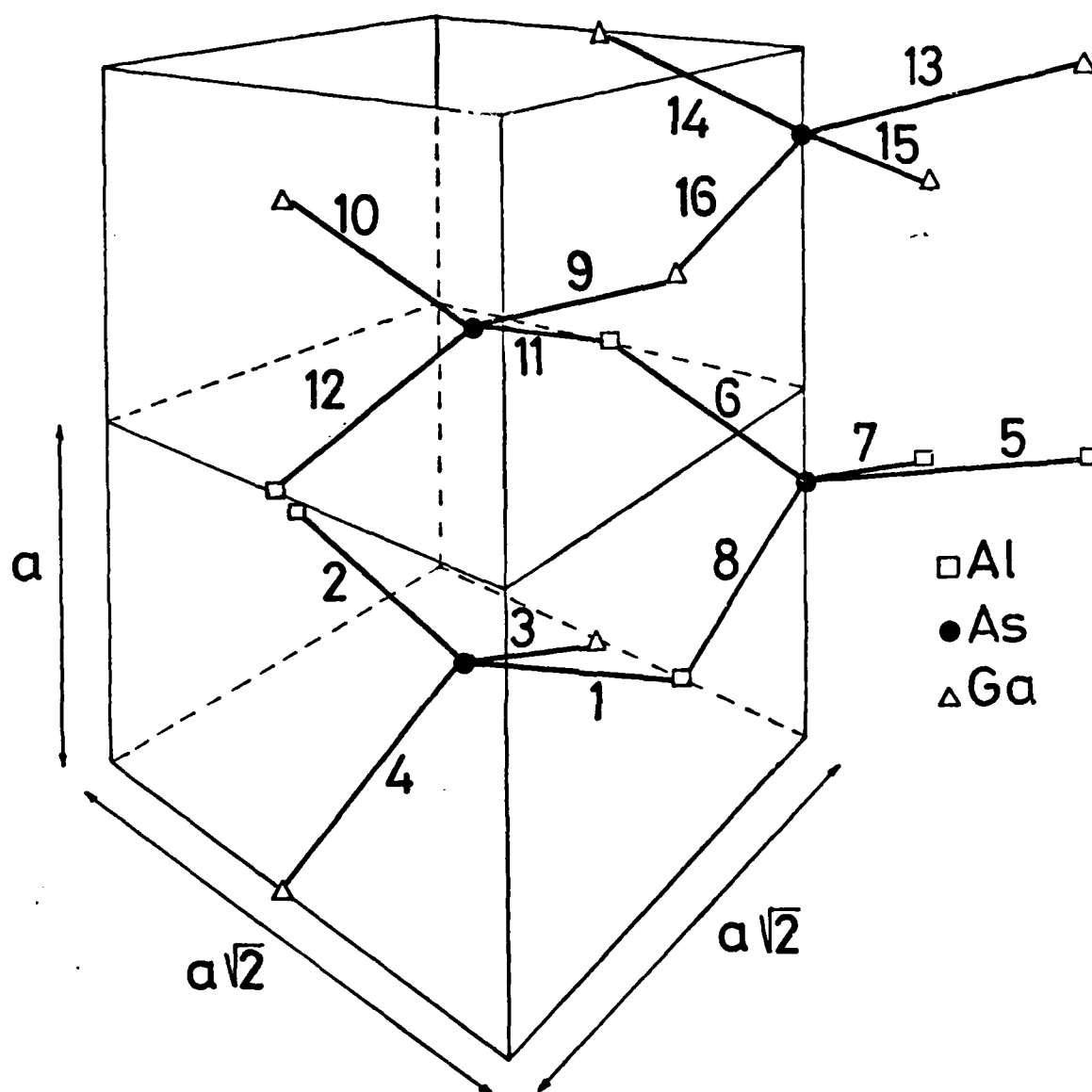is the lattice constant of the corresponding
zincblende crystal.

FIGURE I.2.- Supercell used in the calculation of a
$(GaAs)_2-(AlAs)_2$ SL oriented along the (001)
direction. Heavy lines represent the bonds
from which WF's are built up. Parameter a
is the lattice constant of the corresponding
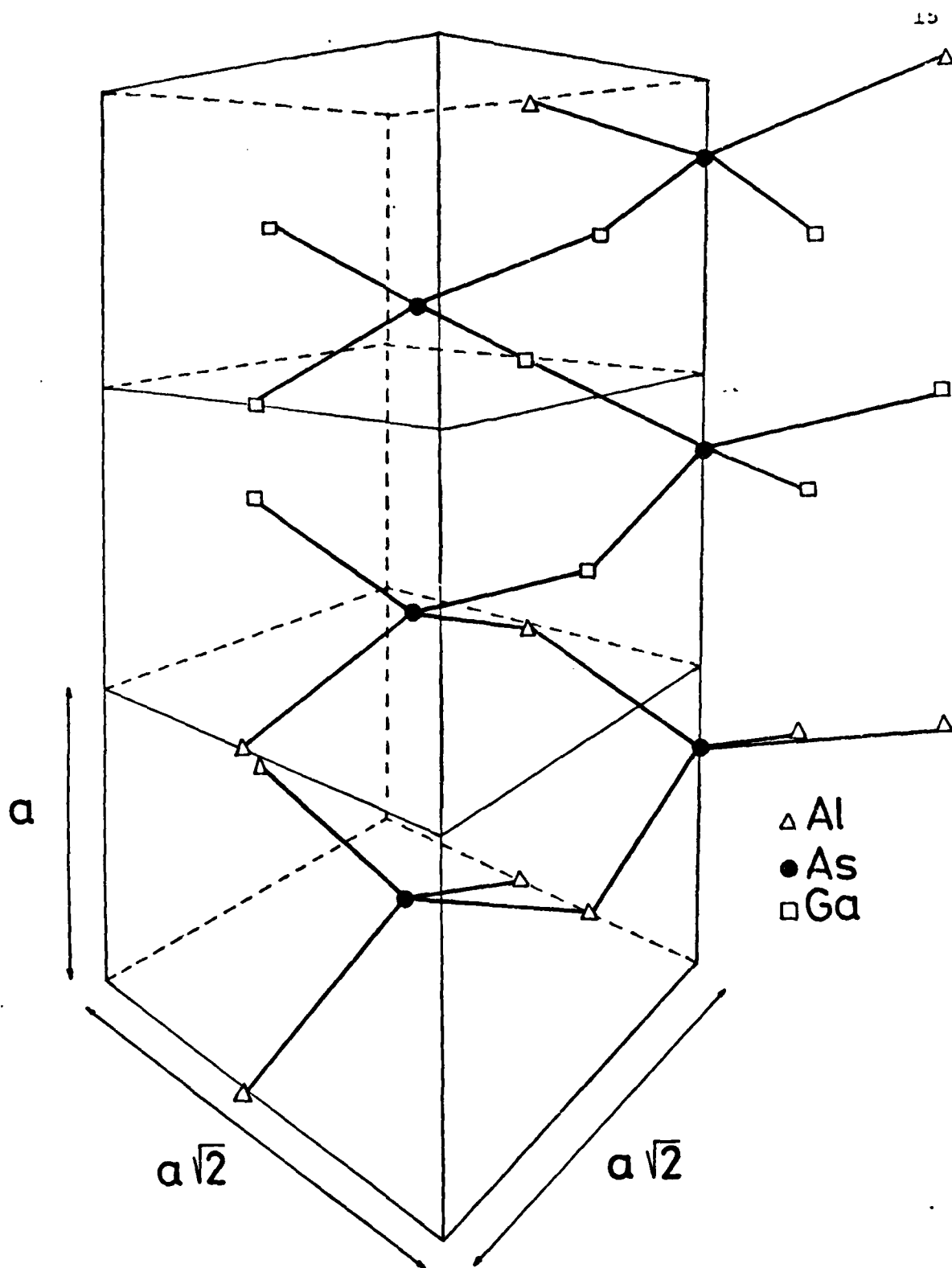zincblende crystal.

△ Al
● As
□ Ga

a

a √2   a √2

FIGURE I.3- Supercell used in the calculation of a
           (GaAs)$_3$-AlAs)$_3$ SL oriented along the (001)
           direction. Heavy lines represent the bonds from
           which WF's are built up. Parameter a is the
           lattice constant of the corresponding crystal.

No significant variations exist for the exponents of the STO
with respect to the bulk values. The main changes at the
interface are those of the mixture parameters λ appearing in
eq. (I.8). Table I.4 gives our results for such parameter for
the three SL's under study. The comparison between bulk and
interface values shows that the combination between Ga and
As orbitals does not change significantly. The main variation
is that of the mixture of Al and As orbitals. The connection

TABLE I.4.- Values of the mixture parameter λ for bonds in
the bulk and at the interface for (001)-type
superlattices. λ_A is for the combination in Al-As
bonds, and λ_G for Ga-As bonds (eq. (I.8)).

	Bulk	Interface
m = 1	—	$\lambda_A = 1.005$ $\lambda_G = 1.043$
m = 2	$\lambda_A = 1.014$ $\lambda_G = 1.042$	$\lambda_A = 0.991$ $\lambda_G = 1.040$
m = 3	$\lambda_A = 1.014$ $\lambda_G = 1.042$	$\lambda_A = 0.974$ $\lambda_G = 1.046$

of these results with physical properties is far from
straightforward because the main change produced in going
from perfect crystals to SL is not in the orbitals shape but
in the way in which these orbitals combine to give the WF's
of the system. In other words, the effect of the SL is
essentially contained in the orthogonalization procedure.
Therefore it is better to directly analyze physical results

as the charge density or the potential self-consistently calculated for the SL. Figure I.4 shows the potential average parallel to the interface plane for $(GaAs)_3$-$(AlAs)_3$. The mean value of $V(z)$ is 6 meV higher in the GaAs region than in the AlAs one. The three different contributions to this step are: the ionic potential V_i, the Hartree potential V_H, and the exchange potential V_{xc}

$$\Delta \bar{V}_i = \bar{V}_i (GaAs) - \bar{V}_i (AlAs) = -0.0232 \text{ eV}$$

$$\Delta \bar{V}_H = \bar{V}_H (GaAs) - \bar{V}_H (AlAs) = 0.0284 \text{ eV}$$

$$\Delta \bar{V}_{xc} = \bar{V}_{xc} (GaAs) - \bar{V}_{xc} (AlAs) = 0.0009 \text{ eV} \quad .$$

From these values we can conclude that in the self-consistent process the differences in the ionic potentials are screened by the electrons so that a barrier in the opposite direction results.

Similar results are obtained here for m = 2 and by Pickett et al.(1978) for the (110) oriented SL. The reason of this induced potential barrier is easily understood in terms of the charge transfer. In order to visualize this transfer, Figures I.5 and I.6 show, for m = 2 and 3 respectively, the difference between the SL charge density and the charge of each perfect crystal placed at the adequate spatial region. In both cases, a net charge is transferred from AlAs to GaAs. Such a result could be expected from the Pauling's scale of electronegativities (Pauling 1972), where Ga has a higher value than Al, so that the latter tends to transfer electrons to the former. This effect is mainly concentrated at the interface and it has a clear implication in the interaction between localized orbitals. In our scheme we work with the interaction between WF's $a_i(\vec{r})$ given by

$$\epsilon_{ij}(\vec{R}) = \langle a_i(\vec{r}) | H | a_j(\vec{r}-\vec{R}) \rangle \quad , \tag{I.9}$$

where H is the self-consistent Hamiltonian, $\vec{R}$ a lattice vector and i,j label two WF's of the set associated to the valence
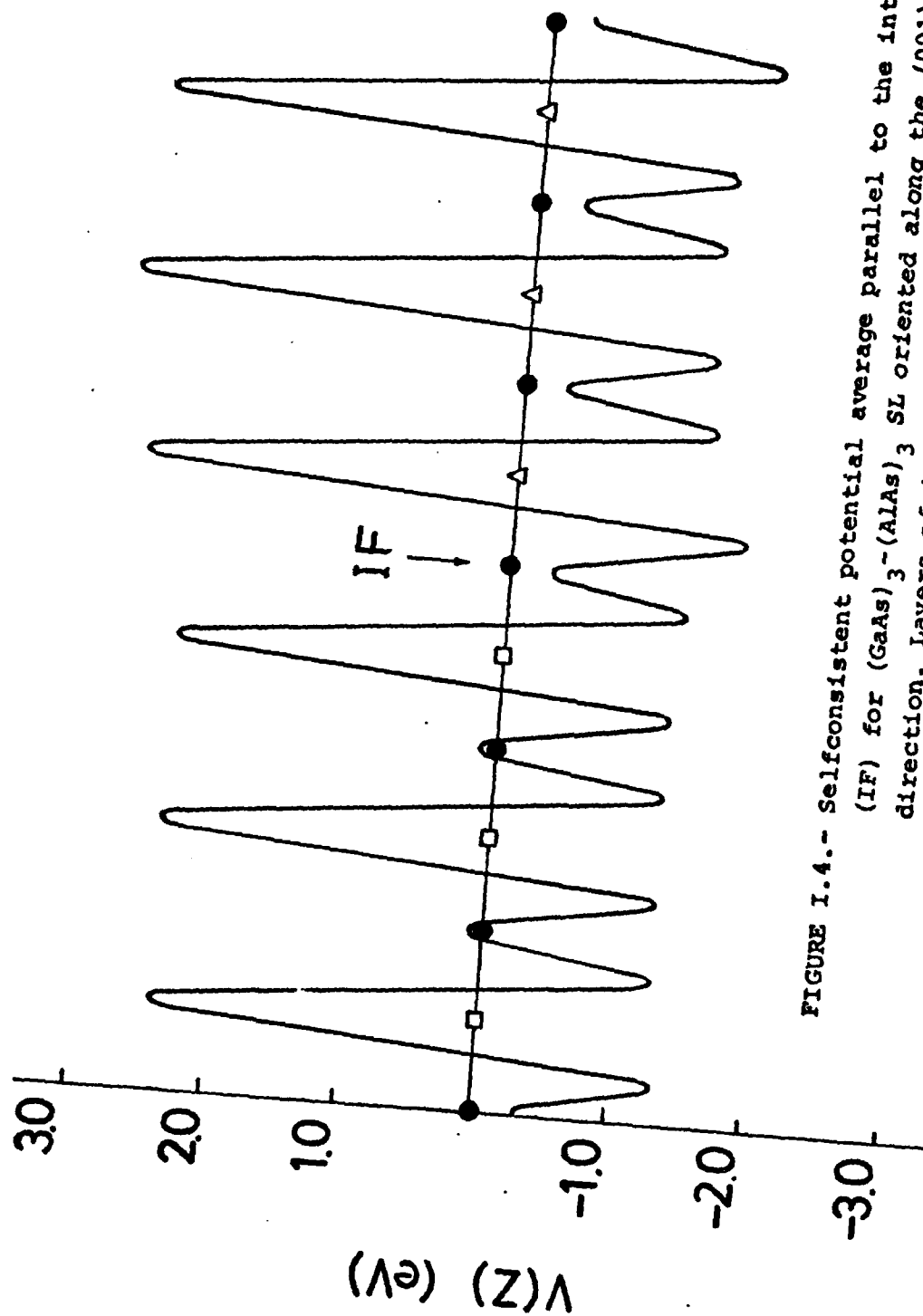
FIGURE I.4.-- Selfconsistent potential average parallel to the interface (IF) for (GaAs)₃-(AlAs)₃ SL oriented along the (001) direction. Layers of ions are represented by ● for As, △ for Al and □ for Ga.
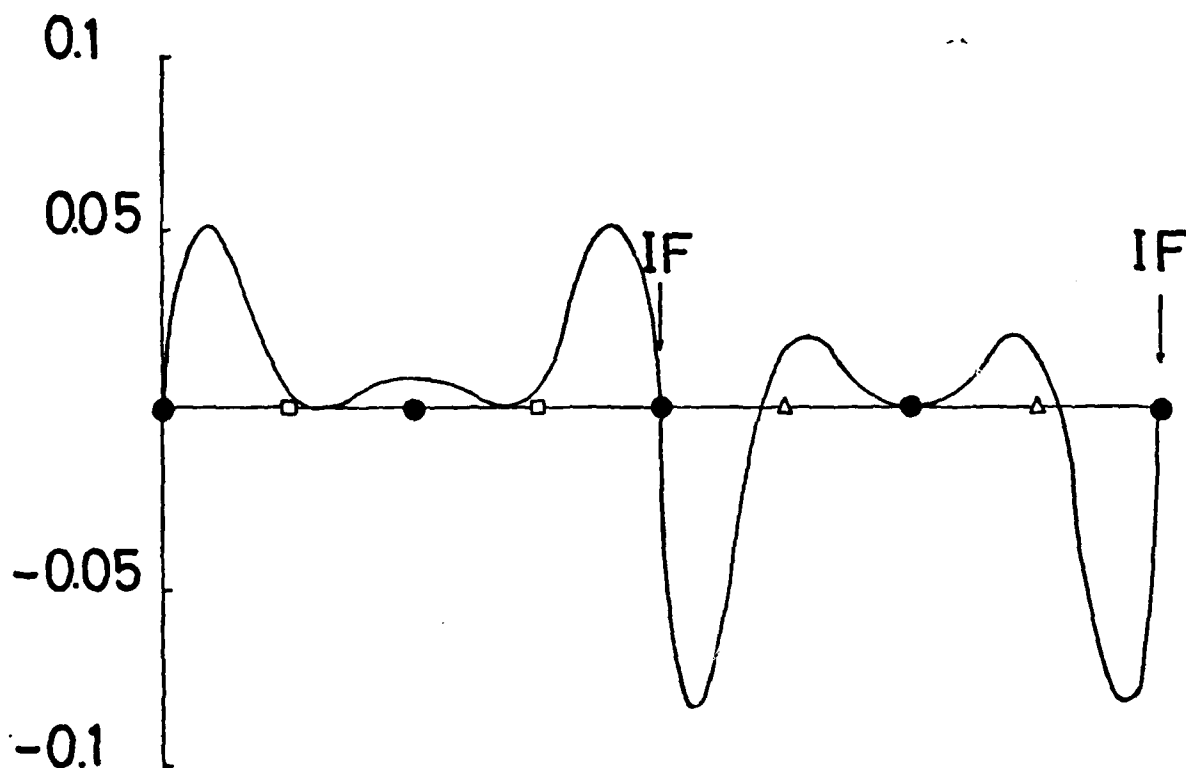
FIGURE I.5.- Charge transfer in electrons per ion
selfconsistently computed for $(GaAs)_2-(AlAs)_2$
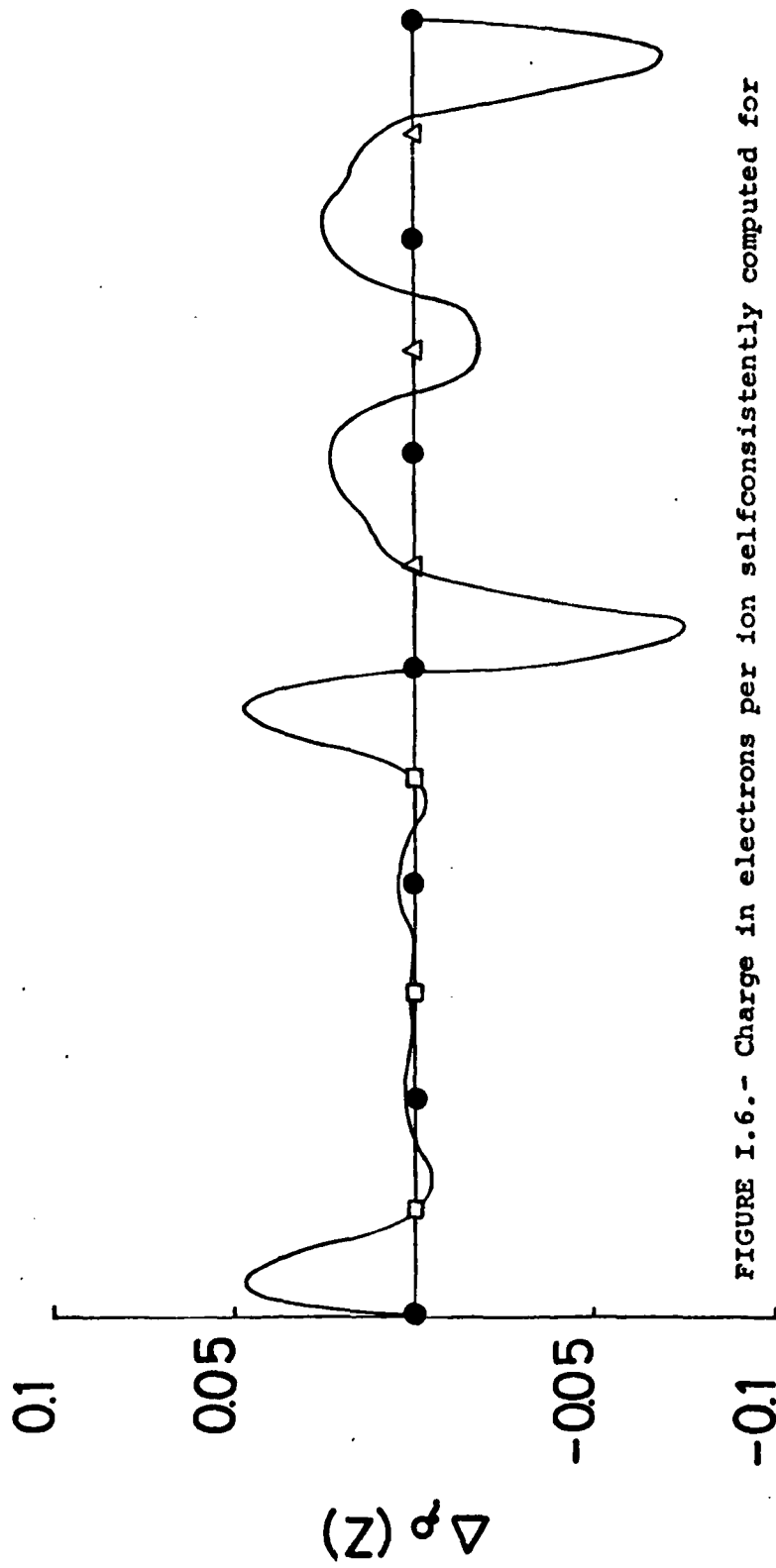SL in the (001) direction. Layers of ions are
represented by ● for As, Δ for Al and □ for Ga.

FIGURE I.6.- Charge in electrons per ion selfconsistently computed for $(GaAs)_3-(AlAs)_3$ SL in the (001) direction. Layers of ions are represented by ● for As, △ for Al and □ for Ga.

bands (Tejedor and Vergés 1979, Sánchez-Dehesa et al.1981b).
In Tables I.5 and I.6 we show some of the interactions for
m = 1 and 2 respectively. In order to compare with simple

TABLE I.5.- Interaction $\varepsilon_{ij}(\vec{R}=0)$ (in a.u.) for the $(GaAs)_1$-
$(AlAs)_1$ SL in the (001) direction. Subindices G
and A refer to interactions in GaAs and AlAs,
respectively. The labels i,j correspond to the
ones in Figure I.1.

Neighbourhood between bonds	$\varepsilon_{ij} = <a_i|H|a_j>$
Zero	$\varepsilon_{GG}(1,1) = 0.1790$
	$\varepsilon_{AA}(3,3) = 0.1648$
First neighbours	$\varepsilon_{GG}(1,2) = -0.05\text{C}8$
	$\varepsilon_{AA}(3,4) = -0.0688$
	$\varepsilon_{GA}(1,3) = -0.0663$
Second parallel neighbours	$\varepsilon_{GA}(1,5) = 0.0144$
non parallel	$\varepsilon_{GA}(1,6) = -0.0018$
	$\varepsilon_{GA}(1,8) = -0.0048$

tight-binding models, it is sufficient to look at the inter-
action of a WF with itself because a WF essentially contains
atomic orbitals of two first neighbours. Table I.7 shows this
magnitude for different WF's in the $(GaAs)_3$-$(AlAs)_3$ SL. The
conclusion drawn from these results is that the self-
interaction of Ga-As bonds at the interface tends to be an
average of the two bulk values in agreement with a simple

TABLE I.6.- Interactions $\varepsilon_{ij}(\vec{R}=0)$ (in a.u.) for the $(GaAs)_2-(AlAs)_2$ SL in the (001) direction. Subindices G and A refer to interactions in GaAs and AlAs respectively. The labels i,j correspond to the ones in Figure 2. We have artificially labelled the centre of each semiconductor as bulk zone.

Neighbourhood between bonds		Interface zone	Bulk zone
Zero		$\varepsilon_{GG}(1,1) = 0.1798$	$\varepsilon_{GG}(5,5) = 0.1821$
		$\varepsilon_{AA}(3,3) = 0.1594$	$\varepsilon_{AA}(13,13) = 0.1662$
First neighbours		$\varepsilon_{GG}(1,2) = -0.0580$	$\varepsilon_{GG}(5,6) = -0..622$
		$\varepsilon_{AA}(3,4) = -0.0666$	$\varepsilon_{AA}(13,14) = -0.0654$
		$\varepsilon_{GA}(1,3) = -0.0703$	
Second neighbours	parallel	$\varepsilon_{GG}(1,5) = 0.0135$	
		$\varepsilon_{GA}(11,15) = 0.0149$	
		$\varepsilon_{AG}(3,7) = 0.0125$	
		$\varepsilon_{AA}(9,13) = 0.0137$	
	non parallel	$\varepsilon_{GG}(1,6) = -0.0020$	
		$\varepsilon_{GA}(12,15) = -0.0014$	
		$\varepsilon_{AG}(9,6) = -0.0034$	
		$\varepsilon_{AA}(9,14) = -0.0026$	

TABLE I.7.- Self-interaction (in a.u.) of different WF's around the interface of the super-lattice $(GaAs)_3-(AlAs)_3$ grown in the (001) direction.

$$\ldots \text{Ga} === \text{As} === \text{Ga} === \text{As} === \text{Al} === \text{As} === \text{Al} === \text{As} === \text{Al} \ldots$$

| | 0.1772 | 0.1771 | 0.1767 | 0.1582 | 0.1711 | 0.1723 |

$\epsilon_{ii}(\vec{R}=0)$

tight-binding model proposed by Schulman and McGill (1979). However, this is not the case of the self-interaction of the Al-As bond at the interface, which is significantly lower than the bulk values. This clear difference with the simple tight-binding model is associated to the change of the mixture parameter λ mentioned above and shown in Table I.4.

Let us finally discuss our results for the band structure. Once the self-consistent potential has been obtained, the valence spectrum is computed by diagonalizing the Hamiltonian represented in a basis of Bloch sums of WF's (Tejedor and Vergés 1979). Then, the calculation is rather simple because the size of the matrix is just 8m×8m. Figures I.7 and I.8 show the valence band structure for m = 1 and 2, respectively. Table I.8 gives the eigenstates at the valence band edges for the three SL's we are concerned with. The main result is the well known (Caruthers and Lin Chung 1978, Schulman and McGill 1979, Andreoni and Car 1980) splitting of some meV of the upper valence states at Γ. As it was obtained by Pickett et al.(1978) in their self-consistent calculation for (110) GaAs-AlAs SL's, we get a non degenerate upper state, but since the width of our SL is too small, such a state is not concentrated at the GaAs region. Therefore, it cannot be considered as a two dimensional SL state as the ones experimentally observed in thicker SL's (Dingle et al.1974, 1975, Manuel et al.1976, Sai-Halasz et al.1978). In order to clarify the meaning of these band structures we present in Table I.9 the levels at the Γ point for perfect crystals treated in the SL framework. A magnitude which gives the trend of the band structure as a function of the SL thickness is the valence band width. Table I.8 shows an increase of this width as m increases. As shown in Table I.10, we also obtain a similar increase for the total energy per atom, a magnitude that, to our knowledge, is not possible to compare with any experimental information.

I.2.2.2. (111) *Superlattices*

No experimental or theoretical information exists, to our knowledge, for SL's grown in this direction. We have

FIGURE I.7.- Band structure for the VB of the $(GaAs)_1$-$(AlAs)_1$ SL in the (001) direction. The origin of energies is taken at the mean potential of the SL.
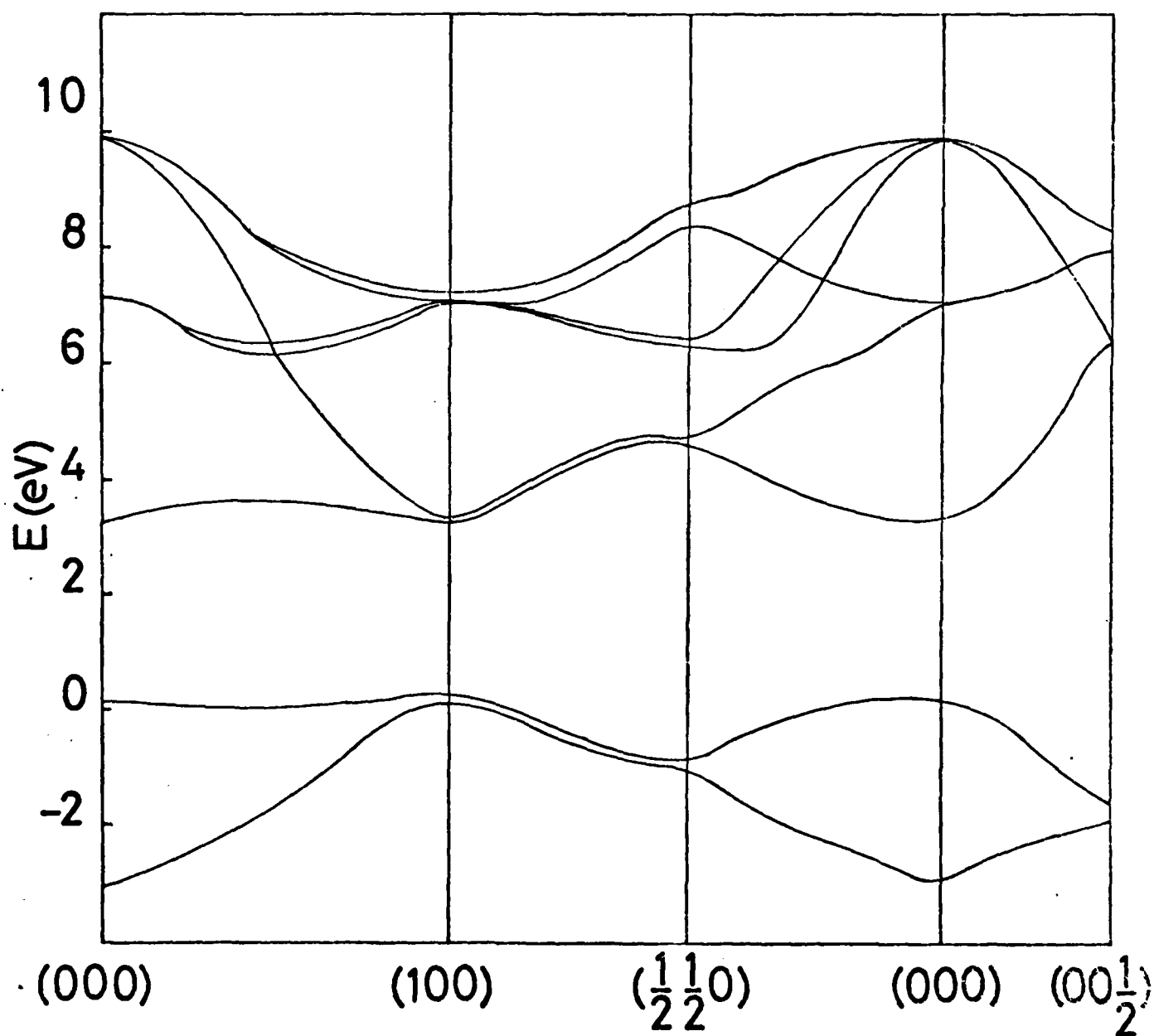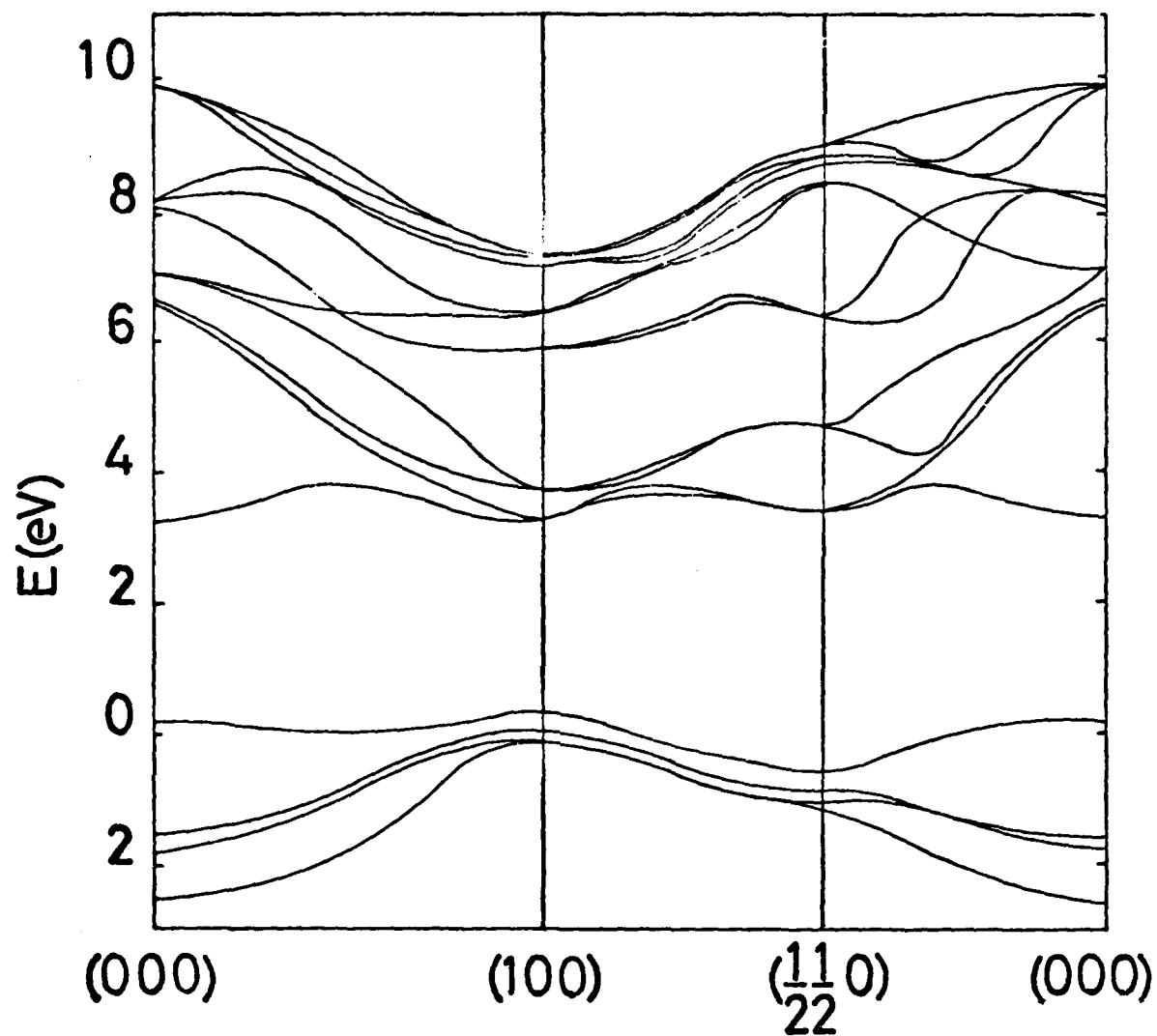
FIGURE I.8.- Band structure for the VB of the
(GaAs)$_2$-(AlAs)$_2$ SL in the (001) direction.
The origin of energies is taken at the mean
potential of the SL.

TABLE I.8.- Eigenstates in $\Gamma \equiv (0,0,0)$ and $J = \frac{2\pi}{a}(\frac{1}{2},\frac{1}{2},0)$ at the valence band edges of a (001) SL. Numbers in parenthesis stand for degeneracies. Results are given in eV with origin at the mean potential for each surperlattice.

$(GaAs)_1-(AlAs)_1$		$(GaAs)_2-(AlAs)_2$		$(GaAs)_3-(AlAs)_3$	
Γ	J	Γ	J	Γ	J
9.906	8.773	9.928	9.006	9.918	8.860 (2)
9.893 (2)	8.245	9.921 (2)	8.781	9.909 (2)	8.705
7.128 (2)	6.443	8.257 (2)	8.751	8.951 (2)	8.571
. . .	. . .	. . .	. . .	. . .	. . .
-2.490	-1.058	-2.526	-1.102	-2.597	-1.110

TABLE I.9.- Eigenstates in $\Gamma \equiv (0,0,0)$ at the band edges of the valence band for $(GaAs)_{2m}-(AlAs)_0$ and $(GaAs)_0-(AlAs)_{2m}$ SL in the (001) directions. Numbers in parenthesis stand for the degeneracy of the eigenstate. The energies (in eV) are referred to the mean value of the potential for each SL.

	$(GaAs)_{2m}-(AlAs)_0$			$(GaAs)_0-(AlAs)_{2m}$		
	m=1	m=2	m=3	m=1	m=2	m=3
	10.040	10.043	10.041	9.764	9.767	9.765
	10.034 (2)	10.039 (2)	10.035 (2)	9.752 (2)	9.755 (2)	9.751 (2)
	7.246 (2)	8.302 (4)	9.050 (4)	7.035 (2)	8.065 (4)	8.785 (4)
	3.190	7.248 (2)	8.168 (2)	3.421	7.036 (2)	8.284 (2)
	0.249	.	.	0.153	.	.
	-2.242	.	.	-2.609	.	.
	.	.	.	.	.	.
	.	-2.236	-2.241	.	-2.606	-2.609

TABLE I.10.- Contributions to the total energy (in a.u.) for the $(GaAs)_m-(AlAs)_m$ SL in the (001) direction for different values of m.

	m = 1	m = 2	m = 3
E_I	-0.9727	-0.9611	-0.9611
E_H	0.2566	0.2571	0.2567
T	1.3223	1.3223	1.3229
E_{xc}	-1.1879	-1.1876	-1.1877
E_{bs}	-0.5817	-0.5693	-0.5682
E_e	-3.4961	-3.4961	-3.4961
E_T	-4.0778	-4.0654	-4.0643

applied our method to such a system because, together with the (001) SL above discussed, they contain the two common polar interfaces. Moreover, we will use the results here obtained to analyze, in the next section, the valence band discontinuities at semiconductor heterojunctions.

Figure I.9 shows the supercell used to calculate the properties of a $(GaAs)_3-(AlAs)_3$ (111) SL with the same approach that the above discussed for the (001) case. Again we start with the ions placed at the ideal bulk positions and minimize the energy as a function of the bond length, l. We get l = 2.403 Å, which is practically the average of l_{GaAs} = 2.401 Å and l_{AlAs} = 2.406 Å; previously obtained in section I.2.1 for perfect zincblende crystals. Once this bulk bond length has been determined, the interface ions are allowed to relax looking for a deeper minimum of the energy. In contrast with the (001) SL where a net relaxation was obtained, now the distance between Al and As interface planes increases in a o.5 %, but the distance between Ga and As interface planes decreases in the same amount. In other words, no
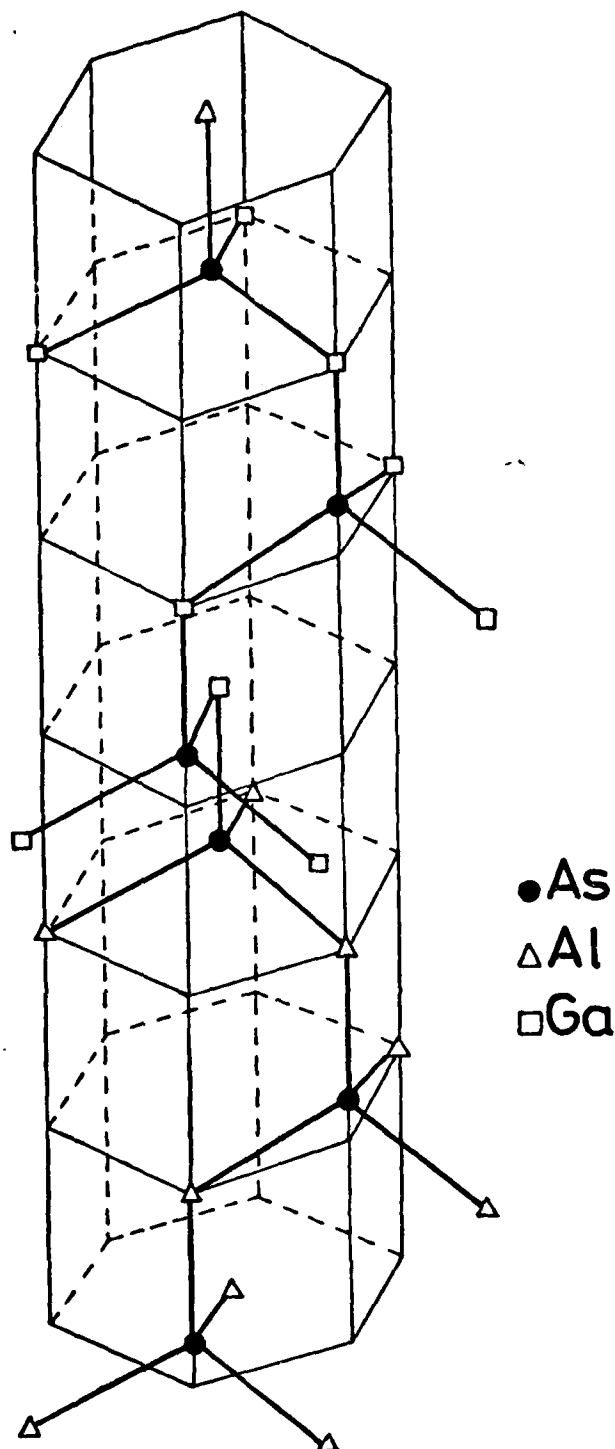
● As
△ Al
□ Ga

FIGURE I.9.- Supercell used in the calculation of the
structure of a $(GaAs)_3$-$(AlAs)_3$ SL oriented
along the (111) direction. Heavy lines
represent the bonds (eq.(I.8)) from which WF's
are built up.

relaxation appears at this interface where just the As plane
slightly moves towards .the Ga plane but the Al-Ga distance
does not change. In spite of this difference, our results for
the variational parameters are rather similar in both systems.
Again the only change at the (111) interface is that the
mixture parameter λ for Al-As bond significantly decreases
with respect to bulk values as shown in Table I.11. This
similitude implies that charge transfer and differences of
mean potentials appear in this (111) SL in the same way as in
the (001) one. So we have

$$\Delta \bar{V} = \bar{V}(GaAs) - \bar{V}(AlAs) = \Delta \bar{V}_i + \Delta \bar{V}_H + \Delta \bar{V}_{xc} =$$

$$= -0.022 + 0.029 + 0.001 \quad (in \ eV).$$

TABLE I.11.- Values of the mixture parameter λ (eq.(8)) for
bonds in the bulk and at the interface (GaAs)$_3$-
(AlAs)$_3$ SL in the (111) direction. λ_A is for the
combination in AlAs bonds and λ_G for Ga-As bonds.

	Bulk	Interface
λ (GaAs)$_3$-(AlAs)$_3$ (111)	$\lambda_A = 1.015$ $\lambda_G = 1.046$	$\lambda_A = 0.999$ $\lambda_G = 1.048$

The charge density that AlAs transfer to GaAs implies that
the mean value of V(z) at GaAs is 8 meV higher than the mean
value of V(z) at AlAs. Since a figure of V(z) or the average
transfer charge would be very similar to Figure I.6, we give
here a different picture of the same points by showing in
Figure I.10 the contour plots of the total charge density
around the interface.

All these results bring to the conclusion that (001)
and (111) SL's are very similar, the main difference being

FIGURE I.10.- Total charge density at the interface of a
(GaAs)$_3$-(AlAs)$_3$ SL oriented along the (111)
direction. Units are in electrons per ion.
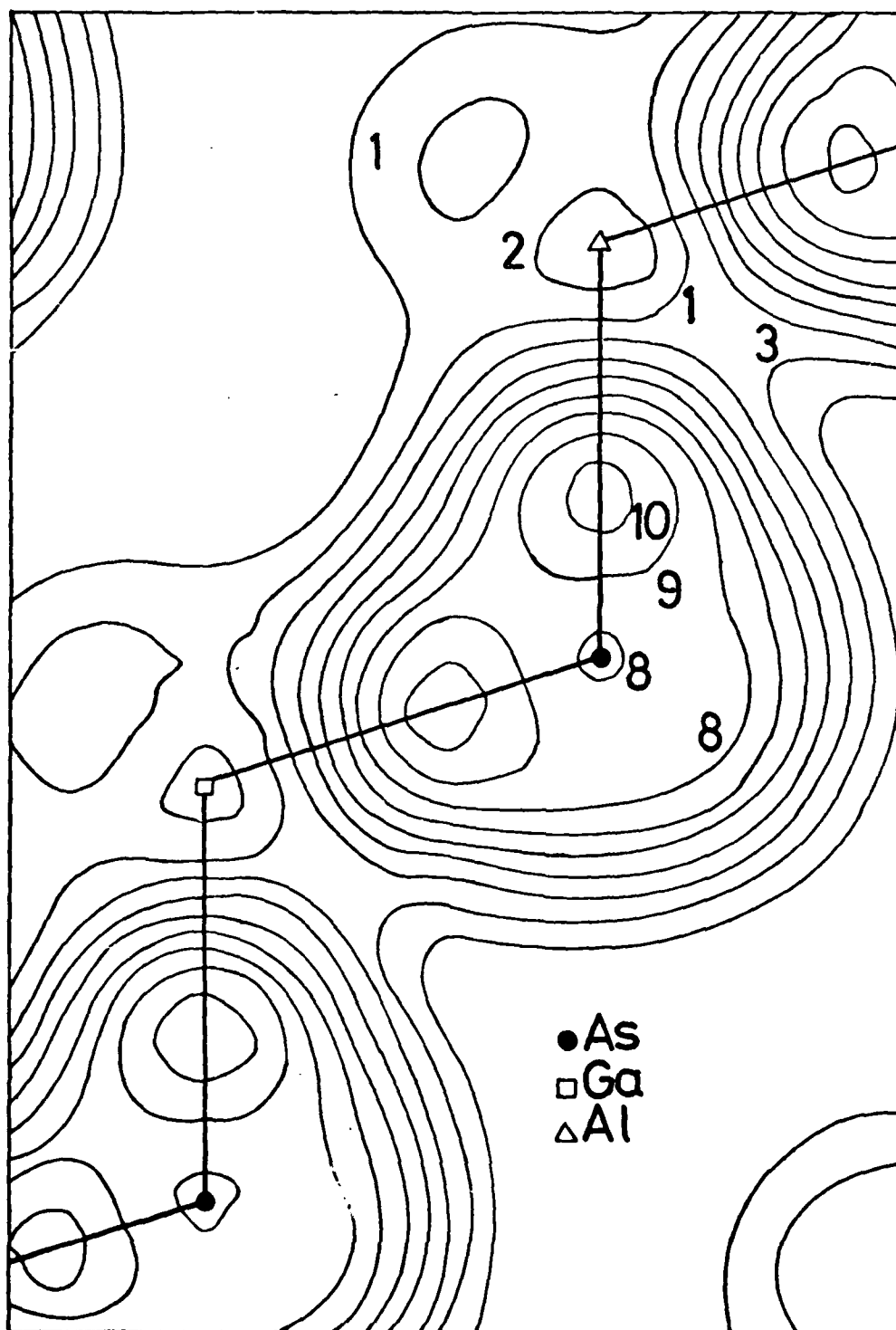
that the former shows ionic relaxation at the interface and the latter does not. One more difference appears when one analyzes the spectrum of this (111) SL given in Table I.12.

TABLE I.12.- Band edges at Γ of the valence band of perfect crystals and $(GaAs)_3-(AlAs)_3$ SL all of them in the (111) direction. Energies in eV are referred to the mean potential for each SL.

$(GaAs)_6-(AlAs)_0$	$(GaAs)_0-(AlAs)_6$	$(GaAs)_3-(AlAs)_3$
10.040(2)	9.760(2)	10.065(2)
10.036	9.751	9.927
9.665(2)	9.394(2)	9.643(2)
9.652(2)	9.393(2)	9.405(2)
.	.	.
.	.	.
.	.	.
-2.253	-2.623	-2.677

Now the upper state at Γ, placed 10.07 eV higher than the mean value of the SL potential, is doubly degenerated and is localized at the GaAs region. Since this type of localized states has been experimentally observed in thicker (001) SL, our result suggests that the transition from 3D to 2D behaviour appears before in (111) SL's than in (001) ones, where we have not obtained states localized in the GaAs region.

I.2.3. Discussion

We have used a self-consistent localized scheme in terms of WF's to analyze the structural and electronic properties of several GaAs-AlAs SL's grown in the (001) and (111)

directions. From the structural point of view, we have found that those SL's with polar interfaces differ each other in that the (001) ones present ionic relaxation while the (111) ones do not. Nevertheless, this difference is not very important because the relaxation around the As ions of the (001) interface just affects to the first Ga and Al planes on each side both increasing in a 2.5 % their distance to the anion. Such small relaxation has no significant effect on the electronic properties. In any case, this relaxation is a purely interface effect so that it seems quite natural to consider that the displacements here obtained can be valid for thicker SL and heterojunctions.

Since we work with a localized scheme the influence of an interface does not enter too much into the deep layers of each semiconductor. Therefore $(GaAs)_m - (AlAs)_m$ SL's, for both orientations, show bulk-like behaviour in the central layer of each semiconductor for m = 3. For instance, our results for these m = 3 cases allow to see how AlAs transfers a small amount of electronic charge to GaAs, so that a potential barrier between both semiconductors appears. At this point, it is very tempting to use this barrier Δ between mean potentials to estimate the shift of the electronic structure of GaAs with respect to AlAs for thicker SL's or even an heterojunction of semiinfinite semiconductors. The best magnitude to measure this shift is the difference ΔE_v between the top of the AlAs and GaAs valence bands, which requires the position of that level E_v for both bulk semiconductors. In order to be consistent with our approach, we have computed that level in a SL framework for $(GaAs)_6 (AlAs)_0$ and $(GaAs)_0 (AlAs)_6$ for both orientations. We have obtained

$$\Delta E_v^{(001)} = \Delta^{(001)} + E_v^{GaAs(001)} - E_v^{AlAs(001)} = 0.282 \text{ eV}$$

$$\Delta E_v^{(111)} = \Delta^{(111)} + E_v^{GaAs(111)} - E_v^{AlAs(111)} = 0.288 \text{ eV} \quad ,$$

which are very similar each other. The unique experimental information for this magnitude is obtained as a extrapolation for $x \to 0$ of this shift measured in GaAs-$Ga_x Al_{1-x}$ thick SL's

oriented along the (001) direction (Dingle et al.1975). The experimental result is $\Delta E_v = (0.15 \pm 0.03) E_g^\Gamma$, where E_g^Γ is the direct gap at the Γ point of the SL. In this work we do not concentrate on conduction bands which are required to know E_g^Γ, but it is straightforward to use the self-consistent Hamiltonian we have obtained to compute such magnitude. We have got $\Delta E_v = 0.135 \, E_g^\Gamma$ which compares fairly well with the above mentioned experimental result. This suggests the possibility of an analysis of thick SL or heterojunctions by using the information obtained for ultrathin SL.

In spite of the similarity of both (001) and (111) SL's with m = 3, the electronic spectrum shows a significant difference. In the (111) SL the upper valence state is spatially localized on the GaAs region as it has been observed experimentally for thicker SL's. However, in the (001) SL's such localization does not exist in our results.


I.3. ELECTRONIC CONDUCTION BANDS

I.3.1. Simple model

Once we have analyzed in detail the VB structure of narrow SL's, we pay some attention to the conduction band (CB) structure. We concentrate on $(GaAs)_4$-$(AlAs)_4$ SL's along the (001) direction because they have been studied experimentally (Barker Jr.et al.1978, Merlin et al.1980, Colvard et al.1980). Since the analysis of the CB is rather more complicated than the one of the VB, we use a simple Hamiltonian which can be justified from the self-consistent calculations discussed above.

We use a tight-binding model (Schulman and McGill 1979) with four orbitals per atom. The tight-binding parameters for perfect semiconductors are fitted to bulk band structures (Osbourn and Smith 1979, Schulman and McGill 1979). So the tight-binding matrix for the superlattice can be straight-forwardly obtained. Its form is shown in Figure I.11. It is organized in 8x8 blocks representing the integrals between

FIGURE I.11.- Superlattice tight-binding matrix. Each block represents an 8x8 submatrix. The upper right-hand corner block, β, links AlAs and GaAs slabs. The matrix is organized in such a way that each block corresponds to matrix elements between orbitals centered on atoms in the same (A and a) or adjacent (B, b or β) SL layers.
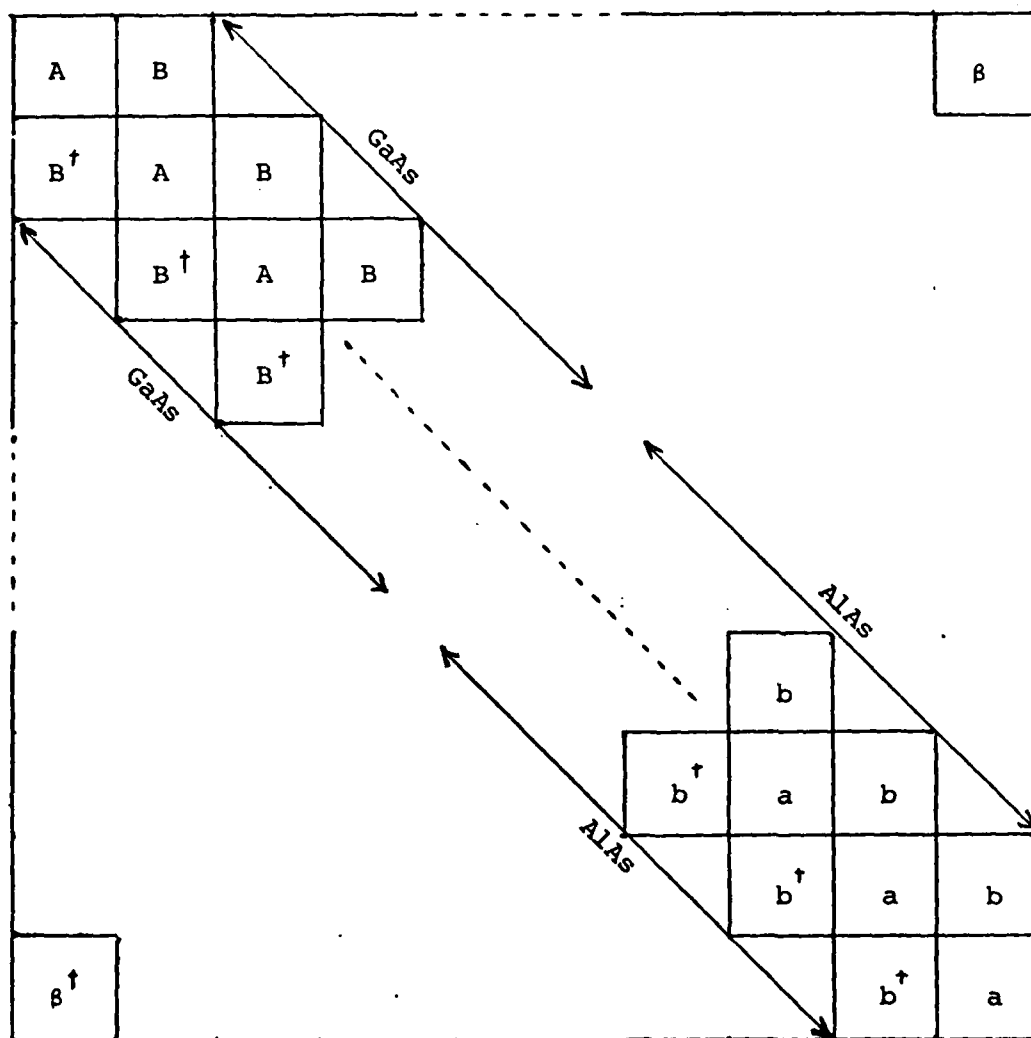
atomic orbitals. Each layer contains a single anion and cation per unit cell. We just retain interaction up to second neighbours so that there are only two types of blocks. The corner blocks contain the integrals between adjacent layers, where each layer is in an adjacent slab. These blocks are the typical ones connected with the SL and they contain the phase factor $\exp(ik_z d)$, where d is the slab width and k_z is the component of the k vector perpendicular to the interface. In this way the total size of the matrix is in our case $16m \times 16m = 64 \times 64$.

The GaAs and AlAs parts of the SL share common As ions at the interface. Therefore, there is no problem in determining the matrix elements for first-neighbours. They are taken from the bulk values. However, the bulk fitting does not provide parameters for second-neighbours at this position. Instead, a simple average of As to As, Al to Al and Ga to Ga parameters has been used.

The direct diagonalization of this matrix gives us the whole band structure we are interested in.

I.3.2. Results

With this model we have computed the band structure along the $\vec{k}$-space direction perpendicular to the interfaces in order to estimate the effective masses of the SL states. Table I.13 shows the energies for different values of $k = 2\pi/d(0,0,k_z)$ obtained with the tight-binding parameters given by Osbourn and Smith (1979). All the SL states given in this table have their eigenfunctions located at the GaAs spatial region, so that, as is well known, this is a SL of type I, i.e. where electrons and holes are in the same region. From these results we can estimate the effective masses (at Γ) of these bonds. We get for the electron, heavy hole and light hole, $m_e^* = 0.69$, $m_{hh}^* = 0.43$ and $m_{lh}^* = 0.19$, respectively. They are rather different from the ones given by a Kronig-Penney model: $m_e^* = 0.073$, $m_{hh}^* = 0.513$ and $m_{lh}^* = 0.08$, which have been used to analyze the experiments of light-scattering (Colvard et al.1980). However, the most

TABLE I.13.- Eigenvalues (in eV) of the SL states in a $(GaAs)_4-(AlAs)_4$ SL along the (001) direction.

	$(4a/\pi)k_z$			
	0	0.4	0.6	1
CB	2.1942	2.1931	2.1921	2.1910
	1.9408	1.9578	1.9735	1.9917
VB	0.00264	-0.02484	-0.05764	-0.12881
	0.00260	-0.02488	-0.05764	-0.12885
	-0.00096	-0.06335	-0.13735	-0.20633

important result is that we get $m^* = 10.6$ for the effective
mass of the second conduction band. The reason is that this
very flat band comes from the lowest CB at X in GaAs. This
is due to the folding of the Brillouin zone. Since that
state has a very high longitudinal mass in perfect GaAs, this
fact appears, and even is increased, for the second
conduction band of the SL. We think that this result can be
of great significance for resonance phenomena as the ones
appearing at the Raman scattering experiment discussed by
Colvard et al.(1980).

CHAPTER II. METAL-SEMICONDUCTOR JUNCTIONS

II.1. INTRODUCTION

The mechanism of Schottky-barrier formation has been the subject of many different interpretations (Rhoderick 1978). In the last few years, new experimental information has been obtained which points to the effect of the metal-semiconductor reactivity on the barrier formation (Brillson 1978, Andrews and Phillips 1975, Ottaviani et al.1980, Williams et al.1978, Brillson et al.1981). In particular, the abruptness of the junction interface seems to be a function of the metal-semiconductor bonding, with the consequent effect on the barrier height (Brillson et al. 1981). Very recent experimental evidence has shown that metal-semiconductor interdiffusion is by no means a rule and that some structural effects, not completely understood, may inhibit interdiffusion, allowing the existence of well-defined abrupt interfaces. Silver on Si and InP (McKinley et al.1979, Williams et al.1977), as well as some silicides on Si (Ho et al.1979), are well-known cases of abrupt junctions.

Other experiments with etched interfaces (Montgomery et al.1979, Spicer et al.1980, Williams 1981, Mottram et al. 1979) show the dependence of the height barrier on the kind of chemical compound and interlayer formed at the interface. These and previous experiments point to the importance of a few layers of the interface on the barrier formation.

This experimental evidence suggests that metal-semiconductor junctions can be classified into three main groups: (i) Abrupt interfaces, for which a rather ideal junction is formed with a well defined separation between the structures of the metal and the semiconductor; (ii) etched interfaces, for which a reactant, say H, O, Cl is left between the metal and the semiconductor; and (iii) reactive interfaces, for which the metal and the semiconductor interdiffuse and/or form a new chemical compound at the interface.

All this rich experimental information has proved a formidable challenge to theoreticians. Even abrupt interfaces are far from a complete understanding, although they have received, due to obvious reasons of simplicity, a greater attention.

Primitive theories have analyzed the Schottky-barrier formation by means of a thermodynamic argument (Schottky 1942) and have included an appropriate density of states at the interface (Bardeen 1947, Heine 1965). Leaving apart other many-body approaches (Inkson 1973, Tejedor et al.1977), we mention two recent models advanced by Spicer and Froeouff, respectively. The defect model (Spicer et al.1980, Williams 1981) seems to be particularly appropriate for metals on cleaved (110)-surfaces of III-V semiconductors, although it does not seem applicable to covalent semiconductors. Froeouff and Woodall (1981) have advanced a different model by a combination of a Schottky model and the formation of clusters at the interface.

At a different level of sophistication, we have the work of Cohen and coworkers (1977), where a very elaborate self-consistent calculation of an abrupt Al-Si junction has been given, within a pseudopotential theory. Unluckily, this line has not been pursued further and no systematic analysis of the height barrier has been given within this framework as a function of different metals and/or interlayers. This lack of systematic analysis for the ideal (abrupt) interface within a selfconsistent approach is the most unfortunate, since this prevents comparing -even for the most simple model (abrupt interfaces)- theory and experiment, a comparison which could allow getting a better understanding of the specific effects associated to interdiffusion and reactivity.

Quite recently, we have used a simple pseudopotential model (Louis and Flores 1981) to explain the main properties of abrupt and etched interfaces. In this approach, the crucial quantity is the amount of charge located in the semiconductor surface states reacting with the etching agent. The selfconsistent redistribution of this charge is analyzed as a function of the interface conditions. The main conclusions

of this analysis are the following: (i) For clean covalent interfaces,the junction behaviour turns out to be near the Bardeen limit; (ii) for etched covalent interfaces, the surface Fermi level may shift to higher (or lower) energies for electronegative (electropositive) reactants.

In this Report, we have further analyzed clean and etched abrupt Si-junctions by means of a realistic self-consistent calculation based on a tight-binding model. The purpose of this calculation is to obtain the barrier height and the change in the semiconductor surface Fermi level due to the barrier formation. As mentioned above, we can expect that, in this barrier formation, the main effects come from the interlayer and a few layers of the interface. We think that tight-binding models are very well suited to analyzing these local effects. In §II.2.1 and II.2.2 we give our method and in §II.2.3 we present our results and give the discussion.

On the other hand, in §II.3 we analyze non-abrupt junctions for III-V semiconductors and discuss the conditions under which the metal and the semiconductor interdiffuse.

II.2. CLEAN AND ETCHED METAL-SI JUNCTIONS

II.2.1. The model

We describe both the semiconductor and the metal electronic structures by means of a tight-binding method. For Si, we use sp^3-hybrids in each atom, and include interaction parameters extending up to second neighbours. This is a standard procedure; details about the parameters used in the actual calculation are given below (Chadi and Cohen 1975, Pandey and Phillips 1976, Menéndez and Vergés 1981). As regards the metal, we use two orbitals in each atom trying to simulate a broad and a narrow band associated with a s- and a d-band, respectively (Harrison 1980). This model is only a rough approximation to the metal structure but, as will be discussed below, the barrier formation is very little

dependent on most of the details of the metal density of
states; in other words, this two-orbital approximation to the
electronic metal structure (a noble or a transition metal)
turns out to be sufficient for our purposes.

The crystallographic structure of the clean interface
may be rather complicated. Even for abrupt interfaces, the
metal atoms do not exactly match the Si-structure. For
instance, for Ag on Si (McKinley et al.1979), Ag-atoms form
a monolayer with a three-fold symmetry having a lateral
separation roughly corresponding to that of the Si-Si bond.
A complete calculation of this structure would be rather
cumbersome. However, since the barrier formation seems to be
dependent only on very general properties of the metal
density of states (see below), we propose to calculate the
metal-semiconductor junction by assuming the metal atoms to
form a (111)-f.c.c. structure matching the (111)-Si face. We
have chosen that structure having the lattice parameter, a,
closer to the actual ones of most noble and transition
metals: this yields a = 3.12 Å (compare with 3.52 Å for Ni
and 4.09 Å for Ag). Note that with this parameter there are
three metal atoms in the surface unit cell defined by the Si
structure. It is worth remarking that although the lattice
parameter is different from the actual value for any metal,
the interaction parameters defining the s- and d-bands have
been chosen (see below) to reproduce approximately the
electron density of states of that metal forming the junction.

On the other hand, we assume to have at the interface
the same interaction parameters for the metal and the semi-
conductor as were chosen in the bulk. The clean junction is
formed by introducing some interaction parameters between
the outermost Si-atom and the metal atom sitting just on top ·
of it; specifically, we assume to have definite interactions
between the dangling-bond Si-hybrid and the two metal
orbitals (see below).

For an etched junction, we introduce an interlayer of
H between the metal and the semiconductor with one ad-atom
in the surface unit cell. For H we use a s-orbital and
introduce definite interactions with the last layers of the

metal and the semiconductor (see below). The dependence of
the interface properties on the electronegativity of the
atom forming the interlayer (say, Cs or Cl instead of H) has
been analyzed by a proper modification of the atomic
parameters.

Let us now turn to discuss how to get selfconsistency
at both the clean and etched junctions. To this end, it is
convenient to analyze in successive steps the following cases:
clean metal surfaces, clean semiconductor surfaces, metal-
metal surfaces, metal-semiconductor junctions and metal-
interlayer-semiconductor interfaces.

II.2.1.1. Clean metal surfaces

In this case, we assume to have until the surface the
same interaction parameters between hybrids defining the
Hamiltonian in the bulk. However, due to the surface
perturbation, it is necessary to introduce a diagonal
perturbation in each layer in order to get selfconsistency
(Desjonqueres and Cyrot-Lackmann 1975). When these diagonal
perturbations are taken zero, it appears in the metal a lack
of charge neutrality which is practically localized in the
last surface layer; then, selfconsistency -which is equivalent
in this case to charge neutrality- can be achieved by a
proper switching on of a diagonal perturbation in the last
surface layer. The effect of this perturbation in successive
layers is negligible in such a way that, practically, they
keep their neutrality with independence of the surface
perturbation.

II.2.1.2. Clean semiconductor surfaces

Here, we again consider the crystal extending up to a
surface, with the same interaction parameters as in the bulk,
but with diagonal perturbations switched on, in principle,
in each layer to get selfconsistency. Let us consider a
(111)-covalent face. For this surface, Kleinman (1975) has
shown that the surface band is half-occupied; with this
condition satisfied, there is complete charge neutrality in

the crystal, although there might be no local neutrality in
different layers. This local neutrality can be achieved by
introducing appropriate diagonal perturbations in each
layer as was the case for the metal. In similarity with this
case, a diagonal perturbation in the last surface layer can
be adjusted to give neutrality in the same layer, and this
gives automatically -due to the complete neutrality of the
crystal- neutrality, in practical terms, in the second and
further layers (Djafari-Rouhani et al.1979). It is of
interest to remark that the condition of local neutrality
for the last surface layer is practically equivalent to the
following condition: charge neutrality in the first sublayer.
This can be understood in the following way: for a semi-
conductor, the surface perturbation produces an important
transfer of charge between the last two layers and leaves
practically unperturbed the rest of the crystal; then, with
a proper adjustment of a local perturbation at the last layer,
this transfer of charge can be reversed and local neutrality
can be obtained. From a different point of view, this
transfer of charge is obtained by shifting the surface band
energy and moving the surface Fermi energy.

II.2.1.3. *Metal-metal interface*

For this case we can also assume to have localized
diagonal perturbations in the last layers of both metals. On
the other hand, a transfer of charge between these two
layers must appear in order to create an electric dipole
which equalizes the Fermi levels of both systems (other
layers keep their neutrality). Then, selfconsistency can be
achieved by adjusting these charges (of opposite signs) to
the values determined by the difference between the Fermi
levels of both metals, by means of two perturbations
localized at the two last layers.

II.2.1.4. *Metal-semiconductor selfconsistency*

We can now discuss how to get selfconsistency at the
clean metal-semiconductor junction. In similarity with the

metal-metal interface, we can expect to have diagonal perturbations and a transfer of charge at the two last layers of both crystals; at variance with the metal-metal interface, these charges, however, are not determined by the condition of equalization of both Fermi levels, since the metal Fermi level can be freely moved across the semiconductor gap. Accordingly, in comparison with the previous case (§II.2.1.3), we have a new freedom in the problem: the relative position of both bulk bands. This freedom -due to the existence of the semiconductor gap- is compensated by a characteristic of the same semiconductor surface: the strong coupling between the last two layers of the crystal (see §II.2.1.2). We shall immediately see how this characteristic allows us to introduce a new condition which completely determine our problem.

According to this discussion, we have three parameters which have to be determined to achieve selfconsistency at the metal-semiconductor interface: the two diagonal perturbations at the last layers of the metal and the semiconductor, and the induced dipole, D, between both crystals. These parameters are determined by the following conditions: (i) the first one is given by the assumption that the interface transfer of charge must be localized in the two last layers; this is a condition which is practically satisfied for the metal (see §II.2.1.1). For the semiconductor, however, the first sublayer is strongly connected with the surface layer. Accordingly, the condition of localization of the transfer of charge to the surface layers give the following equation:

$$\delta n_{sc}^{(1)} = 0 \ , \tag{II.1}$$

which expresses a condition of charge neutrality at the first semiconductor sublayer.

(ii) The second condition is given by the whole charge neutrality. This yields:

$$\delta n_{sc}^{(0)} + \delta n_{M}^{(0)} = 0 \ , \tag{II.2}$$

where superindex (0) stands for the surface layer.

(iii) Finally, the transfer of charge between the metal and the semiconductor, measured by $\delta n_M^{(0)} = -\delta n_{sc}^{(0)}$, give the induced dipole, D, which is proportional to $\delta n_{sc}^{(0)}$ and to the distance, d, between the metal and the semiconductor surface layers:

$$D = \alpha d \delta n_{sc}^{(0)} \quad . \qquad (II.3)$$

Eqs.(II.1), (II.2) and (II.3) give the three conditions determining the three parameters $V_{sc}^{(0)}$, $V_M^{(0)}$ (the two diagonal perturbations at both surface layers) and D. Eq.(II.1) is the new condition associated to the semiconductor characteristic commented on above. (For the metal-metal interface, eq.(II.1) disappears while D is given by the difference between both Fermi levels). It is of interest to note that eq.(II.3) gives, in any case, a very small value for $\delta n_{sc}^{(0)}$, since for a distance of, say, d = 2.69 Å (Ag-Si case) and $\delta n_{sc}^{(0)} = 1$ we obtain D = 37.9 eV, a very high value. Then, in a first approximation we can substitute eq.(II.3) by

$$\delta n_{sc}^{(0)} = 0 \quad . \qquad (II.4)$$

We have now in this approximation the following three conditions:

$$\delta n_{sc}^{(0)} = \delta n_{sc}^{(1)} = \delta n_M^{(0)} = 0 \quad ; \qquad (II.5)$$

let us call $\bar{V}_{sc}^0$, $\bar{V}_M^0$ and $\bar{D}$ to the values of the three parameters $V_{sc}^{(0)}$, $V_M^{(0)}$ and D, as obtained from conditions (II.5). This solution gives a barrier height, $\bar{\phi}_{bn}$, and a Fermi level in the semiconductor gap defining the so-called charge neutrality level (Rhoderick 1978, Tejedor et al.1977).

The general solution for the conditions given by eqs. (II.1), (II.2) and (II.3) is close to the one obtained with eq.(II.5), and it can be obtained from the last one by a linear perturbation of the parameters $\bar{V}_{sc}^{(0)}$, $\bar{V}_M^{(0)}$ and $\bar{D}$. The idea is to obtain the linear modifications in the charges

$\delta n_{sc}^{(0)}$, $\delta n_{sc}^{(1)}$ and $\delta n_{M}^{(0)}$ as introduced by small changes in $\bar{v}_{sc}^{(0)}$, $\bar{v}_{M}^{(0)}$ and $\bar{D}$. Thus, we write:

$$\delta n^{(i)} = \frac{\delta n^{(i)}}{\delta \bar{v}_{sc}^{(0)}} \delta V_{sc}^{(0)} + \frac{\delta n^{(i)}}{\delta \bar{V}_{M}^{(0)}} \delta V_{M}^{(0)} + \frac{\delta n^{(i)}}{\delta \bar{D}} \delta D \quad , \qquad (II.6)$$

where $\delta n^{(i)}$ stands for $\delta n_{sc}^{(0)}$, $\delta n_{sc}^{(1)}$ and $\delta n_{M}^{(0)}$, and the coefficients $\delta n^{(i)}/\delta V_{sc}^{(0)}$, $\delta n^{(i)}/\delta V_{M}^{(0)}$ and $\delta n^{(i)}/\delta D$ are obtained by small changes of $\bar{v}_{sc}^{(0)}$, $\bar{v}_{M}^{(0)}$ and $\delta \bar{D}$ in the solution obtained with conditions (II.5). It is now an easy matter to obtain $\delta V_{sc}^{(0)}$, $\delta V_{M}^{(0)}$ and D by imposing the conditions given by eqs.(II.1), (II.2) and (II.3). This procedure yields the following equations:

$$\frac{\delta n_{sc}^{(1)}}{\delta \bar{v}_{sc}^{(0)}} \delta V_{sc}^{(0)} + \frac{\delta n_{sc}^{(1)}}{\delta \bar{v}_{M}^{(0)}} + \frac{\delta n_{sc}^{(1)}}{\delta \bar{D}} \delta D = 0 \qquad (II.7a)$$

$$\frac{\delta n_{sc}^{(0)}}{\delta \bar{v}_{sc}^{(0)}} \delta V_{sc}^{(0)} + \frac{\delta n_{sc}^{(0)}}{\delta \bar{v}_{M}^{(0)}} \delta V_{M}^{(0)} + \frac{\delta n_{sc}^{(0)}}{\delta \bar{D}} \delta D \equiv \delta n_{sc}^{(0)} \approx \frac{(D^0 + \delta D)}{\alpha d} \quad (II.7b)$$

$$\frac{\delta n_{M}^{(0)}}{\delta \bar{v}_{sc}^{(0)}} \delta V_{sc}^{(0)} + \frac{\delta n_{M}^{(0)}}{\delta \bar{v}_{M}^{(0)}} \delta V_{M}^{(0)} + \frac{\delta n_{M}^{(0)}}{\delta \bar{D}} \delta D \equiv \delta n_{M}^{(0)} = -\delta n_{sc}^{(0)} \quad .(II.7c)$$

In our calculations (see below) we have found that

$$\frac{\delta n_{sc}^{(1)}}{\delta \bar{v}_{M}^{(0)}} \approx \frac{\delta n_{sc}^{(0)}}{\delta \bar{v}_{M}^{(0)}} \approx 0 \quad ,$$

in such a way that eqs.(II.7a) and (II.7b) can be now used to obtain $\delta V_{sc}^{(0)}$ and δD:

$$\frac{\delta n_{sc}^{(1)}}{\delta \bar{v}_{sc}^{(0)}} \delta V_{sc}^{(0)} + \frac{\delta n_{sc}^{(1)}}{\delta \bar{D}} \delta D = 0 \quad . \qquad (II.8a)$$

$$\frac{\delta n_{sc}^{(0)}}{\delta \bar{V}_{sc}^{(0)}} \delta V_{sc}^{(0)} + \frac{\delta n_{sc}^{(0)}}{\delta \bar{D}} \delta D \equiv \frac{\bar{D} + \delta D}{\alpha d} \quad . \tag{II.8b}$$

Note that for $\bar{D}/\alpha d \to 0$, we recover the solution given above: $\delta V_{sc}^{(0)} = \delta D = 0$. In general, these equations give δD, the change in the height barrier as a function of $\bar{D}$ and other parameters. Note that $\bar{D} = \Phi_M - \chi - \bar{\Phi}_{bn}$, where Φ_M is the metal workfunction and χ the semiconductor affinity. Thus, we write:

$$\delta D = \frac{\bar{D}/\alpha d}{\left[-\frac{\delta n_{sc}^{(0)}}{\delta \bar{V}_{sc}^{(0)}} \frac{\delta n_{sc}^{(1)}/\delta \bar{D}}{\delta n_{sc}^{(1)}/\delta \bar{V}_{sc}^{(0)}} + \frac{\delta n_{sc}^{(0)}}{\delta \bar{D}} - \frac{1}{\alpha d} \right]} \equiv S \left[\Phi_M - \chi - \bar{\Phi}_{bn} \right]. \tag{II.9}$$

Apparently, this equation defines a linear relationship between δD, the change in the barrier height, and $(\Phi_M - \chi)$; note, however, that S is, in general, a function of the interface properties as defined by the metal and semiconductor densities of states. Once S is obtained from the actual properties of the interface, eq.(9) gives the change in the barrier height with respect to the charge neutrality level and the final interface Fermi energy.

II.2.1.5. *Metal-interlayer-semiconductor selfconsistency*

Let us now discuss how to get selfconsistency at the metal-interlayer-semiconductor junctions. Comparing with the metal-semiconductor interface we have ı new freedom in the junction: the one associated with u.e interlayer. Thus, we have to determine selfconsistently its charge, n_H, and its mean level, E_H.

Accordingly, we have in this junction four parameters to be determined selfconsistently: the two diagonal perturbations at the last layers of the metal and the semi-conductor, $V_M^{(0)}$ and $V_{sc}^{(0)}$, the induced dipole, D, between both crystals, and the mean atomic level for the interlayer, E_H. The conditions determining these parameters are the following: (i) as in the metal-semiconductor junction, we

impose charge neutrality at the first semiconductor sublayer:

$$\delta n_{sc}^{(1)} = 0 \quad .$$ (II.10)

(ii) The condition of whole charge neutrality yields the following equation:

$$\delta n_{sc}^{(0)} + \delta n_H + \delta n_M^{(0)} = 0 \quad .$$ (II.11)

(iii) On the other hand, the induced dipole, D, is determined by δn_H and $\delta n_{sc}^{(0)}$, according to the equation:

$$D = \alpha\{d\delta n_{sc}^{(0)} + d'\delta n_H\} \quad ,$$ (II.12)

where d (d') is the distance between the semiconductor surface layer (interlayer) and the metal surface layer (compare eqs. (II.12) and (II.3).

(iv) Finally, we need a selfconsistent equation for the mean atomic level, E_H. This can be obtained by using a Hartree model; within this approximation, the mean atomic level depends on the electrostatic potential induced in the interlayer and on the electrostatic repulsion between electrons of different spins inside the atom. Thus:

$$E_H = E_H^{(0)} + \alpha(d-d')\delta n_{sc}^{(0)} + \frac{1}{2} U\delta n_H \quad .$$ (II.13)

In this equation, $E_H^{(0)}$ is the mean atomic level for the isolated atom, $\alpha(d-d')\delta n_{sc}^{(0)}$ is the electrostatic potential induced at the interlayer as measured from the semiconductor, and $\frac{1}{2} U\delta n_H$ gives the mean intraatomic repulsion $(\delta n_H^{\uparrow} = \frac{1}{2} U\delta n_H)$. Note that a reasonable approximation to $E_H^{(0)}$ is to take for it the mean value of the ionization and affinity levels for the ad-atom.

Eqs.(II.10), (II.11), (II.12) and (II.13) give the four conditions which determine the four parameters $V_M^{(0)}$, $V_{sc}^{(0)}$, D and V_H. It is worth noting that, in similarity with the metal-semiconductor interface, condition (II.12) can be substituted by the following equation:

$$\delta D = S' \left[\phi_M - \chi - \bar{\phi}'_{bn} \right] \quad , \tag{II.15}$$

where, as discussed above, $\bar{\phi}'_{bn}$ is the charge neutrality level of the etched junction and S' a parameter depending on the interface properties.

II.2.2. Method of calculation

In order to obtain the charge and the density of states associated to a given layer, we have calculated the Green function, $\bar{\bar{G}}$, defined by the following equation:

$$(\omega - \bar{\bar{H}}) \cdot \bar{\bar{G}} = \bar{\bar{I}} \quad , \tag{II.16}$$

where ω is the energy, $\bar{\bar{H}}$ the Hamiltonian written in a tight-binding basis, and $\bar{\bar{I}}$ the unit tensor. In our representation, we write $\bar{\bar{H}}$ and $\bar{\bar{G}}$ in a basis defined by a superlayer number, m, an orbital index, α, and a momentum, $\vec{\kappa}$, parallel to the surface and belonging to the first Brillouin zone of our two-dimensional surface lattice. Let us call a the number of independent orbitals in each superlayer.

In this representation, a matrix element of, say, the Green function, $\bar{\bar{G}}$, takes the form $G_{\alpha m, \alpha' m'}(\vec{\kappa})$. In the following, instead of using this notation, we shall write $\underset{\approx}{G}_{m,m'}(\vec{\kappa})$ or $\underset{\approx}{G}_{m,m'}$ ($\vec{\kappa}$ understated), in such a way that an element (α, α') of the matrix $\underset{\approx}{G}_{m,m'}(\vec{\kappa})$ is $G_{\alpha m, \alpha' m'}(\vec{\kappa})$. Moreover, in order to simplify the discussion, we consider the case of a clean semiconductor surface. Later on, we shall see how to analyze an interface.

For a clean semiconductor surface, we write equation (II.16) in the tight-binding representation by taking the elements $(\alpha m, \alpha' o)$, where o stands for the surface superlayer; this yields:

$$\omega \underset{\approx}{G}_{m,o} - \sum_{m'} \underset{\approx}{H}_{m,m'} \underset{\approx}{G}_{m',o} = \underset{\approx}{\delta}_{m,o} \quad . \tag{II.17}$$

Let us now assume that the interaction between orbitals extend up to second neighbour superlayers; with this particular

case we try to show how to generalize the procedure to long
distance interactions. Then, eq.(II.17) can be explicitly
written as follows:

$$\left[\omega - \underset{\approx}{H}_{0,0}\right] \cdot \underset{\approx}{G}_{0,0} - \underset{\approx}{H}_{0,1} \cdot \underset{\approx}{G}_{1,0} - \underset{\approx}{H}_{0,2} \cdot \underset{\approx}{G}_{2,0} = \underset{\approx}{I} \qquad \text{(II.18a)}$$

$$-\underset{\approx}{H}_{1,0} \cdot \underset{\approx}{G}_{0,0} + \left[\omega - \underset{\approx}{H}_{1,1}\right] \cdot \underset{\approx}{G}_{1,0} - \underset{\approx}{H}_{1,2} \cdot \underset{\approx}{G}_{2,0} - \underset{\approx}{H}_{1,3} \cdot \underset{\approx}{G}_{3,0} = 0 \qquad \text{(II.18b)}$$

$$-\underset{\approx}{H}_{2,0} \cdot \underset{\approx}{G}_{0,0} - \underset{\approx}{H}_{2,1} \cdot \underset{\approx}{G}_{1,0} + \left[\omega - \underset{\approx}{H}_{2,2}\right] \cdot \underset{\approx}{G}_{2,0} - \underset{\approx}{H}_{2,3} \cdot \underset{\approx}{G}_{3,0} -$$

$$- \underset{\approx}{H}_{2,4} \cdot \underset{\approx}{G}_{4,0} = 0 \qquad \text{(II.18c)}$$

$$\vdots \qquad\qquad \vdots$$

$$-\underset{\approx}{H}_{m,m-2} \cdot \underset{\approx}{G}_{m-2,0} - \underset{\approx}{H}_{m,m-1} \cdot \underset{\approx}{G}_{m-1,0} + \left[\omega - \underset{\approx}{H}_{m,m}\right] \cdot \underset{\approx}{G}_{m,0} -$$

$$- \underset{\approx}{H}_{m,m+1} \cdot \underset{\approx}{G}_{m+1,0} - \underset{\approx}{H}_{m,m+2} \cdot \underset{\approx}{G}_{m+2,0} = 0 \ , \qquad \text{(II.18d)}$$

where the different interactions between superlayers m and
m' are given by $\underset{\approx}{H}_{m,m'}$ and use has been made of the fact that
interactions extend only up to second neighbours superlayers.
It is convenient to remark at this point that a superlayer,
in the language used here, may be built up by several
crystal layers; the number of crystal layers forming a
layer is given by that number allowing us to write eq.(II.16),
well inside the bulk (Lee and Joannopoulos 1981), in the
form given by eq.(II.18d). For Si, a superlayer has two
crystal layers.

For an ideal structure,

$$\underset{\approx}{H}_{m,m'} = \underset{\approx}{H}(m-m') \qquad \text{(II.19a)}$$

and

$$\underset{\approx}{H}_{\alpha,\beta}(m-m') = \underset{\approx}{H}^{*}_{\beta,\alpha}(m'-m) \qquad . \qquad \text{(II.19b)}$$

For simplicity we limit our discussion to the case in which for the third superlayer (eq.(II.18c)) we recover the general equation (II.18d). (In our second neighbours approximation, this implies an ideal unrelaxed surface). A more general case can be readily obtained. For the case of an ideal unrelaxed surface, eq.(II.19a) can be used for all the matrix elements $H_{m,m'}$ appearing in eqs.(II.18).

In the literature, these equations have been solved by the transfer-matrix method (Falicov and Yndurain 1975, Louis and Yndurain 1977, Vergés 1978), by reducing them to a finite system by taking a slab (Pandey and Phillips 1976), or by other methods (Lee and Joannopoulos 1981). In our procedure, we have followed decimation techniques as applied in the renormalization group method (Goncalvez da Silva and Keiller 1981). The advantage of our procedure is its quick convergence and its saving of computer time.

It is now convenient to rewrite eqs.(II.18) in the following way:

$$
\begin{bmatrix} \omega - H(0) & -H(\bar{1}) \\ -H(1) & \omega - H(0) \end{bmatrix} \begin{bmatrix} G_{0,0} \\ G_{1,0} \end{bmatrix} + \begin{bmatrix} -H(\bar{2}) & 0 \\ -H(\bar{1}) & -H(\bar{2}) \end{bmatrix} \begin{bmatrix} G_{2,0} \\ G_{3,0} \end{bmatrix} = \begin{bmatrix} I \\ 0 \end{bmatrix} ,
$$

$$(II.20)$$

$$
\begin{bmatrix} -H(2) & -H(1) \\ 0 & -H(2) \end{bmatrix} \begin{bmatrix} G_{m-2,0} \\ G_{m-1,0} \end{bmatrix} + \begin{bmatrix} \omega - H(0) & -H(\bar{1}) \\ -H(1) & \omega - H(0) \end{bmatrix} \begin{bmatrix} G_m \\ G_{m+1} \end{bmatrix} +
$$

$$
\begin{bmatrix} -H(\bar{2}) & 0 \\ -H(\bar{1}) & -H(\bar{2}) \end{bmatrix} \begin{bmatrix} G_{m+2,0} \\ G_{m+3,0} \end{bmatrix} = 0
$$

$$(II.21)$$

m even, or equivalently, with an obvious notation:

$$
W \cdot G_0 + T_1 \cdot G_2 = \begin{bmatrix} I \\ 0 \end{bmatrix}
$$

$$(II.22a)$$

$$
T_2 \cdot G_{m-2} + W \cdot G_m + T_1 \cdot G_{m+2} = 0 .
$$

$$(II.22b)$$

In these equations, $0,2,4,...,$ are the numbers associated to the different *superlayers* formed by the superlayers $(0,1)$, $(2,3)$, $(4,5),...$ and so on. Note that the number of superlayers defined inside each *superlayer* is related to the order of the interaction (second order here). According to decimation techniques, we proceed in successive steps by eliminating the even Green functions associated to superlayers $2,6,10,...,$ in eqs.(II.22). Thus, in a first step we consider the following equations:

$$\underset{\sim}{\mathbf{T}}_2 \cdot \underset{\sim}{\mathcal{G}}_0 + \underset{\sim}{\mathbf{W}} \cdot \underset{\sim}{\mathcal{G}}_2 + \underset{\sim}{\mathbf{T}}_1 \cdot \underset{\sim}{\mathcal{G}}_4 = 0 \qquad\qquad \text{(II.23a)}$$

$$\underset{\sim}{\mathbf{T}}_2 \cdot \underset{\sim}{\mathcal{G}}_4 + \underset{\sim}{\mathbf{W}} \cdot \underset{\sim}{\mathcal{G}}_6 + \underset{\sim}{\mathbf{T}}_1 \cdot \underset{\sim}{\mathcal{G}}_8 = 0 \qquad\qquad \text{(II.23b)}$$

$$\underset{\sim}{\mathbf{T}}_2 \cdot \underset{\sim}{\mathcal{G}}_8 + \underset{\sim}{\mathbf{W}} \cdot \underset{\sim}{\mathcal{G}}_{10} + \underset{\sim}{\mathbf{T}}_1 \cdot \underset{\sim}{\mathcal{G}}_{12} = 0 \qquad\qquad \text{(II.23c)}$$

and write

$$\underset{\sim}{\mathcal{G}}_2 = -\underset{\sim}{\mathbf{W}}^{-1} \left[\underset{\sim}{\mathbf{T}}_2 \cdot \underset{\sim}{\mathcal{G}}_0 + \underset{\sim}{\mathbf{T}}_1 \cdot \underset{\sim}{\mathcal{G}}_4 \right] \qquad\qquad \text{(II.24a)}$$

$$\underset{\sim}{\mathcal{G}}_6 = -\underset{\sim}{\mathbf{W}}^{-1} \left[\underset{\sim}{\mathbf{T}}_2 \cdot \underset{\sim}{\mathcal{G}}_4 + \underset{\sim}{\mathbf{T}}_1 \cdot \underset{\sim}{\mathcal{G}}_8 \right] \qquad\qquad \text{(II.24b)}$$

$$\underset{\sim}{\mathcal{G}}_{10} = -\underset{\sim}{\mathbf{W}}^{-1} \left[\underset{\sim}{\mathbf{T}}_2 \cdot \underset{\sim}{\mathcal{G}}_8 + \underset{\sim}{\mathbf{T}}_1 \cdot \underset{\sim}{\mathcal{G}}_{12} \right] \;. \qquad\qquad \text{(II.24c)}$$

Now, these equations are used to eliminate $\underset{\sim}{\mathcal{G}}_2$, $\underset{\sim}{\mathcal{G}}_6$, $\underset{\sim}{\mathcal{G}}_{10},...$ from eqs.(II.22). This procedure yields

$$\left[\underset{\sim}{\mathbf{W}} - \underset{\sim}{\mathbf{T}}_1 \cdot \underset{\sim}{\mathbf{W}}^{-1} \cdot \underset{\sim}{\mathbf{T}}_2 \right] \cdot \underset{\sim}{\mathcal{G}}_0 - \left[\underset{\sim}{\mathbf{T}}_1 \cdot \underset{\sim}{\mathbf{W}}^{-1} \cdot \underset{\sim}{\mathbf{T}}_1 \right] \cdot \underset{\sim}{\mathcal{G}}_4 = \begin{bmatrix} \underset{\sim}{\mathbf{I}} \\ 0 \end{bmatrix} \qquad \text{(II.25a)}$$

$$-\left[\underset{\sim}{\mathbf{T}}_2 \cdot \underset{\sim}{\mathbf{W}}^{-1} \cdot \underset{\sim}{\mathbf{T}}_2 \right] \cdot \underset{\sim}{\mathcal{G}}_0 + \left[\underset{\sim}{\mathbf{W}} - \underset{\sim}{\mathbf{T}}_2 \cdot \underset{\sim}{\mathbf{W}}^{-1} \cdot \underset{\sim}{\mathbf{T}}_1 - \underset{\sim}{\mathbf{T}}_1 \cdot \underset{\sim}{\mathbf{W}}^{-1} \cdot \underset{\sim}{\mathbf{T}}_2 \right] \cdot \underset{\sim}{\mathcal{G}}_4 -$$

$$- \left[\underset{\sim}{\mathbf{T}}_1 \cdot \underset{\sim}{\mathbf{W}}^{-1} \cdot \underset{\sim}{\mathbf{T}}_1 \right] \cdot \underset{\sim}{\mathcal{G}}_8 = 0 \qquad\qquad \text{(II.25b)}$$

$$-\left[\underset{\sim}{\mathbf{T}}_2 \cdot \underset{\sim}{\mathbf{W}}^{-1} \cdot \underset{\sim}{\mathbf{T}}_2 \right] \cdot \underset{\sim}{\mathcal{G}}_4 + \left[\underset{\sim}{\mathbf{W}} - \underset{\sim}{\mathbf{T}}_2 \cdot \underset{\sim}{\mathbf{W}}^{-1} \cdot \underset{\sim}{\mathbf{T}}_1 - \underset{\sim}{\mathbf{T}}_1 \cdot \underset{\sim}{\mathbf{W}}^{-1} \cdot \underset{\sim}{\mathbf{T}}_2 \right] \cdot \underset{\sim}{\mathcal{G}}_8 -$$

$$- \left[\underset{\sim}{\mathbf{T}}_1 \cdot \underset{\sim}{\mathbf{W}}^{-1} \cdot \underset{\sim}{\mathbf{T}}_1 \right] \cdot \underset{\sim}{\mathcal{G}}_{12} = 0 \;. \qquad\qquad \text{(II.25c)}$$

These equations coincide with eqs.(II.22) by an appropriate renormalization of the different matrixes. Thus, with the following definitions:

$$\underset{\sim}{W}'_s = \underset{\sim}{W} - \underset{\sim}{\tau}_1 \cdot \underset{\sim}{W}^{-1} \cdot \underset{\sim}{\tau}_2 \tag{II.26a}$$

$$\underset{\sim}{W}'_b = \underset{\sim}{W} - \underset{\sim}{\tau}_1 \cdot \underset{\sim}{W}^{-1} \cdot \underset{\sim}{\tau}_2 - \underset{\sim}{\tau}_2 \cdot \underset{\sim}{W}^{-1} \cdot \underset{\sim}{\tau}_1 \tag{II.26b}$$

$$\underset{\sim}{\tau}'_1 = -\underset{\sim}{\tau}_1 \cdot \underset{\sim}{W}^{-1} \cdot \underset{\sim}{\tau}_1 \tag{II.26c}$$

$$\underset{\sim}{\tau}'_2 = -\underset{\sim}{\tau}_2 \cdot \underset{\sim}{W}^{-1} \cdot \underset{\sim}{\tau}_2 \tag{II.26d}$$

we recover formally eqs.(II.22) with new renormalized parameters. For instance, $\underset{\sim}{\tau}'_1$ and $\underset{\sim}{\tau}'_2$ measure the effective interaction between renormalized superlayers 0 and 4, 4 and 8, and so on, while $\left[\underset{\sim}{W} - \underset{\sim}{\tau}_1 \cdot \underset{\sim}{W}^{-1} \cdot \underset{\sim}{\tau}_2\right]$ can be defined as the effective matrix of $(\omega - \underset{\sim}{H})$ for layer 0 and $\left[\underset{\sim}{W} - \underset{\sim}{\tau}_1 \cdot \underset{\sim}{W}^{-1} \cdot \underset{\sim}{\tau}_2 - \underset{\sim}{\tau}_2 \cdot \underset{\sim}{W}^{-1} \cdot \underset{\sim}{\tau}_1\right]$ the same effective matrix for superlayers 4,8, ...

Now, the procedure can be iterated, and at any step, say p, we obtain the following matrixes as a function of the ones obtained in step (p-1):

$$\underset{\sim}{W}_s^{(p)} = \underset{\sim}{W}_s^{(p-1)} - \underset{\sim}{\tau}_1^{(p-1)} \cdot \left[\underset{\sim}{W}_b^{(p-1)}\right]^{-1} \cdot \underset{\sim}{\tau}_2^{(p-1)} \tag{II.27a}$$

$$\underset{\sim}{W}_b^{(p)} = \underset{\sim}{W}_b^{(p-1)} - \underset{\sim}{\tau}_1^{(p-1)} \cdot \left[\underset{\sim}{W}_b^{(p-1)}\right]^{-1} \cdot \underset{\sim}{\tau}_2^{(p-1)} -$$

$$- \underset{\sim}{\tau}_2^{(p-1)} \cdot \left[\underset{\sim}{W}_b^{(p-1)}\right]^{-1} \cdot \underset{\sim}{\tau}_1^{(p-1)} \tag{II.27b}$$

$$\underset{\sim}{\tau}_1^{(p)} = -\underset{\sim}{\tau}_1^{(p-1)} \cdot \left[\underset{\sim}{W}_b^{(p-1)}\right]^{-1} \cdot \underset{\sim}{\tau}_1^{(p-1)} \tag{II.27c}$$

$$\underset{\sim}{\tau}_2^{(p)} = -\underset{\sim}{\tau}_2^{(p-1)} \cdot \left[\underset{\sim}{W}_b^{(p-1)}\right]^{-1} \cdot \underset{\sim}{\tau}_2^{(p-1)} \quad . \tag{II.27d}$$

Note that for the second step, $\underset{\sim}{\tau}_1^{(2)}$ and $\underset{\sim}{\tau}_2^{(2)}$ give the effective interaction between renormalized superlayers 0 and 8, 8 and 16, and so on, while $\underset{\sim}{\tau}_1^{(3)}$ and $\underset{\sim}{\tau}_2^{(3)}$ measure the effective interaction for superlayers 0 and 16, 16 and 32,... In general, after p steps, $\underset{\sim}{\tau}_1^{(p)}$ and $\underset{\sim}{\tau}_2^{(p)}$ give the effective interaction between superlayers 0 and 2^{p+1}, having

renormalized out 2^p superlayers. This is the important point of the procedure followed in this paper, since the number of renormalized superlayers grows with an exponential power of the number of steps. On the other hand, we can expect both $\tau_1^{(p)}$ and $\tau_2^{(p)}$ to decrease, for any value of ω, with the increasing number of steps; this is a conclusion that can be reached on physical grounds by noting that the effective interaction between superlayers must be small when they are far apart. Let us assume that, after p_0 steps, $\tau_1^{(p_0)}$ and $\tau_2^{(p_0)}$ are negligible. Then, eqs.(II.25) reduce to:

$$W_s^{(p_0)} \cdot \mathcal{G}_0 = \begin{bmatrix} I \\ 0 \end{bmatrix} \qquad\qquad (II.28a)$$

$$W_b^{(p_0)} \cdot \mathcal{G}_{(2^{p_0}+1)} = 0 \quad . \qquad\qquad (II.28b)$$

It is obvious from eqs.(II.27) that when $\tau_1^{(p_0)}$ and $\tau_2^{(p_0)}$ are small enough, a new step produces no change on the values of $W_s^{(p_0)}$ and $W_b^{(p_0)}$; the physical meaning of this result is clear: the surface and bulk superlayers are practically decoupled. Then, $W_s^{(p_0)}$ and $W_b^{(p_0)}$ give the effective matrixes of $(\omega-H)$, for the surface and bulk superlayers, respectively.

In practical terms, $\tau_1^{(p)}$ and $\tau_2^{(p)}$ become small as a function of the chosen degree of accuracy for our effective Hamiltonians. Accordingly, we neglect $\tau_1^{(p_0)}$ and $\tau_2^{(p_0)}$ when, for step (p_0+1), the differences between the values of every term of $W_s^{(p_0)}$ (or $W_b^{(p_0)}$) and $W_s^{(p_0+1)}$ (or $W_b^{(p_0+1)}$) are smaller than a given number, for any frequency. This is equivalent to say that, to a given accuracy, a slab of 2^{p_0} superlayers is large enough to decouple both surfaces. Note that our results, after p_0 steps, are equivalent to the ones given by the matrix transfer method after 2^{p_0} steps.

$W_s^{(p_0)}$ and $W_b^{(p_0)}$ give the effective Hamiltonians for the isolated surface and bulk superlayers, respectively, and allows us to obtain, for instance, the density of states not only for the surface but for the bulk too. As

regards $\underset{\approx S}{W}{}^{(p_0)}$, this matrix gives for Si an effective Hamiltonian in a basis which includes not only the dangling-bond orbital, but the 8 orbitals associated to the last two layers.

A similar argument can be applied to obtain the same surface matrix for the metal. In this case, $\underset{\approx S}{W}$ is a (6x6) matrix, as corresponds to two orbitals per atom, three atoms in the surface unit cell, and a nearest neighbour interaction.

Once that $\underset{\approx S}{W}$ has been determined for both the metal and the semiconductor, we analyze the clean junction by introducing the corresponding hopping interaction; in this way, the clean interface is analyzed by inverting a 14x14 matrix. As regards the etched junction, we have one more atom in the surface unit cell, and thus we obtain for this case a 15x15 effective Hamiltonian.

From the point of view of the actual calculation it is worth commenting three points: (i) as is well-known, in all the matrix-transfer methods a finite broadening must be introduced to get meaningful results. This amounts to substituting ω by $\omega + i\delta$, where δ is a quantity related to the degree of accuracy accepted for the calculation. In our case, we have taken $\delta = 0.05$ eV, in such a way that the accuracy of our results can be expected to be better that 0.1 eV. (ii) On the other hand, in order to get the same accuracy in the effective Hamiltonians, $\underset{\approx S}{W}$, we have to give 6 steps in our calculation ($p_0 = 6$). (iii) Finally, let us comment that in order to obtain averages in the surface Brillouin zone, we have taken 45 points in the irreducible part of it (Chadi and Cohen 1974).

II.2.3. Results and discussion for the clean metal-semiconductor junction

In our actual calculation we have adjusted our parameters to a Si-Ag interface. For this case, the metal Fermi level lies in the s-band; however, in order to analyze the dependence of the junction properties on the metal

density of states at the Fermi level, we have used the same parametrized metal band structure, but have changed its Fermi level position.

In Table I.1 we give the different parameters used to calculate the Si-band structure: we have considered the three different cases given by Pandey and Phillips (P-P) (1976), Chadi and Cohen (C-C) (1975) and Menéndez and Vergés (M-V) (1981). P-P and C-C parameters give a very good valence band description. However, a free semiconductor surface calculated with the P-P parameters has its Fermi level almost coinciding with the valence band edge, while for the C-C interactions there appears a too much wide thermal gap. With the M-V parameters we obtain a better description of the main gap and the electron surface states, although the valence band is not so well described as with the P-P and C-C interactions.

As regards the metal, we have used the following parameters adjusted to give an appropriate density of states for Ag (Harrison 1980):

$$V_{ss} = -1.00 \text{ eV}, \quad V_{sd} = -0.25 \text{ eV}, \quad V_{dd} = -0.25 \text{ eV},$$
$$\epsilon_d - \epsilon_s = -3.00 \text{ eV};$$

here V_{ss}, V_{sd} and V_{dd} are the interactions between the nearest neighbours s-s, s-d and d-d orbitals, respectively, while ϵ_d and ϵ_s are the d and s orbitals levels.

The junction is formed by introducing a given interaction between the Si-dangling-bond hybrid and the orbitals of the on the top-Ag atom. We have chosen the parameters defining these interactions by taking a geometrical mean value between the interaction of two hybrids forming a Si-bond and the s-s (or the d-d) interaction for the metal. In Table II.2 we give the values used in the calculations for the different semiconductor models: a second set of values defining the interactions (the smaller ones in Table II.2) have been used in order to analyze the dependence of the barrier properties on the strength of the metal-semiconductor bond.

TABLE II.1.- Interaction parameters used in the calculation of the Si-band structure. P-P: Pandey and Phillips. C-C: Chadi and Cohen. M-V: Menéndez and Vergés (in eV). V_1, V_2, V_3, V_4, V_5 define the first-neighbours interactions in C-C notation; $(pp\sigma)_2$ and $(pp\pi)_2$ define the (P-P) second neighbours interactions.

	P-P	C-C	M-V
V_1	-1.10	-1.80	-2.04
V_2	-4.10	-5.85	-4.90
V_3	-0.55	-0.20	-0.43
V_4	0.24	0.85	0.24
V_5	-0.27	-0.60	0.57
$(pp\sigma)_2$	0.58	0.00	0.60
$(pp\pi)_2$	-0.10	-0.36	0.02

TABLE II.2.- Interaction between the dangling-bond hybrid of Si and the on the top-Ag atom orbitals. V_{Hs} and V_{Hd} refer to the s and d orbitals respectively, while (a) and (b) stand for the weak and strong coupling (in eV).

		P-P	C-C	M-V
V_{Hs}	(a)	-1.50	-1.23	-1.50
	(b)	-2.50	-3.42	-3.00
V_{Hd}	(a)	-0.50	-0.35	-0.50
	(b)	-0.70	-1.02	-1.15

In Figures I.1 to I.6 we give the density of states for the semiconductor surface layer, as calculated with the conditions given by eq.(II.5) and the P-P and the C-C parameters, for the following cases: (i) free surface; (ii) Ag-Si interface for weak-semiconductor-metal coupling (see Table II.2); (iii) same as (ii) for strong coupling. These figures have been calculated by assuming that the Fermi level in the metal lies in the d-band; for this case, the following general results of our calculation are better illustrated: (a) the Fermi level at the junction, as measured from a fixed point in the semiconductor bulk, moves towards the valence band for increasing values of the metal-semiconductor interaction; (b) the density of states at the Fermi level decreases for an increasing coupling between the metal and the semiconductor; (c) as far as the density of states in the main gap decreases with the metal-semiconductor bond strength, we find a corresponding increase in the density of states of the valence band near the top band-edge.

A word of caution must be put here. For the P-P parameters, the Fermi level at the free semiconductor surface practically coincides with the valence band edge. As the junction is formed, the Fermi level enters the valence band; then, the procedure followed in this work is not fully appropriate since selfconsistency cannot be achieved in the inner semiconductor layers. However, we have solved the junction for this case by looking for a selfconsistent solution only in the last two semiconductor layers, and neglecting the lack of neutrality which must appear in the inner layers. For this reason, the results obtained with the P-P parameters must be taken only as indicative.

Due to this comment and to the fact that the C-C parameters give a too wide semiconductor gap, we consider that the results obtained with the M-V parameters, as regards the change in the Fermi level, δE_F, between the free surface and the junction and S, are the best ones given by our calculations, For the case of a specific Ag-Si junction (with the metal Fermi level lying in the s-band) we have obtained the following results:
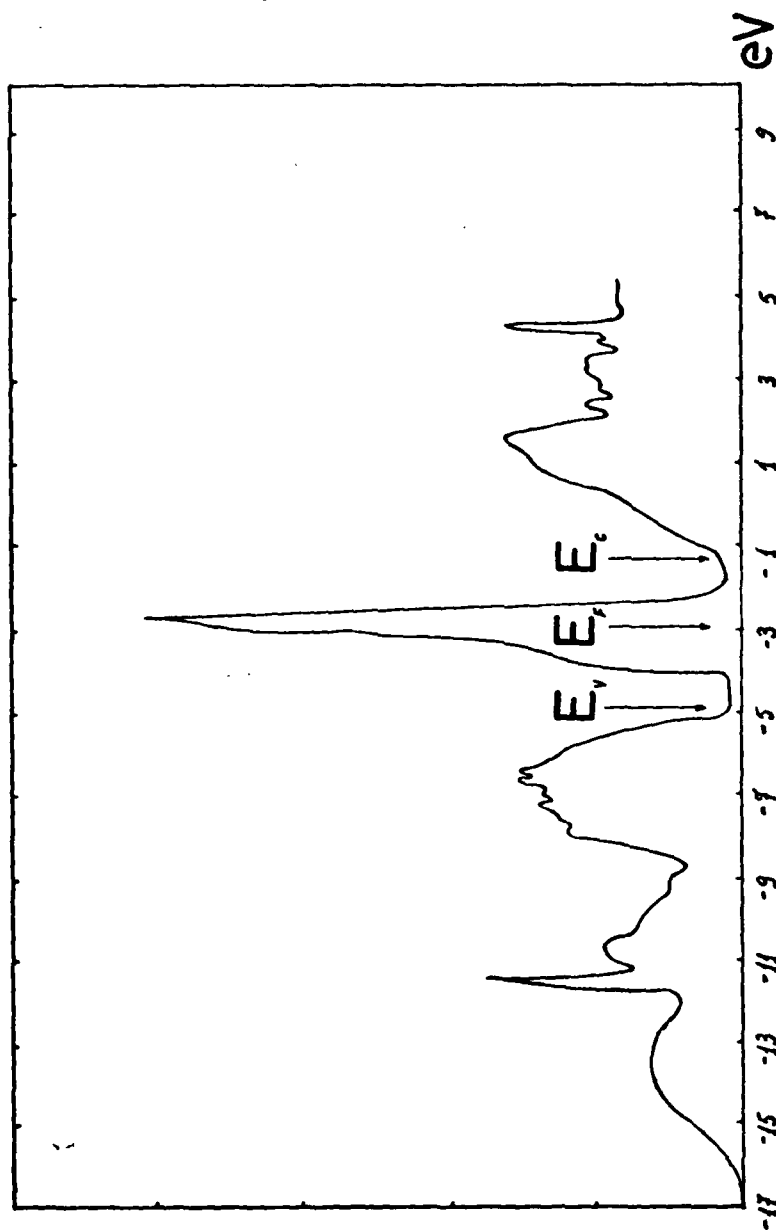
Fig II·1

Density of states for the semiconductor surface layer. Free surface and C-C parameters. E_F = Fermi level. E_C = Conduction band edge. E_V = Valence band edge.
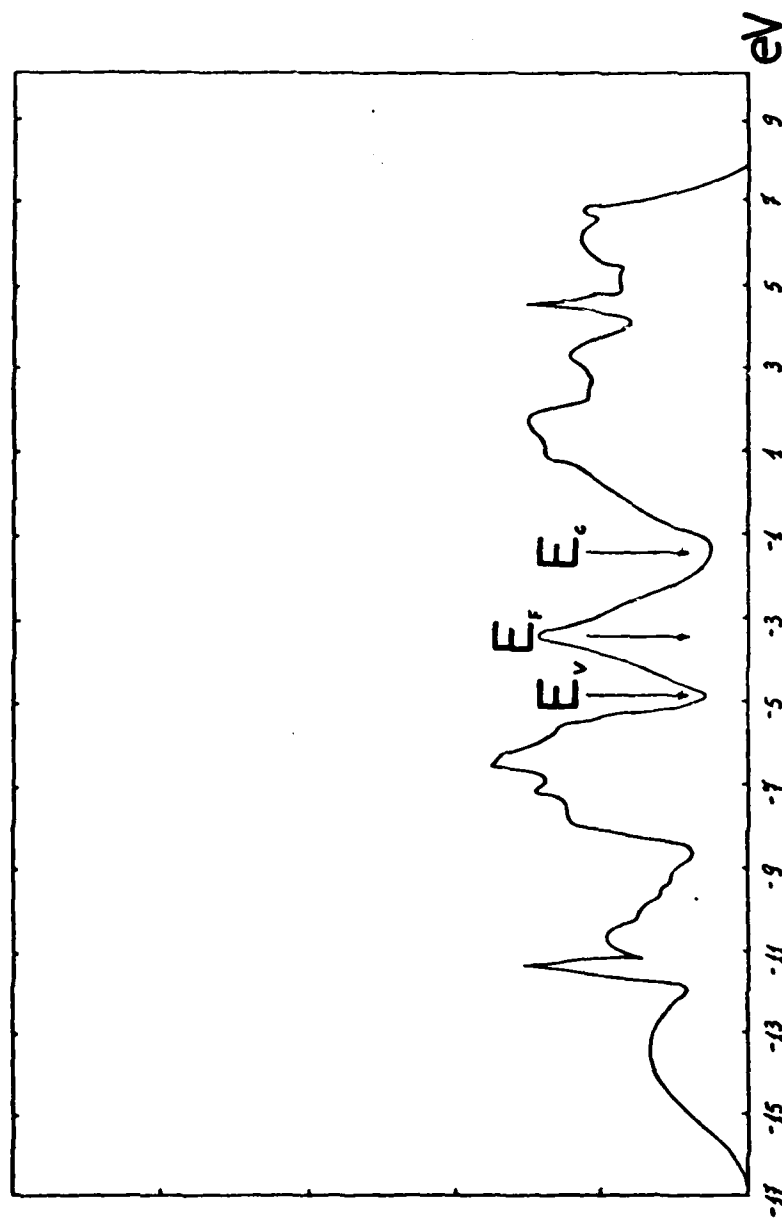
Fig II·2

Density of states for the semiconductor surface layer. Weak metal-
semiconductor coupling and C-C parameters. E_F = Fermi level. E_C =
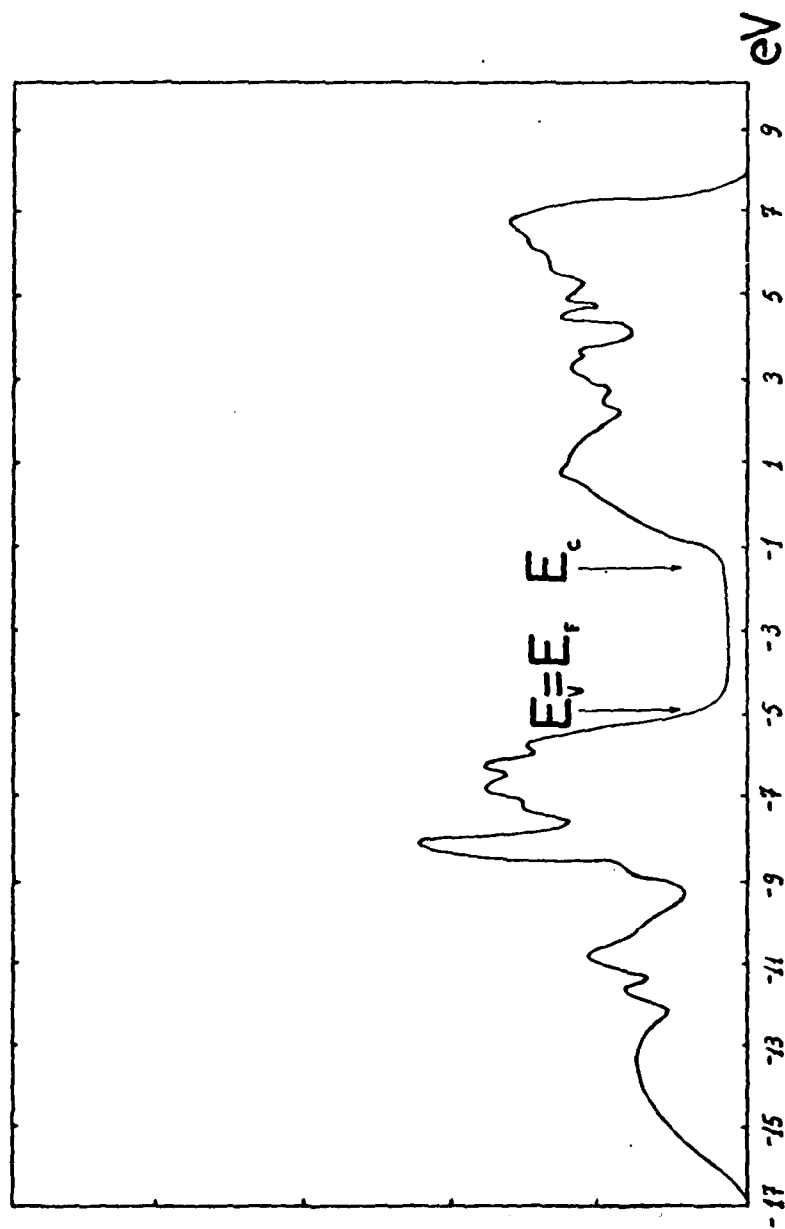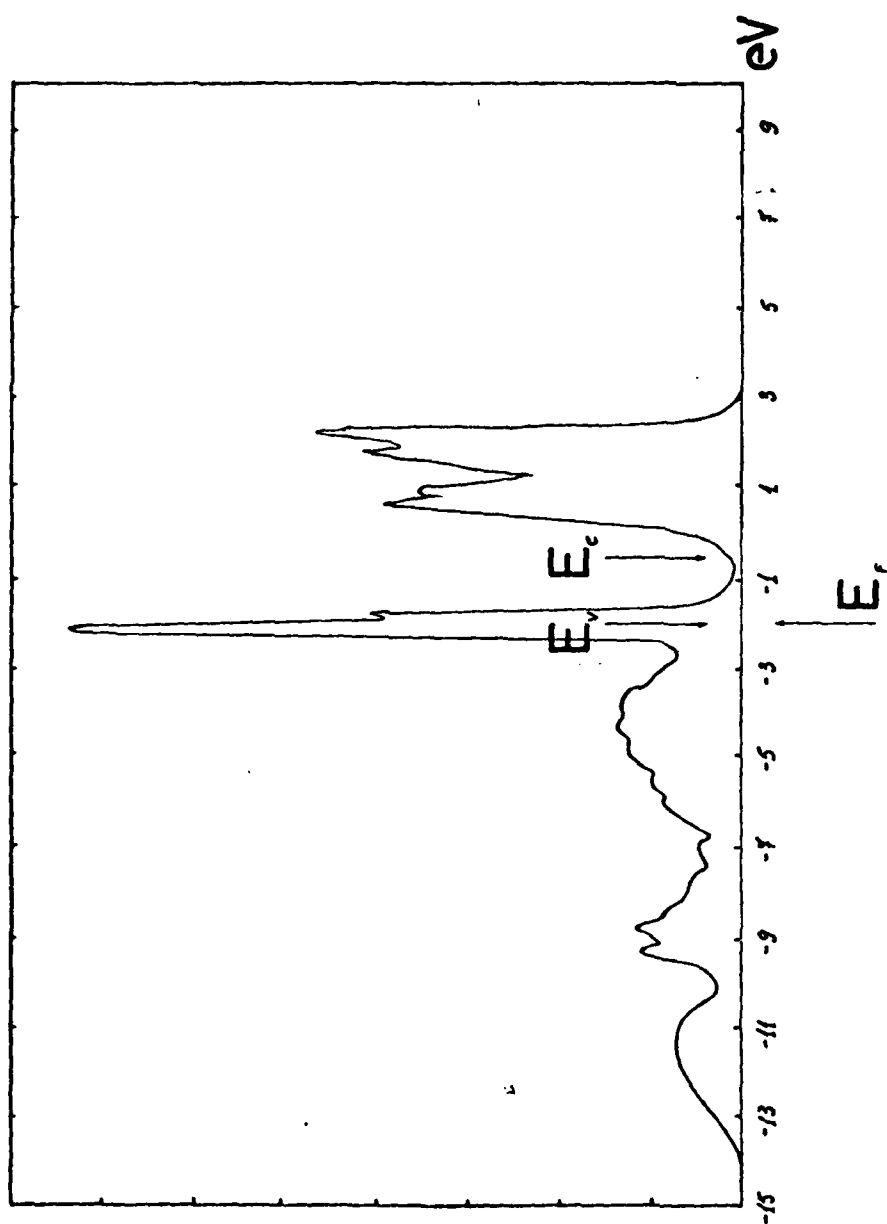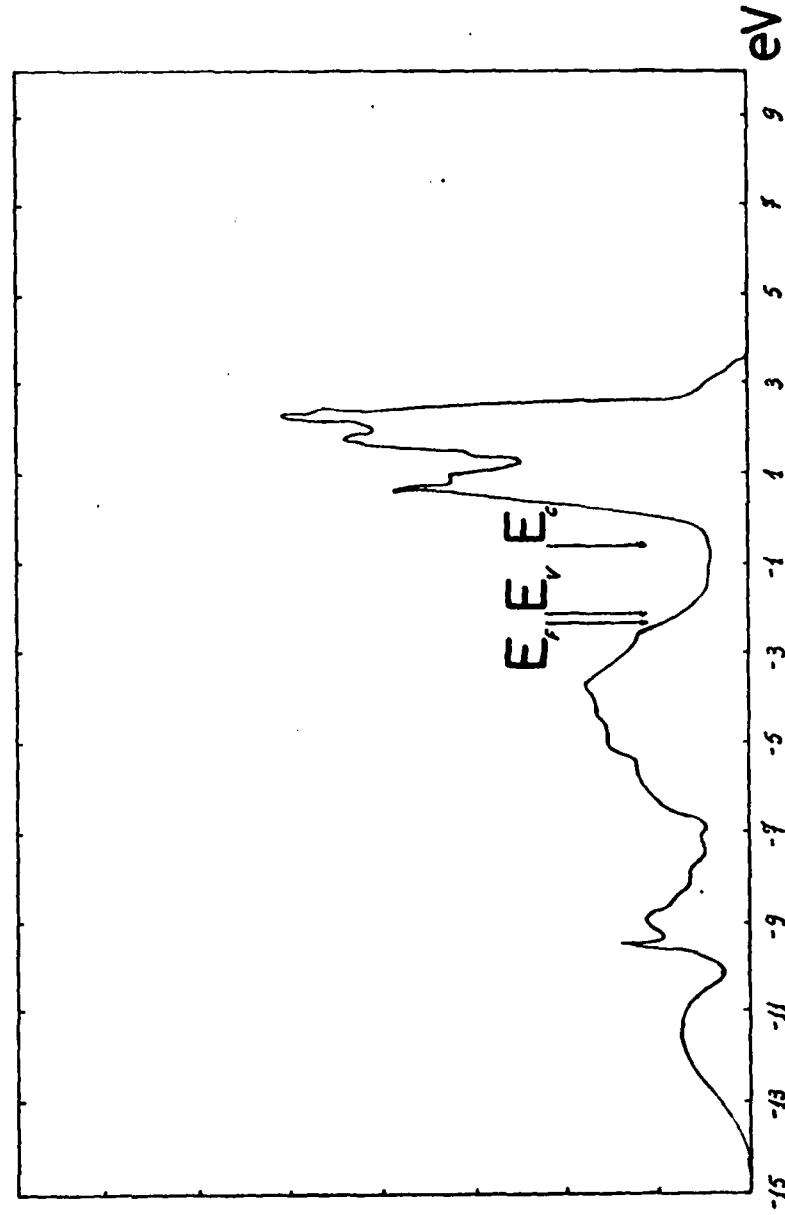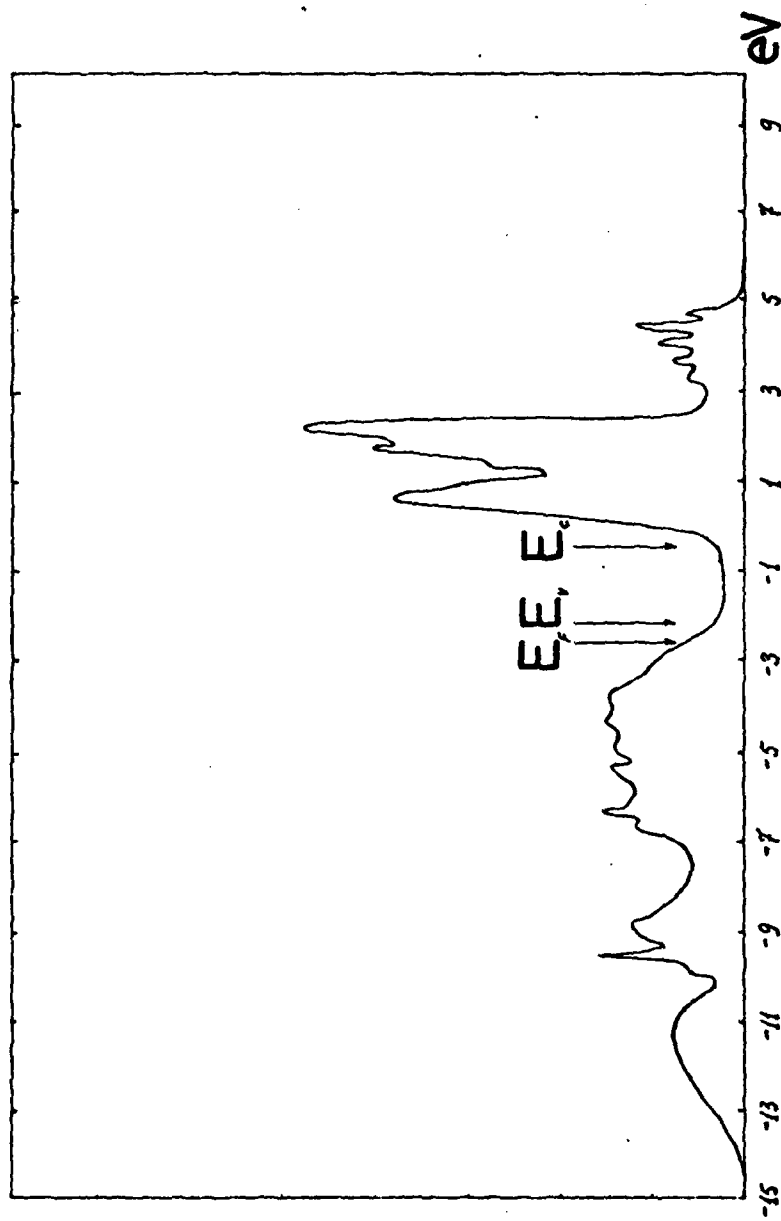Conduction band edge. E_V = Valence band edge.

Fig II.3

Density of states for the semiconductor surface layer. Strong metal-semiconductor coupling and C-C parameters. E_F ≡ Fermi level. E_C ≡ Conduction band edge. E_V ≡ Valence band edge.

Density of states for the semiconductor surface layer.
Free surface and P-P parameters. E_F ≡ Fermi level. E_C ≡
Conduction band edge. E_V ≡ Valence band edge.

Fig II·5

Density of states for the semiconductor surface layer. Weak metal-semiconductor coupling and P-P parameters. E_F ≡ Fermi level. E_C ≡ Conduction band edge. E_V ≡ Valence band edge.

Fig II·6

Density of states for the semiconductor surface layer. Strong metal-semiconductor coupling and p-p parameters. E_F = Fermi level. E_C = Conduction band edge. E_V = Valence band edge.

$\delta E_F = 0 \pm 0.05$ eV, $\qquad$ S = 0.07 $\qquad$ (weak coupling) ,

and

$\delta E_F = -0.15 \pm 0.05$ eV, $\qquad$ S = 0.14 $\qquad$ (strong coupling).

According to the way the interaction parameters for the metal-semiconductor coupling were chosen, we expect the actual junction to be closer to the strong coupling case.

The effect of the metal density of states at the Fermi level on the junction properties has been analyzed by assuming, in a second case, that the metal Fermi level lies in the d-band. With the M-V parameters we have obtained the following results:

$\delta E_F = -0.35 \pm 0.05$ eV, $\qquad$ S = 0.04 $\qquad$ (weak coupling)

$\delta E_F = -0.60 \pm 0.05$ eV, $\qquad$ S = 0.11 $\qquad$ (strong coupling).

These results show an important dependence of δE_F and S on the metal density of states at the Fermi level, although the details of this density around this level are unimportant.

Coming back to the Ag-Si junction, note that the barrier height is a function of the charge neutrality level, the slope S and the metal workfunction ϕ_M. As regards the charge neutrality level, we take into account the experimental evidence (Margaritondo et al.1975) that E_F, at the free semiconductor surface (a 111-7x7 reconstruction), is 0.55 eV above the valence band top. By using the values obtained for the case of strong coupling interaction we find that the charge neutrality level is 0.4 $\pm$ 0.05 eV above the valence band top. With this value and ϕ_M(Ag) = 4.4 eV we obtain the following barrier height:

ϕ_{bn}(Ag-Si) = 0.66 $\pm$ 0.05 eV ,

a value to be compared with the experimental barrier height of 0.79 eV (Rhoderick 1978). This result shows that, indeed, the metal-semiconductor coupling is close to the strong

coupling case, and that the actual parameters defining this coupling must be even a little greater.

It is of interest to consider now the general conclussions that can be reached from the results given above for δE_F and S as a function of the metal-semiconductor coupling strength and the metal density of states at the Fermi level. Our results show that δE_F increases with both the metal-semiconductor coupling and with the density of states at the metal Fermi level. Thus, we can expect δE_F to be close to zero for metals of low electronegativity, for which the metal-semiconductor coupling must be small, and of low electron density; for these cases the barrier height must be a little smaller than 0.55 eV (this is the barrier height for a free surface). On the other hand, δE_F may present important changes, up to 0.5 eV, for metals of high electronegativity and high electron density. In general, these comments seem to be in qualitative agreement with the experimental results collected for the metal-semiconductor junction (Rhoderick 1979).

As regards the change in the Fermi level, δE_F, induced by the barrier formation, it is worth commenting on the experimental evidence given by Margaritondo et al.(1976). By analyzing the cases of Al, Ga and In on Si, those authors have shown that, with the barrier formation, the interface Fermi level shifts towards the valence band in quantities of 0.20, 0.30 and 0.40 eV, for Al, Ga and In, respectively. Considering that these metals have a density of states at the Fermi level between the two cases analyzed above (with the Fermi level lying in the s- or the d-band), we conclude that the observed shifts in the interface Fermi level are in reasonable agreement with our previous calculation. Moreover, according to our previous discussion, we expect the differences between the three metals (Al, Ga and In) to be related to the different bondings between each metal and the semiconductor. In this sense, note that the Pauling electronegativity takes the values 1.5, 1.6 and 1.7 for Al, Ga and In, respectively, suggesting that, indeed, the increase of electronegativity is related to a stronger coupling and to an

increase of the barrier height.

On the other hand, let us comment that most silicides seem to present an abrupt interface. Then, these junctions can by analyzed in the terms presented in this Report. The crucial parameters characterizing the interface are the distance, d, between the last layers of the semiconductor and the metal, and the strength of the metal-semiconductor bond. Due to structural and bonding similarities (Ho et al. 1979), we can expect these junctions to have practically the same charge neutrality point and the same value of S. This suggests that *these junctions* must show a linear relationship between the height barrier and the workfunction of the silicide metal. This seems to be in reasonable agreement with the experimental evidence (Froeouff 1980), although complementary information on the silicide workfunction would be necessary to reach a definite conclusion.

Let us finally make a commment on the barrier height formation: for an abrupt interface, the barrier height is determined by the density of states near the Fermi level in the semiconductor gap. For a clean surface, this density is high and is determined by the surface band; as far as the metal-semiconductor coupling is switched on, this density of states decreases, an effect induced by the broadening of the surface states of the free semiconductor. This process explains why the Fermi level for the junction almost coincides with the Fermi level for the free surface, a result stressed by other researchers (Tejedor et al. 1977, Louis and Flores 1981).

In conclusion:

(a) The Fermi level at the junction -as measured from a fixed point in the semiconductor- moves towards the valence band for increasing values of the metal-semiconductor coupling.

(b) The density of states at the Fermi level decreases for an increasing coupling between the metal and the semiconductor.

(c) As far as the density of states in the main gap decreases with the metal-semiconductor bond strength, we

find a corresponding increase in the density of states of the valence band near the top band edge.

(d) The effect of an increase in the metal density of states at the Fermi level on the junction properties is similar to an increase in the metal-semiconductor coupling.

II.2.4. Results and discussion for the metal-interlayer-semiconductor junction

Let us turn our attention to etched junctions with a monolayer between the metal and the semiconductor. In our calculation we have assumed to have one ad-atom on top of the outermost Si-atom, and the same structure for the metal as the one discussed above in §II.2.3 with one metal-atom on top of the ad-atom. For the ad-atom we have assumed to have a s-orbital per atom, a model appropriate for a H or Cs monolayer, while for the metal we have used those parameters given in §II.2.3 and adjusted to a Ag-case.

The Hamiltonian for the interface is defined by a number of parameters giving the coupling between the ad-atom and the orbitals of the last layers of the metal and the semiconductor. For H we have followed Pandey (1976) and taken the following parameters for the Si-H interaction:

$$V_{ss}^{Si-H} = -3.57 \text{ eV}$$

$$V_{sp\sigma}^{Si-H} = -2.76 \text{ eV} \quad , \tag{II.29}$$

where V_{ss} and $V_{sp\sigma}$ give the interactions between the ad-atom and the s and p orbitals of Si, respectively. For the Ag-H coupling, we need the interactions between the ad-atom and the s- (V_{ss}^{Ag-H}) or d-orbitals (V_{sd}^{Ag-H}); these parameters have been obtained by averaging the Si-H interactions with the Ag-Ag interactions, V_{ss}^{Ag-Ag} and V_{dd}^{Ag-Ag}, given above (§II.2.3). This yields:

$$V_{ss}^{Ag-H} = -2.3 \text{ eV}$$

$$V_{sd}^{Ag-H} = -1.0 \text{ eV} \quad . \tag{II.30}$$

On the other hand, E_H^0, the mean atomic level for the isolated atom, has been adjusted to give an appropriate solution for the case of a H-monolayer adsorbed on a clean 111-Si surface (Appelbaum and Hamann 1975, Pandey 1976). In Figures II.7 and II.8 we give the density of states in the adsorbed monolayer and in the last semiconductor layer as obtained for

$$E_H^0 = -5.4 \text{ eV} \tag{II.31}$$

by means of a selfconsistent calculation. This density of states shows a good agreement with other calculations (Pandey 1976), and it corresponds to a solution for which there is a small transfer of charge, around 0.01 e/atom, from the monolayer to the semiconductor surface layer; this is in agreement with the experimental evidence (Ibach and Rowe 1974). Note that for the monolayer case, we get selfconsistency by means of an equation similar to (II.13); in this equation, U has been taken equal to 8 eV, following many other chemisorption analysis for H (Baldo et al.1983, Newns 1969).

The values given in (II.29), (II.30) and (II.31), and the parameters introduced in II.2.3 for the metal and the semiconductor, define our model Hamiltonian for the H-interlayer.

At this point it is convenient to remark that Figures II.7 and II.8, as well as all the calculations presented in this paragraph for the metal-interlayer-semiconductor junction, have been obtained by using the semiconductor parameters given by Pandey and Phillips (1976) and collected in Table II.1. In spite of the comment made in §II.2.2 for this case, where we stressed the difficulties associated with the fact that the Fermi level for the interface lies in the semiconductor valence band, we have checked that all the main results related to changes in the Fermi level as obtained with the P-P parameters are in good agreement with the results as calculated with the M-V parameters (a case giving a better description of the surface states position).

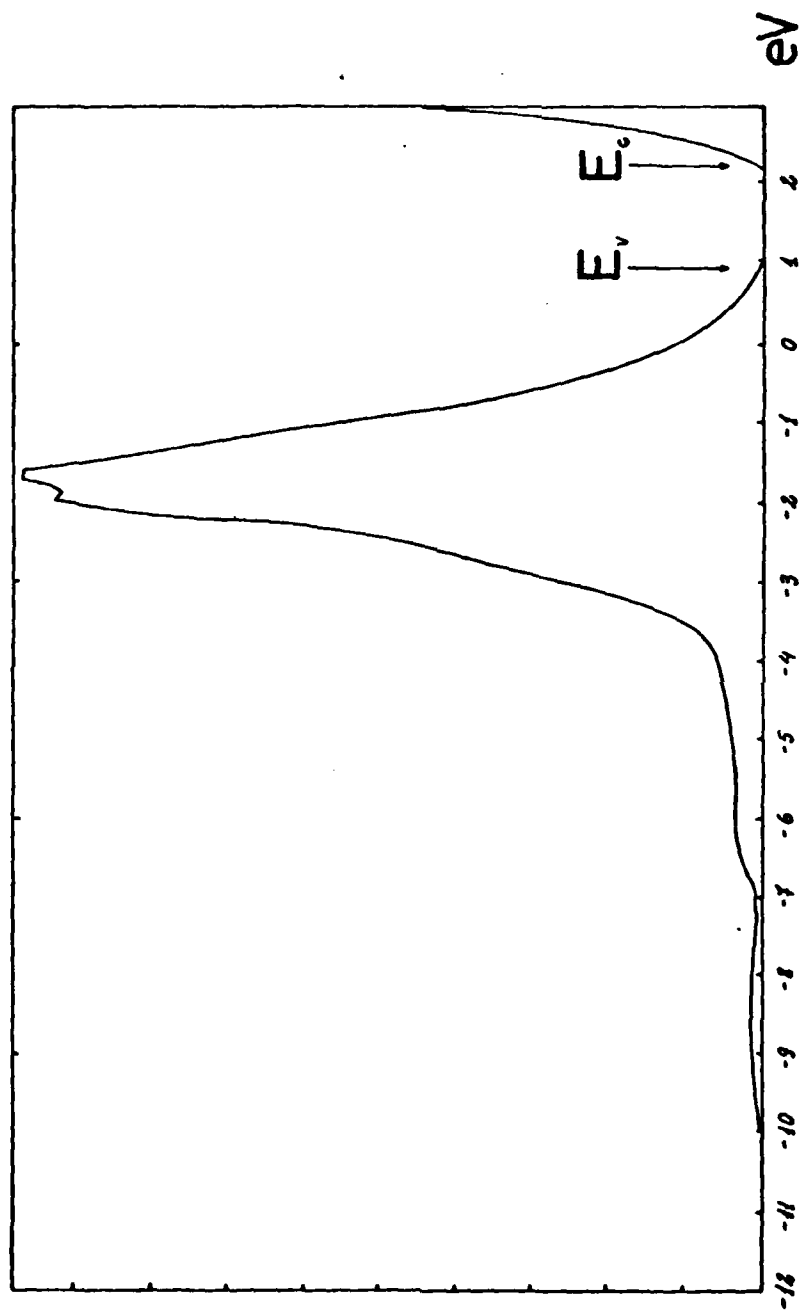As regards the Cs-interlayer, we have determined the

Fig II·7

Density of states in the H-monolayer for the Si-H system. E_C = Conduction band edge. E_V = Valence band edge.
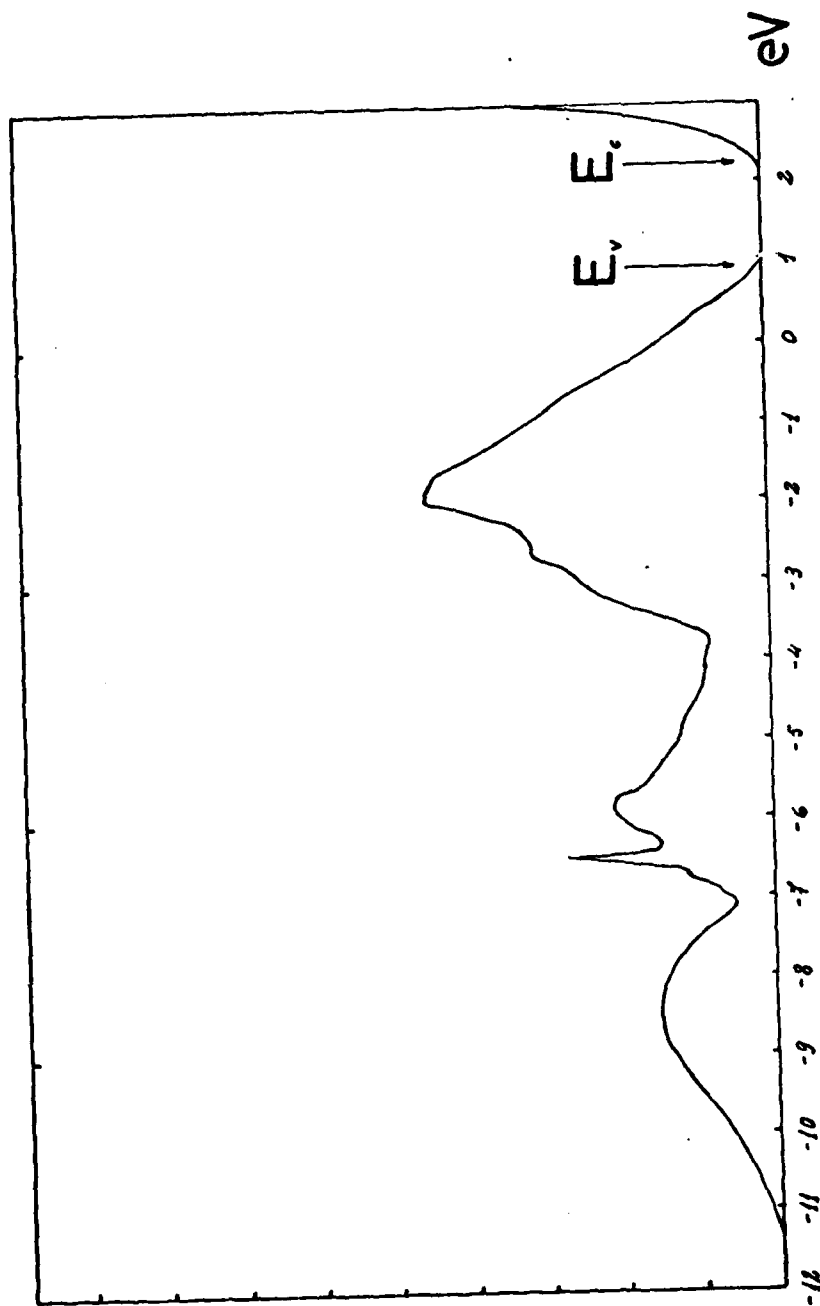
Fig II·8

Density of states in the semiconductor surface layer for the Si-H system. E_c ≡ Conduction band edge. E_v ≡ Valence band edge.

parameters defining the interface in the following way: firstly, we have obtained the effective V_{ss}^{Cs-Cs} interaction by means of the procedure given by Harrison (1980). Then, we have obtained the different Si-Cs and Ag-Cs interaction parameters by averaging that effective interaction, V_{ss}^{Cs-Cs}, with the Si-Si and Ag-Ag interaction parameters. This procedure yields:

$$V_{ss}^{Ag-Cs} = -1.5 \text{ eV}$$

$$V_{sd}^{Ag-Cs} = -1.6 \text{ eV}$$

$$V_{ss}^{Si-Cs} = -1.25 \text{ eV} \tag{II.32}$$

$$V_{sp\sigma}^{Si-Cs} = -0.92 \text{ eV} \quad .$$

On the other hand, $E_{Cl}^{(0)}$ has been taken equal to the average of the affinity and the ionization levels for the free atom:

$$E_{Cs}^{(0)} = -2.0 \text{ eV} \quad . \tag{II.33}$$

Finally, for Cs, the intraatomic interaction, U, has been taken equal to 1.5 eV, close to the difference between the affinity and the ionization levels.

In order to analyze the effect of Cl on the junction properties, we have adapted the previous model, keeping only a s-atomic orbital, but introducing stronger interactions with the metal and the semiconductor. To this end, we have practically scaled the H-Si and H-Ag interactions with the Cl-Si and Cl-Ag ones, by means of the bond energies for H and Cl with Si and Ag (Pauling 1972). This yields:

$$V_{ss}^{Ag-Cl} = -4.5 \text{ eV}$$

$$V_{sd}^{Ag-Cl} = -3.5 \text{ eV}$$

$$V_{ss}^{Si-Cl} = -2.45 \text{ eV} \tag{II.34}$$

$$V_{sp\sigma}^{Si-Cl} = -1.41 \text{ eV} \quad .$$

Moreover, following the criterium given above for Cs, we have selected the following parameters:

$$E_{Cl}^{(0)} = -8.3 \text{ eV}$$

$$U = 7 \text{ eV} \quad ,$$

(II.35)

which completely determine our interface model Hamiltonian.

One more comment must be made before discussing our results: selfconsistency has to be reached by using eqs. (II.10), (II.11), (II.12) and (II.13). However, in order to apply eq. (II.13) we need the distances d and d' between the last metal layer and the interface semiconductor layer or the ad-atom interlayer, respectively. For H and Cl we can assume, as discussed above, that the ad-atom is located on top of the outermost Si-atom (Pandey 1976, Schluter and Cohen 1978), and the distances d and d' can be approximately obtained by adding the covalent atomic radii. However, for Cs a more appropriate position would be for the ad-atom to sit above the center of three Si-atoms. Then, the distance between the interlayer and the last semiconductor layer, (d'-d), would be substantially reduced. This fact can have considerable effect in the final selfconsistency: we shall discuss its implications later on. (In spite of this comment, for the sake of simplicity, we shall calculate the Cs-interlayer case with a model Hamiltonian appropriate for an ad-atom adsorbed on the top position; the effect of the adsorption site will be only simulated by changing the distance (d'-d)).

In Figures II.9 and II.10 we present the density of states in the interlayer and the last semiconductor layer as calculated for the Si-H-Ag junction. In Figures II.11 and II.12 we give the same quantities for the Si-Cs-Ag junction, by assuming no transfer of charge from or to the interlayer (see below).

Our calculation shows the following general results:

(i) The parameter S', giving through eq. (II.15) δD, is practically zero in all the cases (H, Cs and Cl). Then, the Fermi level for these junctions practically coincides with
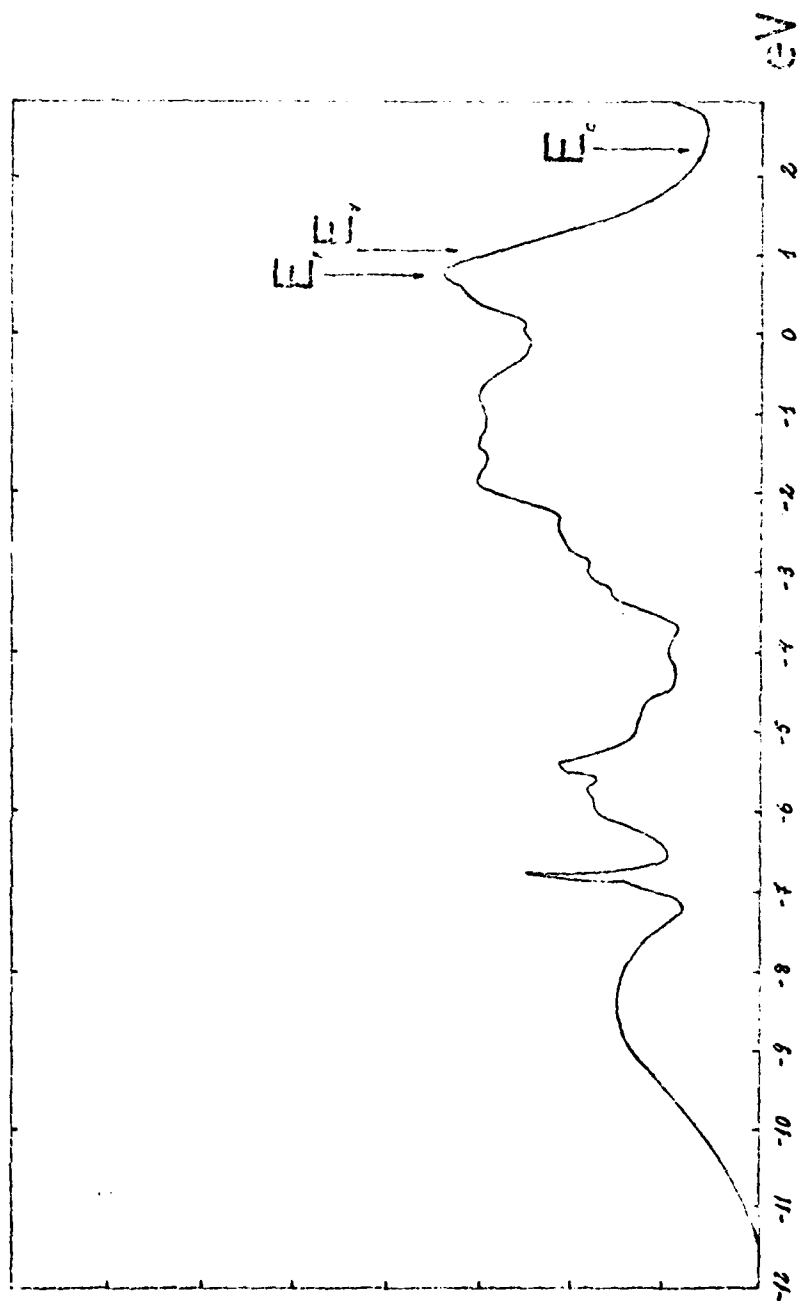
Fig II·9

Density of states in the semiconductor surface layer for the Si-Al-Ag junction. E_F = Fermi level. E_C = Conduction band edge. E_V = Valence band edge.
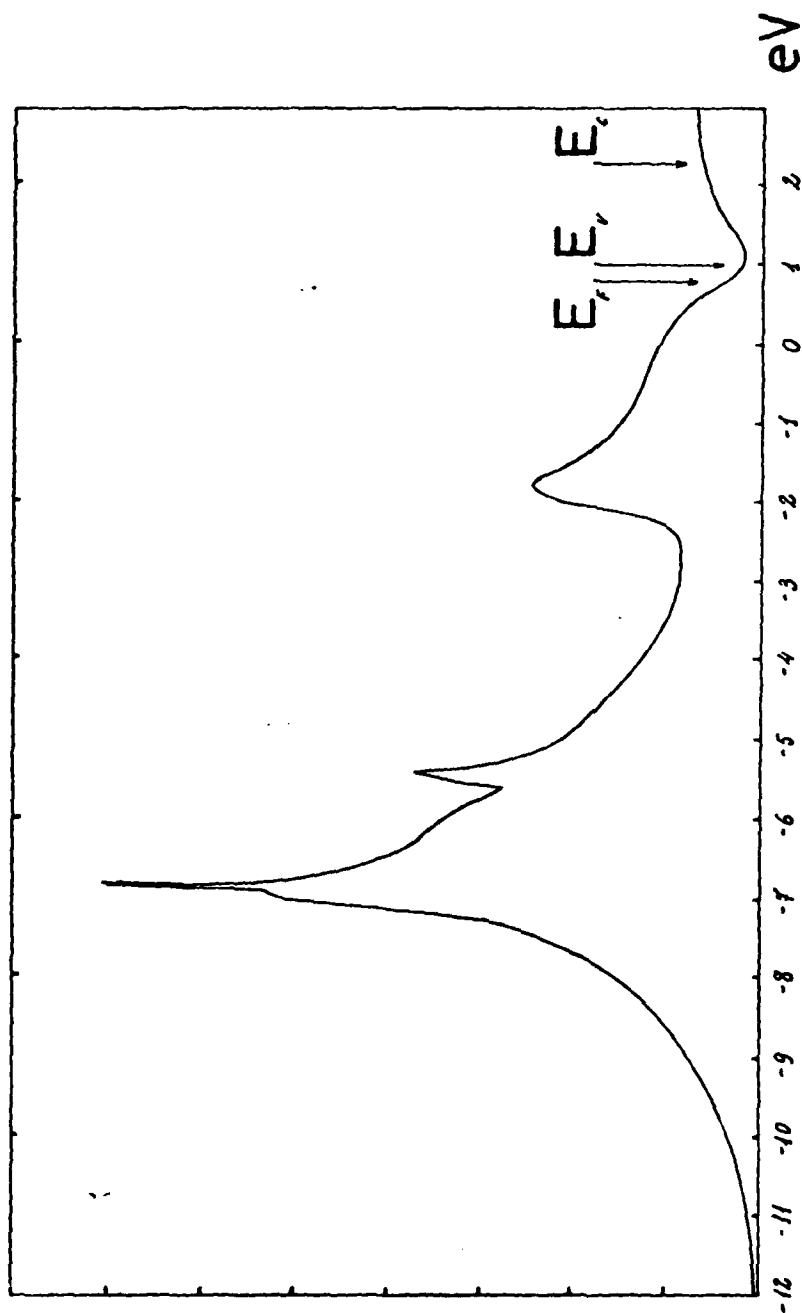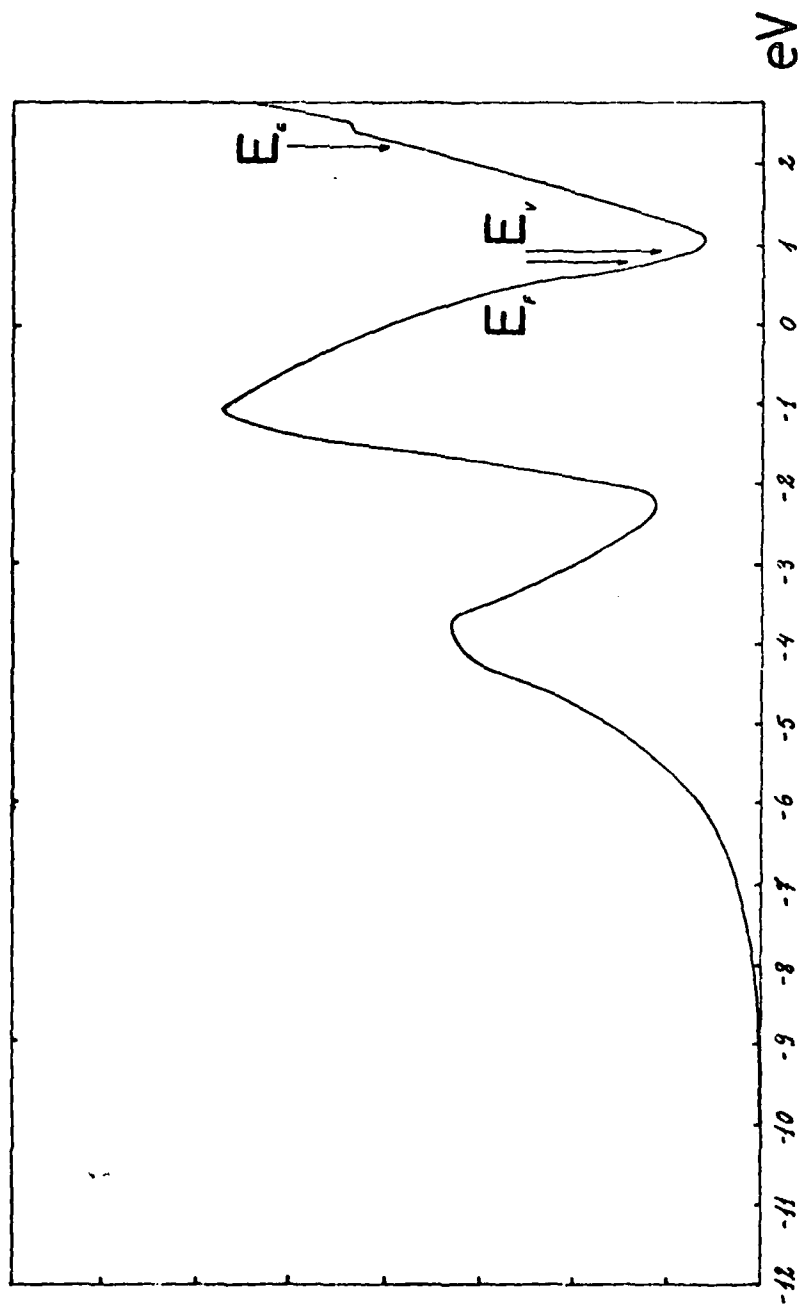
Fig II·10

Density of states in the H-monolayer for the Si-H-Ag junction. E_F ≡ Fermi level. E_C ≡ Conduction band edge. E_V ≡ Valence band edge.

Fig II·11

Density of states in the Cs-monolayer for the Si-Cs-Ag junction. E_F = Fermi
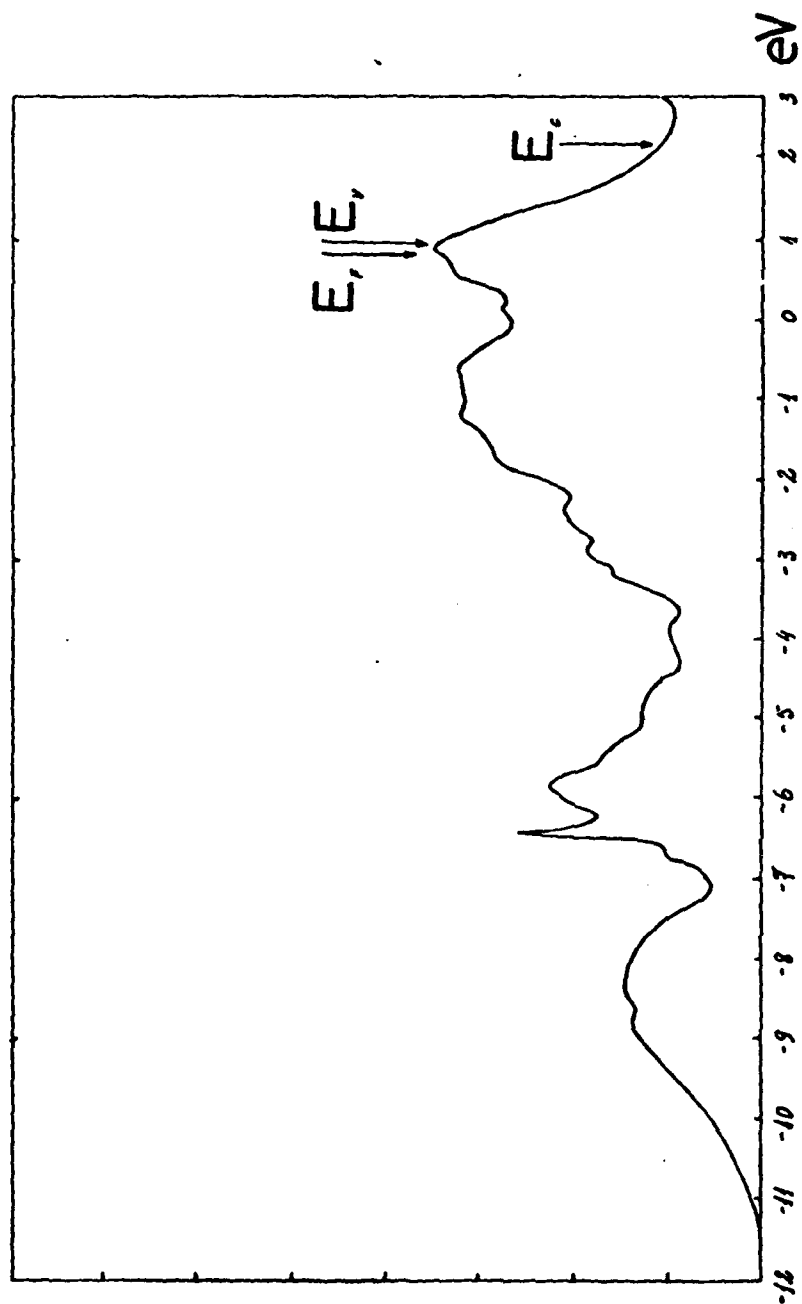level. E_C = Conduction band edge. E_V = Valence band edge.

Fig II·12

Density of states in the semiconductor surface layer for the Si-Cs-Ag
junction. $E_F \equiv$ Fermi level. $E_C \equiv$ Conduction band edge. $E_V \equiv$ Valence
band edge.

the charge neutrality level.

(ii) The charge neutrality level can be obtained in two steps. In a first step, this level has been obtained by assuming no transfer of charge from the ad-atom to the semiconductor: this is practically the case for H. In a second step, the charge neutrality level is modified by the transfer of charge from (or to) the interlayer, due to the low or high ad-atom electronegativity.

For H, with an electronegativity similar to Si and Ag, there is practically no transfer of charge between the interlayer and the semiconductor. Then, the charge neutrality level is given by the first step. Our calculation shows that this level is 0.13 ± 0.05 eV below the Fermi level for the free surface. It is worth remarking that this level almost coincides with the one obtained for the clean Ag-Si junction. We conclude that for H, the interface Fermi level is very close to the one obtained for the clean Si-Ag junction.

For Cs, there is an important transfer of charge from the ad-atom to the semiconductor. The first step mentioned above gives a charge neutrality level located 0.07 ± 0.05 eV below the free surface Fermi level. On top of this, the charge neutrality level shifts to lower energies due to the transfer of charge from the ad-atom to the semiconductor. Our calculation shows that this shift δE_F is related to the transfer of charge, Δn_{Cs}, by the equation:

$$\delta E_F \simeq 0.4 \ \Delta n_{Cs} \qquad \qquad (II.36)$$

with δE_F given in eV and Δn_{Cs} in units of electronic charge per atom. Now, it is important to note that Δn_{Cl} is very dependent on (d-d'), the distance between the ad-atom interlayer and the last semiconductor layer. For a position on top of the Si atom, we have estimated Δn_{Cs} to be around 0.16 units of electronic charge. However, for a site above the mid-point of three Si-atoms, we have estimated that Δn_{Cs} must be around 0.5 units of electron charge. For the two cases, the charge neutrality level shifts towards lower energies in 0.08 eV and 0.25 eV, respectively. Considering the second

case to be the most likely to happen, we obtain a Fermi level for the Si-Cs-Ag located 0.32 ± 0.05 eV below the Fermi level for the free surface, and 0.17 ± 0.05 eV below the Fermi level for the clean Si-Ag interface.

For Cl, we find an important transfer of charge to the ad-atom. With the first step (no transfer of charge), the charge neutrality level is located at 0.17 ± 0.05 eV below the Fermi level for the free surface. In the second step, we find that the charge neutrality level shifts to higher energies; δE_F is related to Δn_{Cl} by the equation:

$$\delta E_F \simeq 0.6 \ \Delta n_{Cl} \quad , \tag{II.37}$$

with Δn_{Cl} measured in units of electronic charge per atom. With the on the top position for Cl, we have estimated that $\Delta n_{Cl} \simeq 0.14$, and $\delta E_F \simeq 0.08$ eV. Accordingly, we obtain a Fermi level for the Si-Cl-Ag junction located around 0.09 ± 0.05 eV below the Fermi level for the free surface and 0.04 ± 0.05 eV above the Fermi level for the Si-Ag junction.

Summarizing the last results: the Fermi level for the Si-Cs-Ag, Si-H-Ag and Si-Cl-Ag junctions have been obtained at energies: -0.17 ± 0.05 eV, 0.02 ± 0.05 eV and 0.04 ± 0.05 eV, respectively, referred to the Fermi level for the Si-Ag junction.

The main changes in the Fermi level (and the corresponding changes in the barrier height) are induced by ad-atoms of very low affinity. This is mainly due to the fact that Cs has been supposed to sit on the mid of three Si-atoms. In other words, had we assumed Cl to sit on the same position, we had obtained a greater shift, around 0.2 eV, in the Fermi level but towards *higher* energies. This conclusion seems to be in agreement with the results obtained by Mottram et al. (1975) for an interlayer of O; in this case, O sits in the mid-position and induces a shift in the interface Fermi energy of 0.2 eV towards the conduction band.

(iii) Finally, we have analyzed the effect of the metal density of states at the Fermi level on the previous results

by changing the Fermi level position in Ag. For the case in
which the Fermi level was located at the d-band, we have
found no significative change in our previous conclusions.
Thus, the barrier height for the interlayer junctions seems
to be practically independent on most of the metal properties.
Note that this result is contrary to the one obtained for
the clean metal-semiconductor junctions, where a high
density of states at the metal Fermi level was found to
induce an important shift in the interface Fermi level (see
§II.2.3). This suggests that the barrier height for etched
junctions is mainly determined by the semiconductor-ad-atom
interaction.

In conclusion, the crucial physical quantities
determining the barrier formation in the metal-interlayer-
semiconductor junctions seem to be the ad-atom electro-
negativity and the adsorption site for the ad-atom. In other
words, the barrier height is practically determined by the
coupling between the semiconductor and the ad-atom
interlayer.

II.3. NON-ABRUPT METAL-SEMICONDUCTOR JUNCTIONS

II.3.1. Introduction

The mechanism of Schottky-barrier formation has been
the subject of a variety of proposed interpretations
(Schottky 1942, Bardeen 1947, Heine 1965, Rhoderick 1978,
García-Moliner and Flores 1979). Very recently (Andrews and
Phillips 1975, Brillson 1978, Ottaviani et al.1980), new
experimental information has been obtained, which point to
the effect of the metal-semiconductor reactivity on the
barrier height of the junction. Another interesting feature
which occurs at some of these interfaces is the atomic
rearrangement that takes place at the metal-semiconductor
junction (Cheng et al.1980, Brillson et al.1981). In
particular, Brillson et al (1981) have shown that, in III-V
semiconductors, the abruptness of the junction interface is

a function of the stregth of the metal-(III-V) semiconductor bonding. Interface widths have been measured, and correlated with the metal-semiconductor heat of interface reaction ΔH_R (defined as H_F(semiconductor)-H_F(metal-anion complex of lowest energy), H_F being the heat of formation per metal atom). Both magnitudes appear to correlate linearly, with the interface width extending from 20 Å down to practically abrupt surfaces.

Here, we advance a simple theory to explain existing data on the widths of these interfaces, and to make predictions about some materials not hitherto examined experimentally. We assume that no structural effect at the interface may prevent both crystals to interdiffuse, and reach their thermodynamical equilibrium (Proc.Conf.on Surfaces 1982).

II.3.2. Reference system: Ga on Ga-As, etc.

To apply chemical solution theory, it will be instructive to discuss first a reference system.

This we choose, as in the Ga-GaAs interface, such that the metal ion is identical to the semiconductor cation. For this reference system, it is evident that the heat of interface reaction ΔH_R (which is a measure of the energy required to substitute the semiconductor cation by the metal) must be identically zero.

This is a binary system which we shall analyze using methods related to the pioneering studies of Cahn and Hilliard (1958). Figure II.13 shows schematically the density profiles of Ga and of As perpendicular to the planar interface of Ga-GaAs, N_1 and N_2 being the respective numbers of anions and cations in volume V. We assume no change in N across the interface (in Ga metal, $N = 5.1 \times 10^{22}$ cm^{-3}, while in GaAs, $N = 4.3 \times 10^{22}$ cm^{-3}: so the approximation is fairly reasonable in this material).

The formulation used below to analyze this reference system can be viewed as based on that of Fleming et al. (1976). This theory treats inhomogeneities by local theory,
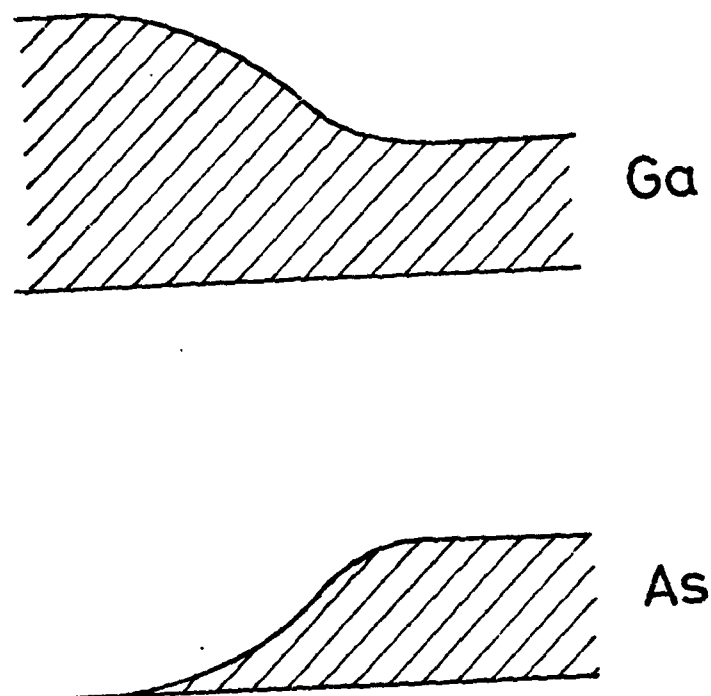
FIGURE II.13.- Density profiles of Ga and As at
the planar interface.

corrected by low order density gradients. The relation between such a theory and the Cahn-Hilliard phenomenological approach employed by Bathia and March (1978) has been clarified by Bathia, March and Sutton (1978). With the simplifications discussed here, the free energy density required, denoted by $\psi(\vec{r})$, as a function of the densities N_1, N_2 and their derivatives can be written as the sum of two parts, ψ_1 and ψ_2, ψ_1 being a local part and ψ_2 proportional to the gradients of N_1 and N_2. The local part ψ_1 can be expressed in the form

$$\frac{1}{k_T N^2} \left[\Delta N + N \delta \Delta c \right]^2 + \frac{1}{V} (\frac{\partial^2 G}{\partial c^2}) (\Delta c)^2 \quad , \qquad \text{(II.37)}$$

where $N = N_1 + N_2$, k_T is the appropriate isothermal compressibility, G is the Gibbs free energy, while

$$\Delta N = \Delta N_1 + \Delta N_2$$

and

$$\Delta c = N^{-1} \left[(1-c) \Delta N_1 - c \Delta N_2 \right] \quad .$$

Evidently the second term in eq.(II.37) comes from the concentration fluctuations, while the first term represents contributions from fluctuations in the total density, but combined with the effect of the size factor δ, which multiplies again the change in concentration Δc. Evidently, in the first term in eq.(II.37), the presence of size differences leads directly to an interference term between ΔN and Δc. For the reference system we assume $\Delta N = 0$ while we shall also take the size difference δ to be unimportant, and put that to zero as well. The only contribution remaining then in the local part of the free energy is therefore coming from the concentration-concentration function $S_{cc}(0)$ defined by

$$\frac{1}{V} \frac{\partial^2 G}{\partial c^2} (\Delta c)^2 = \frac{N k_B T}{S_{cc}(0)} (\Delta c)^2 \quad .$$

The second part of the free energy, ψ_2, can be written

$$\psi_2 = \frac{1}{2} \left\{ A_{11}(N_1,N_2) + A_{22}(N_1,N_2) - 2A_{12}(N_1,N_2) \right\} (\vec{\nabla} N_1)^2$$

$(N = N_1+N_2 = \text{constant})$, or equivalently as

$$B(N_1,N_2) (\vec{\nabla} N_1)^2 ,$$

where B is essentially a homogeneous quantity, evaluated at the local densities N_1 and N_2.

II.3.2.1. *Regular solution model of concentration fluctuations*

In a solution, the most elementary model for the Gibbs free energy, G, is to construct it as a concentration weighted average of the Gibbs energies, G_1 and G_2, for the two components, plus the usual expression for the entropy of mixing. This leads immediately to $S_{cc}(0)$ defined above in terms of $\partial^2 G/\partial^2 c$ as $c(1-c)$. But this elementary treatment is appropriate to an ideal solution, i.e. in the absence of interactions between the two components. Once one introduces an energy to measure these interactions, one is led to the so-called regular solution model (see, for example, Bathia, Hargrove and March 1973), namely

$$S_{cc}(0) = \frac{c(1-c)}{1+ \frac{2W}{k_B T} c(1-c)} .$$

Here 2W is the total decrease in the energy of the system when two atoms, A and B, of each solution are interchanged. For the case under discussion, we identify 2W with the energy of formation of the compound, say GaAs, minus the energy of each one of the atoms, say Ga and As, in their own solution. We see that $S_{cc}(0)$ decreases with increasing W, the heat of reaction for the system. We show data for 2W, obtained from tabulations which can be found in Kittel (1971), in Table II.3:

TABLE II.3.- Interchange energy 2W in kcal/mol.

AlP	AlAs	InSb	GaSb	InP	GaP	InAs	GaAs
39	27	8	8	23	20	17	17

and it is interesting to note that of the systems examined by Brillson et al.(1981), InP, InAs and GaAs have rather similar values of 2W, and we expect the *reference* interface thicknesses to be similar (see below).

As regards $B(N_1 N_2)$ above, we assume that the most important contribution comes from the metallic electrons which have not reacted to form III-V-like bonding. This density is given by

$$N_\Delta = 3\left[N(cation) - N(anion)\right] = 3\left[N-2N_1\right] \quad ,$$

where the factor of 3 comes because we are dealing with trivalent metals, and now, following the gradient expansion of Kirznits (1957), we write the second contribution as

$$\frac{1}{72N_\Delta} (\vec{\nabla}N_\Delta)^2 \quad .$$

Following Bathia and March (1978), we obtain the interfacial free energy σ by integrating the free energy density $\psi_1 + \psi_2$ through the interface, remembering that this interface is of thickness l, in the form

$$\sigma \sim \frac{Nk_B T}{S_{cc}(0)} l(\Delta c)^2 + \frac{l(\vec{\nabla}N_\Delta)^2}{72N_\Delta} \sim$$

$$\sim \frac{Nk_B T}{c(1-c)} \left[1+ \frac{2W}{k_B T} c(1-c)\right] l(\Delta c)^2 + \frac{l(\vec{\nabla}N_\Delta)^2}{72N_\Delta} \quad .$$

Now, we take the mean values $\Delta c \sim 1/2$, $c \sim 3/4$, $N_\Delta \sim 3N/2$ and $|\vec{\nabla}N_\Delta| \sim 3N/l$, and by minimization we find the interface thickness from

$$l^2 \sim \frac{3}{8} \frac{1}{k_B T\left[1+ \frac{3}{4} \frac{W}{k_B T}\right]} \quad .$$

We now note that $2W/k_B T$ in Table II.3 varies between 60 and 10, in such a way that to a good approximation

$$l^2 \sim \frac{1}{2W} (au)^2 \quad . \tag{II.38}$$

If we take $2W = 1/2$ eV, then $l \sim 7.5$ a.u. ~ 4 Å. It is interesting that this value is already a factor of about 10 larger than for surface thickness of, say, the liquid-metal-vapour interface as obtained from a similar argument (Bathia and March 1978).

It is important to emphasize that in the theory presented above, the interface thickness, l, depends only on the heat of reaction (in this reference system). One merit of this is that possible ambiguities associated, for example, with the choice of the value of the isothermal compressibility in eq.(II.37) do not play any part in the final expression for the interface thickness. However, at first sight, the dependence of l solely on the heat of reaction predicted by eq.(II.38) ($l^2 \sim 1/W$) does not seem to be in agreement with experiment. But since experimental evidence has been collected for the following III-V semiconductors, GaAs, InAs, InP and GaSb, we have already remarked that from Table II.3 the first three have very similar values of W and hence would have much the same interface thickness on the present theory. However for GaSb, W is smaller and hence the interface thickness l is expected to be larger, which seems to be reflected in the only one experimental value for this material (Brillson et al.1981), while for AlP and AlAs we can expect the interface thickness, l, to be smaller.

II.3.3. General metal-semiconductor interface (eg. In-GaAs)

Let us now turn to the three-component system, but consider only cases for which the metal has a similar reactivity to the cation, say In on GaAs. The corresponding density profiles are shown schematically in Figure II.14. The profiles for Ga and In, when combined, must give the Ga profile for Ga-GaAs. We take into account the effect of the metal on the As profile by assuming that $2W$, the heat of reaction for the two-component case, has changed by a quantity which is equal to 1/2 of the heat of interface reaction, as given by Brillson et al.(1981). This heat of interface reaction is a measure of the different reactivity
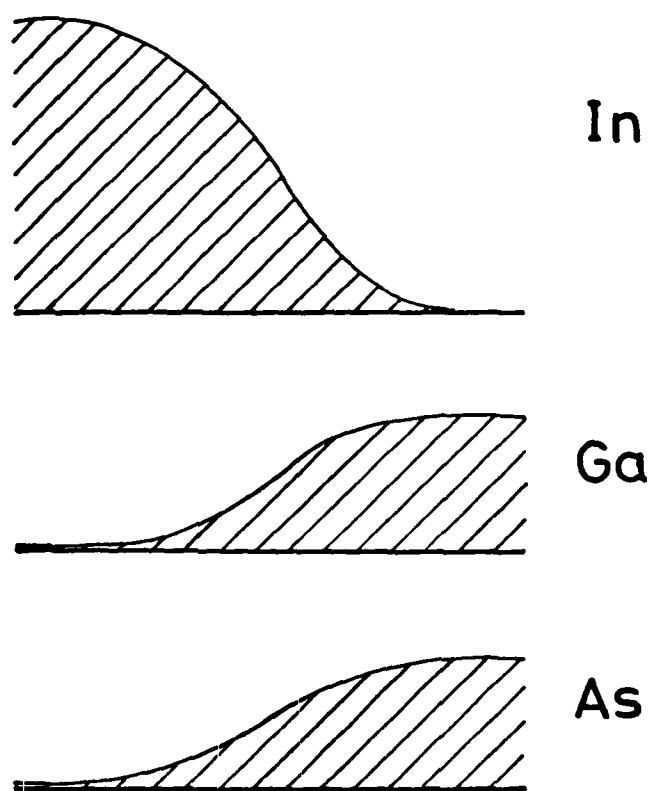
FIGURE II.14.- Density profiles of Ga, As and
In at the planar interface.

for In: the factor of 1/2 appears since As sees Ga and In at the interface.

With this model, we can calculate $dl/d(\Delta H_R)$ $\left[d(\Delta H_R/2)=-d(2W)\right]$ and a simple differentiation gives the desired result

$$\frac{1}{1}\frac{dl}{d(\Delta H_R)} = \frac{1}{4W} \quad .$$

For $2W = 0.5$ eV, we find that $1/1\ dl/d(\Delta H_R) \simeq 1(eV)^{-1}$, in excellent agreement with the slope of the straight line plot given by Brillson et al.(1981).

II.3.4. Conclusion

The main conclusion of this section II.3 is that the interface thickness is not only a function of ΔH_R, but of 2W, the heat of reaction for the semiconductor. The experimental data of Brillson et al.(1981) have been mainly obtained for those semiconductors having a similar heat of reaction, thus giving a unique dependence of l on ΔH_R. However, interface lengths must be greater for decreasing heats of reactivity 2W. (For the reference system $l \sim 1/W^2$). Table II.3 indicates the interest in making measurements on AlP (larger 2W) and on InSb and GaSb (smaller 2W) to test the dependence of the interface lengths on 2W.

CHAPTER III. CONCLUSIONS

In this Project we have analyzed some electronic
properties of GaAs-AlAs heterojunctions and of metal-
semiconductor junctions.

III.1. GaAs-AlAs HETEROJUNCTIONS

By means of a selfconsistent localized scheme, the
structural and electronic properties of several GaAs-AlAs
SL's grown in the (001) and (111) directions have been
obtained. Our results show that small ionic relaxations
appear at the (100)-interfaces, while no appreciable
relaxation is found at (111)-interfaces. For the (100)-
interfaces, the ionic relaxation affects to the first Ga
and Al planes on each side of the As ions, by increasing the
anion-cation distances in a 2.5 %. This relaxation is a
purely interface effect and we conclude that the displacements
obtained in finite SL's are valid for thicker SL's and
heterojunctions.

Our calculation also shows a small transfer of charge
from AlAs to GaAs, so that a potential barrier between both
semiconductors appears. By using this barrier we have
obtained the shift of the electronic structure of GaAs with
respect to AlAs for thicker SL's and semiinfinite hetero-
junctions. We have obtained the following difference, ΔE_V,
between the top of the AlAs and GaAs valence bands:

$$\Delta E_V(001) = -.282 \text{ eV},$$

$$\Delta E_V(111) = 0.288 \text{ eV} \quad ,$$

in remarkable agreement with the experimental evidence.

The electronic spectrum of different SL's have also
been obtained, and we have found that in the (111)-SL's,
the upper valence state is spatially localized on the GaAs

MICROCOPY RESOLUTION TEST CHART
NATIONAL BUREAU OF STANDARDS-1963-A
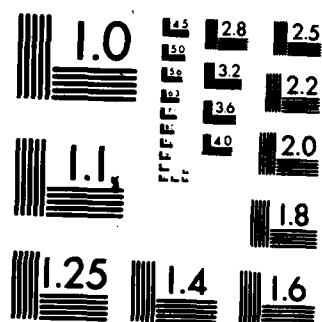
region. At the same time, the conduction band for the (100)-
SL's has been calculated as well. Our calculation shows a
very high effective mass, m* = 10.6 m, for the second
conduction band. This result may have important implications
for Raman scattering.

III.2. METAL-SEMICONDUCTOR JUNCTIONS

III.2.1. Clean metal-semiconductor junctions

Abrupt (111)-Si-Ag junctions have been analyzed by a
selfconsistent tight-binding calculation. For this junction
we have found that the interface Fermi level shifts with
respect to the Fermi level of a clean semiconductor surface,
moving towards the valence band. The extent of this shift
depends essentially on the strength of the metal-semiconductor
coupling.

By changing the parameters defining the junction, we
have analyzed the barrier formation of a general junction
and conclude that:

(i) The Fermi level at the interface -as measured from
a fixed point in the semiconductor- moves towards the
valence band as a function of the strength of the metal-
semiconductor coupling.

(ii) The density of states at the Fermi level decreases
for an increasing coupling of the metal and the semiconductor.

(iii) The effect of an increase in the metal density
of states at the Fermi level on the junction properties is
similar to an increase in the metal-semiconductor coupling.

(iv) The barrier height is essentially
determined by the coupling between the semiconductor and the
last metal layer.

III.2.2. Etched metal-semiconductor junctions

We have performed a realistic calculation of a Si-H-Ag
junction by means of a selfconsistent tight-binding
calculation. By an appropriate change of the interface

parameters, we have explored the effect of having a Cs or a
Cl monolayer at the interface.

Our calculation shows:

(i) The Fermi level for the Si-Cs-Ag, Si-H-Ag and
Si-Cl-Ag junctions are at -0.17 ± 0.005 eV, 0.02 ± 0.05 eV
and 0.04 ± 0.05 eV, respectively, referred to the Fermi
level for the Si-Ag junction.

(ii) The main changes in the Fermi level and in the
barrier height are induced by ad-atoms of low and high
electronegativity when they are supposed to sit on the mid
of three Si atoms. For atoms of low (high) electronegativity,
the Fermi level shifts towards the valence (conduction)
band.

(iii) The crucial physical quantities determining the
barrier formation in the metal-interlayer-semiconductor
junctions are the ad-atom electronegativity and the
adsorption site for the ad-atom. The barrier height is
practically determined by the coupling between the semi-
conductor and the ad-atom interlayer.

III.2.3. Non-abrupt metal-semiconductor junctions

Non-abrupt (III-V) semiconductor-metal junctions have
been analyzed by means of chemical solution theory. Our main
conclusion for these junctions is that the interface
thickness is not only a function of the metal-semiconductor
heat of reaction , as suggested by Brillson et al.(1981),
but of the heat of reaction for the semiconductor too. Interface
lengths must increase for decreasing heats of reactivity.
Thus, it can be expected smaller interface thicknesses for
AlP than for InSb and GaSb.

REFERENCES

Andreoni W and Car R 1980 Phys.Rev.B, 21, 3334

Andrews J M and Phillips J C 1975 Phys.Rev.Lett., 35, 56

Appelbaum J A and Hamann D R 1975 Phys.Rev.Lett., 34, 806

Baldo M, Flores F, Martín-Rodero A, Piccittu G and Pucci R
    1983 to be published

Bardeen J 1947 Phys.Rev., 71, 717

Barker Jr A S, Merz J L and Gossard A C 1978 Phys.Rev.B, 17,
    3181

Bathia A B, Hargrove W A and March N H 1973 J.Phys.C, 6, 621

Bathia A B and March N H 1978 J.Chem.Phys., 68, 4651

Bathia A B, March N H and Sutton J 1978 J.Chem.Phys. 69, 2258

Brillson L J 1978 Phys.Rev.Lett., 40, 260

Brillson L J, Brucker C F, Stoffel N G, Katuani A D and
    Margaritondo G 1981 Phys.Rev.Lett., 46, 838

Caruthers E and Lin Chung P J 1978 Phys.Rev.B, 17, 2705

Cahn J W and Hilliard J E 1958 J.Chem.Phys., 28, 258

Chadi D J and Cohen M L 1974 Phys.Rev.B, 10, 4988

——————————   1975 Phys.Stat.Sol.(b), 68, 405

Cheng N W, Culberston R J, Feldman L C, Silverman P J, West
    K W and Mayer J W 1980 Phys.Rev.Lett., 45, 129

Colvard C, Merlin R, Klein M V and Gossard A C 1980 Phys.Rev.
    Lett., 45, 298

Desjonqueres M C and Cyrot-Lackmann I 1975 J.Phys.F, 5, 1368

Dingle R, Gossard A C and Wiegmann W 1975 Phys.Rev.Lett., 34,
    1327

Dingle R, Wiegmann W and Henry C H 1974 Phys.Rev.Lett., 33,
    827

Djafari-Rouhani B, Dobrzynski L, Flores F, Lannoo M and
    Tejedor C 1979 Surface Sci., 80, 134

Ducastelle F and Cyrot-Lackmann I 1970 J.Phys.Chem.Solids, 31,
    1295

Duke C B and Ford W K 1981 Surface Sci., 111, L685

Esaki L and Chang L L 1974 Phys.Rev.Lett., 33, 495

Falicov L and Yndurain F 1975 J.Phys.C, 8, 147

Fleming P D, Yang A J M and Gibbs J H 1976 J.Chem.Phys., 65, 7

Froeouff J L 1980 Solid Stat.Commun., 33, 1059

Froeouff J L and Woodall J M 1981 Appl.Phys.Lett., 39, 727

García-Moliner F and Flores F 1979 *Introduction to the theory
    of solid surfaces* (Cambridge Univ.Press)

Gonçalves da Silva C E T and Keiller B 1981 Solid Stat.
Commun., 40, 215

Gormik E, Schwarz R, Tsui D C, Gossard A C and Wiegmann W 1981
Solid Stat.Commun., 38, 541

Guinea F, Tejedor C, Flores F and Louis E, to be
published

Harrison W A 1966 *Pseudopotentials in the theory of metals*
(Benjamin)

Harrison W A 1980 *Electronic structure and the properties of
solids* (Freeman)

Heine V 1965 Phys.Rev., 138A, 1689

Hess K and Holonyak Jr H 1981 Comments Solid Stat.Phys., 10, 67

Ho P S, Tan T Y, Lewis J E and Rubloff G W 1979 J.Vac.Sci.
Technol., 17, 924

Holonyak Jr H, Laidig W D, Camras M D, Morkoç H, Drummond T J
and Hess K 1981 Solid Stat.Commun., 40, 71

Holonyak Jr H, Laidig W D, Vojak B A, Hess K, Coleman J J,
Dapkus P D and Bardeen J 1980 Phys.Rev.Lett., 45, 1703

Ibach H and Rowe J E 1974 Surface Sci., 43, 481

Ihm J, Lam P K and Cohen M L 1979 Phys.Rev.B, 20, 4120

Inkson J C 1973 J.Phys.C, 6, 1350

Kittel C 1971 *Introduction to solid state physics* (Wiley)

Kirschnitz D A 1957 Sov.Phys.JETP, 5, 64

Kleinman L 1975 Phys.Rev.B, 11, 3900

Kohn W 1973 Phys.Rev.B, 7, 4383

Kunc K and Martin R M 1981 Phys.Rev.B, 24, 3445

Lannoo M and Allan G 1982 Surface Sci., 115, L137

Lee D H and Joanopoulos J D 1981 Phys.Rev.B, 23, 4988

Lohez D, Lannoo M, Masri P, Soonckindt L and Lassabatere L
1980 Surface Sci., 99, 132

Louie S G, Chelikowsky J R and Cohen M L 1977 Phys.Rev.B, 17,
1528

Louis E, Flores F, Guinea F and Tejedor C 1982 Solid Stat.
Commun., 44, 1633

Louis E and Flores F 1981 J.Physique, 42, 1313

Louis E and Yndurain F 1977 Phys.Rev.B, 16, 1542

Manuel P, Sai-Halasz G A, Chang L L, Chang C A and Esaki L
1976 Phys.Rev.Lett., 37, 1701

Margaritondo G, Rowe J E and Christman S B 1975 Phys.Rev.B,
    14, 5396

McKinley A, Williams R H and Parke A W 1979 J.Phys.C, 12, 2447

Menéndez C and Vergés J A 1981 Surface Sci., 112, 359

Merlin R, Colvard C, Klein M V, Morkoc H, Cho A Y and Gossard
    A C 1980 Appl.Phys.Lett., 36, 43

Montgomery V, McKinley A and Williams R H 1979 Surface Sci.,
    89, 635

Mottran J D, Northrap D C, Reed C M and Thanailakis A 1979
    J.Phys.D, 12, 773

Newns D M 1969 Phys.Rev., 178, 1123

Northrup J E, Ihm J and Cohen M L 1982 Phys.Rev.Lett., 47, 1910

Osbourn G C and Smith D J 1979 Phys.Rev.B, 19, 2124

Ottaviani G, Tu K N and Mayer J W 1980 Phys.Rev.Lett., 44, 284

Pandey K C 1976 Phys.Rev.B, 14, 1557

Pandey K C 1982 Phys.Rev.Lett., 49, 223

Pandey K C and Phillips J C 1976 Phys.Rev.B, 13, 750

Pauling L 1972 *The nature of the chemical bond* (Cornell Univ.
    Press, 3rd ed.)

Pickett W E, Louie S G and Cohen M L 1978 Phys.Rev.B, 17, 815

Pinczuk A, Shah J, Gossard A C and Wiegmann W 1981a Phys.Rev.
    Lett., 46, 1341

Pinczuk A, Worlock J M, Stormer H L, Gossard A C and Wiegmann
    W 1981b J.Vac.Sci.Technol., 19, 561

Proceedings of the Conference on Surfaces and Interfaces,
    Trieste 1982

Rhoderick E H 1978 *Metal-semiconductor contacts* (Oxford Univ.
    Press)

Sai-Halasz G A, Pinczuk A, Yu P Y and Esaki L 1978 Solid Stat.
    Commun., 25, 381

Sánchez-Dehesa J 1982 Ph.D.Thesis, Autonomous University of
    Madrid

Sánchez-Dehesa J, Guinea F and Tejedor C 1981a J.Phys.C, 14,
    3355

Sánchez-Dehesa J, Vergés J A and Tejedor C 1981b Phys.Rev.B,
    24, 1006

Sánchez-Dehesa J, Vergés J A and Tejedor C 1981c Solid Stat.
    Commun., 38, 871

Schlüter M and Cohen M L 1978 Phys.Rev.B, <u>17</u>, 716

Schottky W 1942 Z.Phys., <u>118</u>, 539

Schulman J N and Chang Y C 1981 Phys.Rev.B, <u>24</u>, 4445

Schulman J N and McGill T C 1979 Phys.Rev.B, <u>19</u>, 6341

——————————— 1981 Phys.Rev.B, <u>23</u>, 4149

del Sole R and Chadi D J 1981 Phys.Rev.B, <u>24</u>, 7430

Spicer W E, Lindau I, Skeath P R and Su C Y 1980 J.Vac.Sci.
    Technol., <u>17</u>, 1019

Stukel D J and Euwema R N 1969 Phys.Rev., <u>188</u>, 1173

Tejedor C, Flores F and Louis E 1977 J.Phys.C, <u>10</u>, 2163

Tejedor C and Vergés J A 1979 Phys.Rev.B, <u>24</u>, 3445

Vergés J A 1978 Ph.D.Thesis, Autonomous University of Madrid

Vergés J A and Tejedor C 1979a J.Phys.C, <u>12</u>, 499

——————————— 1979b Phys.Rev.B, <u>20</u>, 4251

Walter J R and Cohen M L 1969 Phys.Rev., <u>183</u>, 763

Weast R C 1980 *Handbook of chemistry and physics* (CRC, 61st ed.)
    pp.E103-106

Weisbuch C, Dingle R, Gossard A C and Wiegmann W 1981a Solid
    Stat.Commun., <u>38</u>, 709

Weisbuch C, Miller R C, Dingle R, Gossard A C and Wiegmann W
    1981b Solid Stat.Commun., <u>37</u>, 219

Williams R H, Montgomery V, Varma R R and McKinley A 1977
    J.Phys.D, <u>10</u>, L253

Williams R H, Montgomery V and Varma R R 1978 J.Phys.C, <u>11</u>,
    1989

Williams R H 1981 J.Vac.Sci.Technol., <u>18</u>, 929

van der Ziel J P and Gossard A C 1978 Phys.Rev.B, <u>17</u>, 765

EN

DAT
FILM

9-

DT